Università degli Studi "Roma Tre"

FACOLTÁ DI SCIENZE MATEMATICHE, FISICHE E NATURALI

Dipartimento di Matematica e Fisica

Double Higgs production at NLO in the SM and in the MSSM

Author:
Agostini Alessio

Supervisor:
Prof. Giuseppe Degrassi

PhD XXX Cycle

Contents

Introduction

The puzzle of the Standard Model of the particle and interactions has been completed with the discovery of the Higgs boson at Run 1 of the LHC [1, 2]. The SM provides a theoretical framework describing the fundamental forces of nature in terms of a gauge field theory, apart from the gravitational force. The Higgs boson is a crucial part of the SM. It emerges as a remnant of the mechanism of electroweak symmetry breaking (EWSB) [3–7], which gives mass to gauge bosons and fermions and is essential for the consistency of the theory. Its discovery hence marks the beginning of a new era of particle physics.
Even though the SM describes the so-far gathered data with high accuracy, there are indications that it is not the ultimate theory of nature. Neither is gravitation implemented in the SM nor does the SM provide a candidate for Dark Matter or an explanation for Dark Energy. Furthermore, the Higgs boson mass in the SM seems to be unnatural since contributions from very high-scale physics lead to large quantum corrections to the Higgs boson mass. This poses the question why the Higgs boson mass scale is so much smaller than the Planck scale, known as the hierarchy problem. A large amount of fine-tuning between the different loop contributions is needed to achieve a Higgs boson mass at the electroweak (EW) scale. This hints to New Physics which becomes relevant at a scale that might be reachable at the LHC. In the past, this theoretical problem acted as a guideline for numerous extensions of the SM.

A solution to many shortcomings of the SM is provided by supersymmetry (SUSY). Supersymmetry is a space-time symmetry which enhances the Poincaré symmetry by additional anti-commuting generators. These generators transform bosonic states into fermionic states and vice versa. Each particle is hence paired with a superpartner, which only differs by the spin. None of these superpartners, however, have been discovered yet. Thus, SUSY cannot be an exact symmetry. This problem can be evaded by introducing SUSY breaking sources, leading to different masses for the particles and their superpartners. If SUSY is supposed to solve the naturalness problem of the SM Higgs

boson, the discovery reach of the superpartners lies within the range of the LHC. By now, all experiments could only report exclusion limits on the SUSY particle masses, but large parts of the parameter space remain to be explored.

In this thesis we analyze the double Higgs production in the SM and MSSM. In the chapter 1, we introduce the Low Energy Theorems, a powerful instruments to calculate the NLO QCD corrections to cross section, and we summarise the result for double Higgs production cross section. However, by using the LET, we make an approximation and we will discuss the validity of this approach. At the end of the chapter we present the newest prediction of the double Higgs production and the relative error in the SM.
In the chapter 2, we show our result for the double Higgs production in the MSSM. In particular, making always use of LET, we obtain analytic results for the one- and two-loop squark contributions to Higgs pair production in the limit of vanishing external momenta. We also obtain, by direct calculation of the relevant two-loop diagrams, the subset of bottom/sbottom contributions that involve the D-term-induced EW Higgs-squark coupling and survive in the limit of vanishing bottom mass. To assess the importance of the newly-computed corrections, we include the squark contributions to both triangle and box form factors in a private version of the public code HPAIR, which computes the NLO-QCD cross section for Higgs pair production in the SM and in the MSSM. We find that the two-loop squark contributions can have a non-negligible effect in scenarios with stop masses below the TeV scale.
Finally in the chapter 3 we discuss the calculation of the process $gg \to hhg$, the most relevant process for the real NLO QCD corrections in the double Higgs production. First of all we evaluate a set of orthogonal projectors through which we can calculate the amplitude. Then, from the exact result we made an expansion in the top mass to obtain, for the first time, the analytic results of the large top-mass-expansion evaluation of cross section up to and including $\mathcal{O}(1/m_t^2)$ terms.

Chapter 1

Double Higgs production in the Standard Model at NLO

In Run 1, the couplings of the Higgs boson to fermions and to gauge bosons have already been measured, and found to be compatible with the predictions of the Standard Model (SM) within an experimental accuracy of $(10-20)\%$ [8]. One of the major goals of the forecoming runs of LHC is to improve the experimental results of the Run 1 and the complete exploration of the properties of the Higgs boson, in particular the self interactions. This is the only way to reconstruct the scalar potential of the Higgs doublet field Φ, that is responsible for spontaneous electroweak symmetry breaking,

$$V_h = \mu^2 \Phi^\dagger \Phi + \frac{1}{2}\lambda(\Phi^\dagger\Phi)^2 \; ; \quad \lambda = \frac{m_h^2}{v^2} \text{ and } \mu^2 = -\frac{1}{2}m_h^2 \, , \tag{1.0.1}$$

with $v = 246$ GeV. Rewriting the Higgs potential in terms of a physical Higgs boson leads to the trilinear Higgs self–coupling λ_{hhh}, which in the SM is uniquely related to the mass of the Higgs boson and the VEV,

$$\lambda_{hhh} = \frac{3m_h^2}{v} \, , \tag{1.0.2}$$

and the quartic self couplings $\lambda_{hhhh} = 3m_h^2/v^2$, which is further suppressed by a power of v compared to the triple Higgs coupling. The triple Higgs coupling is accessible in Higgs pair production processes and the quartic coupling in Higgs triple production process. A measurement of the quartic Higgs self-coupling lies beyond the reach of the LHC [9,10], on the contrary previous studies showed that the Higgs pair production process, and hence the trilinear Higgs self-coupling, might be accessible for high integrated luminosities

in the $b\bar{b}\gamma\gamma$ [11–16], $b\bar{b}\tau\bar{\tau}$ [12, 17], $b\bar{b}W^+W^-$ [18] and $b\bar{b}b\bar{b}$ [19–21] final states.

In this chapter we summarize some general results on the Higgs boson pair production via the gluon fusion mechanism in proton–proton collisions, $pp \to hh$ up to next-to-leading order. First of all we briefly discuss the Low Energy Theorem and his application in Higgs sector. Then we present the exact results for the LO cross section that is known since the late eighties [22]. However, similarly to what happens in single Higgs production, one expects the LO contribution to be subject to large radiative corrections. For the higher order corrections to Higgs pair production we show the NLO cross section by using the effective theory with infinite top mass or, equivalently, the limit of vanishing external momentum [23]. Then we discuss as the effective theory is a bad approximation for the double Higgs production, contrarily than it happens for single Higgs production. Finally we present the more recent numerical estimates of the double Higgs production and the relative theoretical uncertainties.

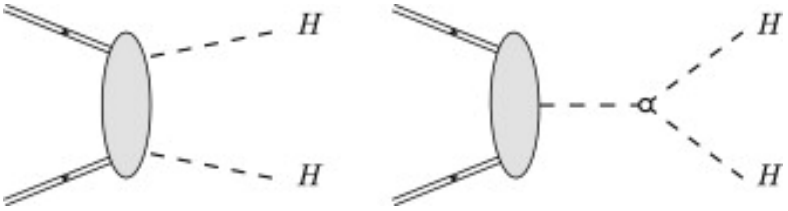

Figure 1.1: Classes of diagrams for Higgs pair production in hadron hadron collisions: double Higgs production without hhh vertices on the left-hand side, and, on the right-hand side, the contribution due to the Higgs self interaction. Final state particles other than the Higgs bosons are understood.

1.1 Double Higgs production at LHC

In the SM, the diagrams contributing to Higgs pair production can be organised in two classes (see 1.1): those where both Higgs bosons couple only to vector bosons or to heavy quarks, and those that feature the Higgs self coupling. Analogously to single-Higgs production, several channels can lead to a final state involving two Higgs bosons. They entail the Higgs coupling to either the top quark (as in the case of gluon-gluon fusion and of $t\bar{t}$ associated production), or vector bosons (in VBF, and in W and Z associated production), or both (for single-top associated production). The dominant channel for Higgs pair production is gluon-gluon fusion via virtual top quarks, *i.e.*, box and triangle diagrams, see fig. 1.2. This process therefore starts at the leading order with a loop, exactly as single-Higgs production. In the "triangle" contribution a single Higgs boson splits via an s-channel exchange into two Higgs bosons, thus it contains the trilinear Higgs self-coupling. The "box" contribution plays the role of an irreducible background, as it does not incorporate the trilinear Higgs self-coupling. A precise prediction of the gluon fusion Higgs-pair production channel is essential to constrain new physics or to determine the Higgs self-coupling.
The second-largest production channel is vector boson fusion (VBF). At variance with single-Higgs production, the production of a Higgs pair in association with a $t\bar{t}$ pair is the third most important process and, in fact, it is even larger than VBF at high Higgs-pair transverse momenta, or for collider centre-of-mass energies higher than that of the LHC. The other production channels are those with vector boson and top quark associated production, see fig. 1.3 [24].

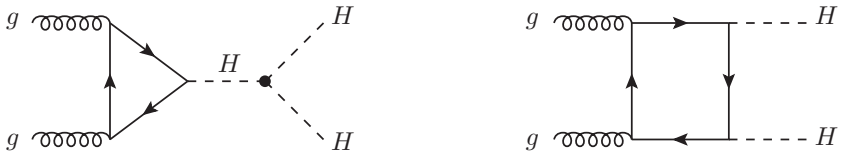

Figure 1.2: Generic Feynman diagrams for box and triangle topologies for Higgs pair production.

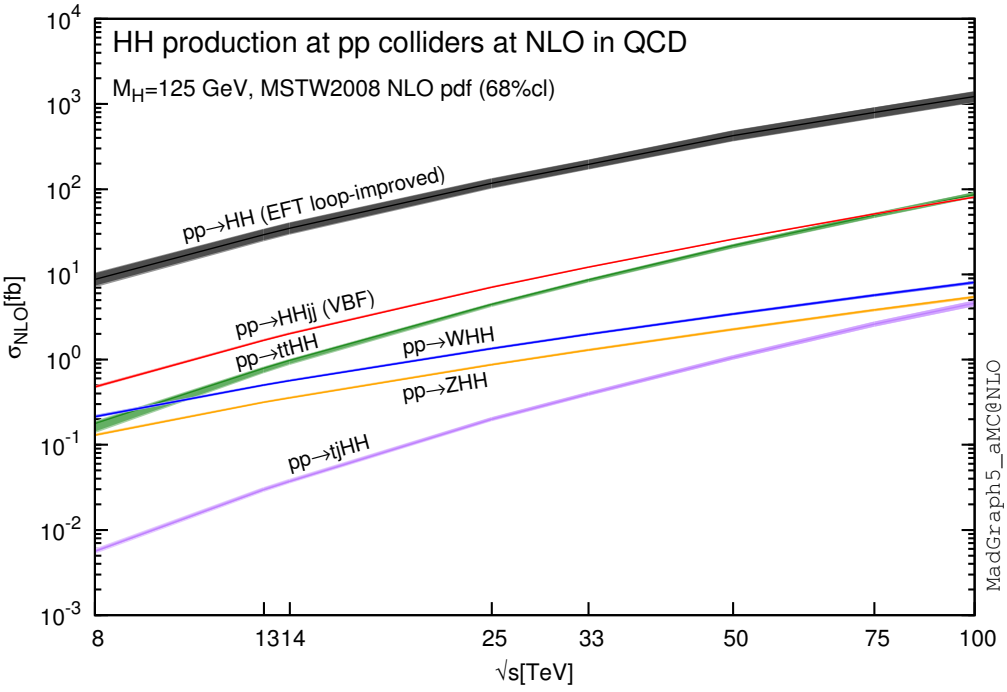

Figure 1.3: Total cross sections at the NLO in QCD for the six largest hh production channels at pp colliders. The thickness of the lines corresponds to the scale and PDF uncertainties.

1.2 The Low Energy Theorem

In this section we briefly expose the low-energy theorem (LET) and its consequences in the Higgs physics. The LET is the starting point of our calculations in SM and also MSSM. The LET for Higgs interactions, relate the amplitude $\mathcal{M}(X, \phi)$ for a generic

particle configuration X plus an external Higgs boson ϕ of vanishing momentum to the corresponding amplitude without the external Higgs boson, $\mathcal{M}(X)$. The LET can be stated as follows: the amplitude $\mathcal{M}(X,\phi)$ can be obtained by considering $\mathcal{M}(X)$ as a field-dependent quantity via the dependence of the relevant parameters (masses, in the SM, and also mixing angles in MSSM) on ϕ. The first term in the expansion of $\mathcal{M}(X)$ in the Higgs field, evaluated at the minimum of the Higgs potential, corresponds to $\mathcal{M}(X,\phi)$. This leads to the following LET [25–27]:

$$\lim_{p_H\to 0}\mathcal{M}(X\,\phi) \;=\; \frac{\partial}{\partial\phi}\,\mathcal{M}(X)\bigg|_{\phi=v} \tag{1.2.1}$$

In case $\mathcal{M}(X)$ contains infrared (IR) divergent terms the theorem applies to the IR-safe part of the two amplitudes. In order to proof the validity of the LET we can apply it at the fermionic and bosonic propagators:

$$\begin{aligned}
\frac{\partial}{\partial\phi}\left(\frac{1}{\not p - m_f}\right)\bigg|_{\phi=v} &= \frac{\partial m_f}{\partial\phi}\frac{\partial}{\partial m_f}\left(\frac{i}{\not p - m_f}\right) = \frac{i m_f}{v}\frac{i}{\left(\not p - m_f\right)^2} \\
&= \frac{i}{\not p - m_f}\frac{-i m_f}{v}\frac{-i}{\not p - m_f}\,, \\
\frac{\partial}{\partial\phi}\left(\frac{1}{p^2 - m_V^2}\right)\bigg|_{\phi=v} &= \frac{\partial m_V^2}{\partial\phi}\frac{\partial}{\partial m_V^2}\left(\frac{1}{p^2 - m_V^2}\right) = \frac{g m_V^2}{m_W^2}\frac{1}{\left(p^2 - m_V^2\right)^2} \\
&= \frac{1}{p^2 - m_V^2}\frac{g m_V^2}{m_W^2}\frac{1}{p^2 - m_V^2}\,.
\end{aligned} \tag{1.2.2}$$

The result of this operation is to obtain vertex with a Higgs null momentum $h\overline{f}f$ or $hVV^\dagger$, for the fermionic and bosonic case respectively, with the exact costant coupling, starting from a propagator. Obviously the amplitude that we can evaluate by using the LET is exactly the same if we use the limit where the top quark mass tends to infinity and in this way the calculation of the NLO corrections are very simplifies. Lagrangians for single and multi-Higgs production in the $m_t \to \infty$ assume this form respectively:

$$\begin{aligned}
\mathcal{L}_{hgg} &= \frac{\alpha_s}{12\pi}G^{a\mu\nu}G^a_{\mu\nu}\frac{h}{v}\,, \\
\mathcal{L}_{h^n gg} &= \frac{\alpha_s}{12\pi}G^{a\mu\nu}G^a_{\mu\nu}\log\left(1+\frac{h}{v}\right)\,,
\end{aligned} \tag{1.2.3}$$

where $G^{a\mu\nu}$ is the gluonic tensor. To use the LET in gluon fusion Higgs production one identify $\mathcal{M}(X,\phi)$ with the gluon-self energy and applies to it the relevant number of derivatives with respect to ϕ.

1.3 Cross section at LO and NLO

In this section we summarize some general results on the gluon-fusion production of a pair of Higgs bosons [28]. The hadronic cross section for the process $p + p \to h + h + X$ at center-of-mass energy $\sqrt{s}$ can be written as

$$M_{hh}^2 \frac{d\sigma}{dM_{hh}^2} = \sum_{a,b} \int_0^1 dx_1 dx_2 \; f_{a,h_1}(x_1, \mu_F)\, f_{b,h_2}(x_2, \mu_F) \int_0^1 dz \; \delta\left(z - \frac{M_{hh}^2}{\hat{s}}\right) M_{hh}^2 \frac{d\hat{\sigma}_{ab}}{dM_{hh}^2} \; , \tag{1.3.1}$$

where: M_{hh}^2 is the invariant mass of the Higgs system; $f_{a,h_i}(x, \mu_F)$ is the density for the parton of type a (with $a = g, q, \overline{q}$) in the colliding proton; μ_F is the factorization scale; $\hat{s} = s\, x_1\, x_2$ is the partonic center-of-mass energy; $\hat{\sigma}_{ab}$ is the cross section for the partonic subprocess $ab \to h + h + X$. The partonic cross section can be written in terms of the LO contribution $\sigma^{(0)}$ as

$$M_{hh}^2 \frac{d\hat{\sigma}_{ab}}{dM_{hh}^2} \;=\; \sigma^{(0)}(z\hat{s})\, z\, G_{ab}(z) \; , \tag{1.3.2}$$

where the coefficient function $G_{ab}(z)$ in eq. (1.3.2) can in turn be decomposed, up to NLO terms, as

$$G_{ab}(z) \;=\; G_{ab}^{(0)}(z) \;+\; \frac{\alpha_s(\mu_R)}{\pi}\, G_{ab}^{(1)}(z) \;+\; \mathcal{O}(\alpha_s^2) \, , \tag{1.3.3}$$

where μ_R denoting the renormalization scale. The LO contribution is given by the gluon-gluon channel by

$$G_{ab}^{(0)}(z) \;=\; \delta(1 - z)\, \delta_{ag}\, \delta_{bg} \, . \tag{1.3.4}$$

The amplitude for $g_a^\mu(p_1) g_b^\nu(p_2) \to h(p_3) h(p_4)$ can be written as:

$$A^{\mu\nu} = \frac{G_\mu}{\sqrt{2}} \frac{\alpha_s(\mu_R)}{2\pi} \delta_{ab}\, T_F\, \hat{s}\, [A_1^{\mu\nu}\, F_1 + A_2^{\mu\nu}\, F_2] \; , \tag{1.3.5}$$

where T_F is the matrix normalization factor for the fundamental representation of $SU(N_c)$ ($T_F = 1/2$) and the form factors F_1, F_2 are functions, besides of m_t^2, of the partonic Mandelstam variables

$$\hat{s} = (p_1 + p_2)^2 \, , \quad \hat{t} = (p_1 - p_3)^2 \, , \quad \hat{u} = (p_2 - p_3)^2 \; . \tag{1.3.6}$$

In eq. (1.3.5) the orthogonal projectors A_1 and A_2 onto the spin-0 and spin-2 states, respectively, in $n_d = 4 - 2\,\epsilon$ dimension and normalized to 2 read

$$A_1^{\mu\nu} = \sqrt{\frac{2}{n_d-2}}\left[g^{\mu\nu} - \frac{p_1^\nu\, p_2^\mu}{(p_1\cdot p_2)}\right], \tag{1.3.7}$$

$$\begin{aligned} A_2^{\mu\nu} &= \sqrt{\frac{n_d-2}{2(n_d-3)}}\left\{\frac{n_d-4}{n_d-2}\left[g^{\mu\nu} - \frac{p_1^\nu\, p_2^\mu}{(p_1\cdot p_2)}\right]\right. \\ &+ \left. g^{\mu\nu} + \frac{p_3^2\, p_1^\nu\, p_2^\mu - 2\,(p_3\cdot p_2)\, p_1^\nu\, p_3^\mu - 2\,(p_3\cdot p_1)\, p_3^\nu\, p_2^\mu + 2\,(p_1\cdot p_2)\, p_3^\mu\, p_3^\nu}{p_T^2\,(p_1\cdot p_2)}\right\}, \end{aligned} \tag{1.3.8}$$

with p_T the transverse momentum of the Higgs particle that can be expressed in terms of the Mandelstam variables as

$$p_T^2 = \frac{\hat{t}\hat{u} - m_h^4}{\hat{s}}\,. \tag{1.3.9}$$

The spin-2 state receives contributions only from box topologies (see fig. 1.2) while in the spin-0 case both box and triangle diagrams contribute such that F_1 takes the form

$$F_1 = F_\Delta \frac{3m_h^2}{\hat{s} - m_h^2} + F_\Box\,, \tag{1.3.10}$$

where $F_\Delta(F_\Box)$ is the contribution of the triangle (box) diagrams. The Born cross section is written as

$$\sigma^{(0)}(\hat{s}) = \frac{G_\mu^2 \alpha_s^2(\mu_R)}{512\,(2\,\pi)^3}\int_{\hat{t}_-}^{\hat{t}_+}\left\{\left|T_F\, F_1^{1\ell}(\hat{s})\right|^2 + \left|T_F\, F_2^{1\ell}(\hat{s})\right|^2\right\}, \tag{1.3.11}$$

with $\hat{t}_\pm = -\hat{s}/2(1 - 2\,m_h^2/\hat{s} \mp \sqrt{1 - 4\,m_h^2/\hat{s}})$. The one-loop form factors $F_1^{1\ell}$, $F_2^{1\ell}$ are fully known analytically [22, 29] and their values in the limit of vanishing external momentum can be obtained via a low energy theorem (LET) calculation giving $F_\Delta^{1\ell,LET} = -F_\Box^{1\ell,LET} = 4/3$, $F_2^{1\ell,LET} = 0$, that correspond to the effective theory $m_t \to \infty$ result. From the eq. (1.3.10) and from the LET values of form factors we can see that there is a strong cancellation, the box and triangle diagram interfere destructively (in particular in effective theory if $\hat{s} = 4m_h^2$ the cancellation is exact). The destructive interference are partial also for the exact form factor.

The NLO terms include, besides the gg channel, also the one-loop induced processes $gq \to qhh$ and $q\bar{q} \to ghh$. The gg-channel contribution, involving two-loop virtual

corrections to $gg \to hh$ and one-loop real corrections from $gg \to hhg$, can be written as

$$\begin{aligned} G_{gg}^{(1)}(z) &= \delta(1-z)\left[C_A\,\frac{\pi^2}{3} + \beta_0\,\ln\left(\frac{\mu_R^2}{\mu_F^2}\right) + \mathcal{C}_{\rm NLO}\right] \\ &+ P_{gg}(z)\,\ln\left(\frac{\hat{s}}{\mu_F^2}\right) + C_A\,\frac{4}{z}\,(1-z+z^2)^2\,\mathcal{D}_1(z) + C_A\,\mathcal{R}_{gg}\,, \end{aligned} \tag{1.3.12}$$

where

$$\mathcal{C}_{\rm NLO} = \frac{\int_{\hat{t}_-}^{\hat{t}_+} d\hat{t}\,\left[\left(T_F\,F_1^{1\ell}\right)^*\,T_F\,\left(\,F_1^{2\ell}+F_1^{2\Delta}\right)\;+\;\left(T_F\,F_2^{1\ell}\right)^*\,T_F\,\left(F_2^{2\ell}+F_2^{2\Delta}\right)\,\right]}{\int_{\hat{t}_-}^{\hat{t}_+} d\hat{t}\,\left(\left|T_F\,F_1^{1\ell}\right|^2+\left|T_F\,F_2^{1\ell}\right|^2\right)} + \text{h.c.}\,. \tag{1.3.13}$$

In eq. (1.3.12), $C_A = N_c$ (N_c being the number of colors), $\beta_0 = (11\,C_A - 2\,N_f)/6$ (N_f being the number of active flavors) is the one-loop β-function of the strong coupling in the SM, $\mathcal{R}_{gg}$ is the contribution of the real corrections, P_{gg} is the LO Altarelli-Parisi splitting function

$$P_{gg}(z) \;=\; 2\,C_A\,\left[\mathcal{D}_0(z) + \frac{1}{z} - 2 + z(1-z)\right]\,, \tag{1.3.14}$$

and

$$\mathcal{D}_i(z)^1 = \left[\frac{\ln^i(1-z)}{1-z}\right]_+\,. \tag{1.3.15}$$

The first line of eq. (1.3.12) displays the two-loop virtual contribution regularized by the infrared singular part of the real-emission cross section. In eq. (1.3.13) the terms $F_1^{2\ell}$ and $F_2^{2\ell}$ contain the contribution of irreducible two-loop diagrams, (see fig. 1.4 a,c,d) and in the limit of vanishing external momenta they read $F_\Delta^{2\ell} = -F_\Box^{2\ell} = -C_F + 5/3\,C_A$, $F_2^{2\ell} = 0$ [23] with $C_F = (N_c^2-1)/(2\,N_c)$. The term $F_1^{2\Delta}$ ($F_2^{2\Delta}$) represents the contribution of the two-loop double-triangle diagrams with a t/u-channel gluon exchange (fig. 1.4 b) to the spin-0 (spin-2) part of the amplitude. In the limit of vanishing external momenta the

[1] The plus-distribution is defined in terms of integrals:

$$\begin{aligned} \int_0^1 dx\,\frac{f(x)}{(x)_+} &= \int_0^1 dx \frac{f(x)-f(0)}{x} \\ \int_0^1 dx\,f(x)\left(\frac{\log(x)}{x}\right)_+ &= \int_0^1 dx\,\left[f(x)-f(0)\right]\frac{\log(x)}{x}\,. \end{aligned}$$

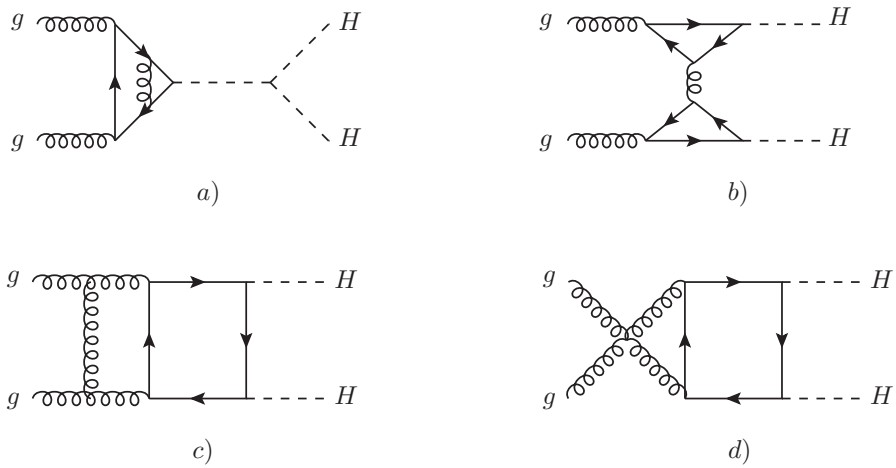

Figure 1.4: Sample of Feynman diagrams for the virtual two-loop corrections to Higgs pair production via gluon fusion.

double-triangle diagrams can be expressed in terms of $F_\Delta^{1\ell,LET}$ as

$$F_1^{2\Delta} \to \frac{1}{2} T_F \left(F_\Delta^{1\ell,LET}\right)^2 \qquad \text{and} \qquad F_2^{2\Delta} \to -\frac{1}{2} T_F \frac{p_T^2}{2\hat{t}\hat{u}} (\hat{s} - 2\, m_h^2) \left(F_\Delta^{1\ell,LET}\right)^2 . \tag{1.3.16}$$

The second line in eq. (1.3.12) contains the non-singular contribution from the real gluon emission in the gluon-fusion process. The function $\mathcal{R}_{gg}$ is obtained from one-loop diagrams where quarks circulate in the loop, and in the limit of vanishing external momenta it becomes $\mathcal{R}_{gg} \to -11(1-z)^3/(6z)$. The contributions of the $gq \to qhh$ and $q\bar{q} \to ghh$ channels are given by:

$$G_{q\bar{q}}^{(1)}(z) \;=\; \mathcal{R}_{q\bar{q}}\,, \qquad\qquad G_{qg}^{(1)}(z) \;=\; P_{gq}(z) \left[\ln(1-z) + \frac{1}{2} \ln\left(\frac{\hat{s}}{\mu_F^2}\right)\right] + \mathcal{R}_{qg}\,, \tag{1.3.17}$$

where

$$P_{gq}(z) \;=\; C_F \, \frac{1 + (1-z)^2}{z}\,. \tag{1.3.18}$$

The functions $\mathcal{R}_{q\bar{q}}$ and $\mathcal{R}_{qg}$ in (1.3.17) are obtained from one-loop quark diagrams, and in the limit of vanishing external momenta become $\mathcal{R}_{q\bar{q}} \to 32\,(1-z)^3/(27z)$, $\mathcal{R}_{qg} \to 2\,z/3 - (1-z)^2/z$.

At the moment, by using the LET approximation, are known the NNLO cross section [30] and recently, the complete NLO fixed order corrections, including all top quark mass effects, have become available [31, 32]. The QCD corrections are large, typically doubling

the cross section from LO to NLO, with another $\sim 20\%$ increase going from NLO to NNLO. The threshold resummation corrections for Higgs boson pair production at NNLL [33] further increase the rate. We presents the numerical results in section 1.5 when we presents also the uncertainties.

1.4 The validity of the LET approximation

As we have been discussed in the section 1.2, the LET is a powerful instruments to calculate the matrix element in the contest of the Higgs physics. However it's necessary to discuss the validity of the LET in our calculation, in particular it is quite sensitive to the hadronic center-of-mass energy and to the choice of the renormalization and factorization scales [34]. In the case of single Higgs production, the LET result gives a quite accurate estimate of the cross section, indeed the region above $\sqrt{\hat{s}} > 2\,m_t$ threshold don't contributes significantly to the hadronic cross section. On the contrary for the double production the region up to $\sqrt{\hat{s}} \sim 600 - 700$ contributes significantly to the hadronic cross section. In this latter region the vanishing external momenta condition is obviously not satisfied and therefore the result obtained in this approximation is unreliable.

The inclusion of more terms in a large top-mass expansion of the form factors does not improve the evaluation of the LO cross section [34,35] and it's evident in Fig.1.5 [28]. Here there's the partonic cross section as a function of $\sqrt{\hat{s}}$. The exact cross section (solid black line), $\sigma_{ex}^{(0)}$, is compared with the approximated ones (dashed colored lines), $\sigma_{app,n}^{(0)}$, obtained using for the form factors the expansions to the order n. An estimate of the hadronic cross section from eq. (1.3.1) based on the use of $\sigma_{app,n}^{(0)}$ depends on the relative weights in the hadronic integral of the regions where $\sigma_{app,n}^{(0)} < \sigma_{ex}^{(0)}$ vs. $\sigma_{app,n}^{(0)} > \sigma_{ex}^{(0)}$ and how these two regions can compensate each other. With the increase in the hadronic energy, regions with larger $\sqrt{\hat{s}}$ are going to contribute more to the hadronic cross section, so that the LET approximation is going to grow in size and therefore become either closer to the full cross section or overestimating it. For instance for $\sqrt{s} = 100$ TeV the LET result overestimates the full cross section by a factor ~ 2.2. Figure 1.5 indicates that an estimate of the LO hadronic cross section obtained employing the large-mass expanded results in the entire range of partonic energies is not going to be realistic.
We arrive at the same conclusions for the hadronic cross section, as it can see in the Fig. 1.6, where we have the hadronic cross section as function of the invariant mass. The inclusion of the $\mathcal{O}(m_t^{-2})$ corrections does not significantly improve the low energy theorem results. The m_t^{-4} terms fail entirely in reproducing the exact distribution, in

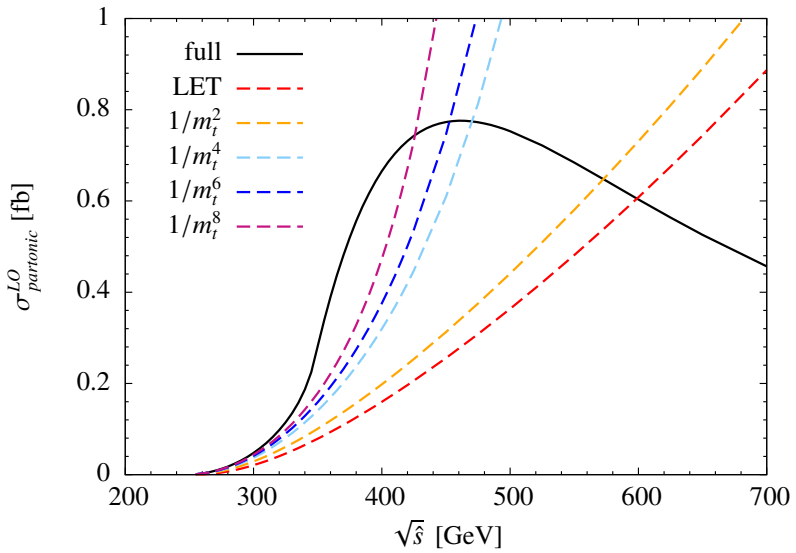

Figure 1.5: Leading order partonic cross section as a function of the partonic center-of-mass energy. The solid line corresponds to the exact result, the dashed ones to the results obtained using different terms in the large top-mass expansion.

particular at large values of M_{HH}.

To conclude, for what it concerns the double production, in the region $\sqrt{\hat{s}} \lesssim 2\,m_t$ the LET result approximates relatively well the exact result but it fails in describing the region $\sqrt{\hat{s}} > 2\,m_t$, that from a physical top of mass $m_t \sim 173$ GeV implies $\sqrt{\hat{s}} \gtrsim 450$ GeV. The sum of the first five terms in the large top-mass expansion reproduces quite well the exact results when $\sqrt{\hat{s}} \lesssim 400$ GeV while the region $\sqrt{\hat{s}} > 400$ GeV is described very badly, worse than in the LET case.

1.5 Theoretical uncertainties

The theoretical uncertainties on the inclusive cross section of the gluon fusion process will be estimated by taking into account the following sources of error [12]:

1. the scale uncertainty, due to the missing higher order contributions and estimated by varying the renormalization scale μ_R and the factorization scale μ_F;

2. the PDFs and related α_s errors. The PDFs are evaluated starting with a parametriza-

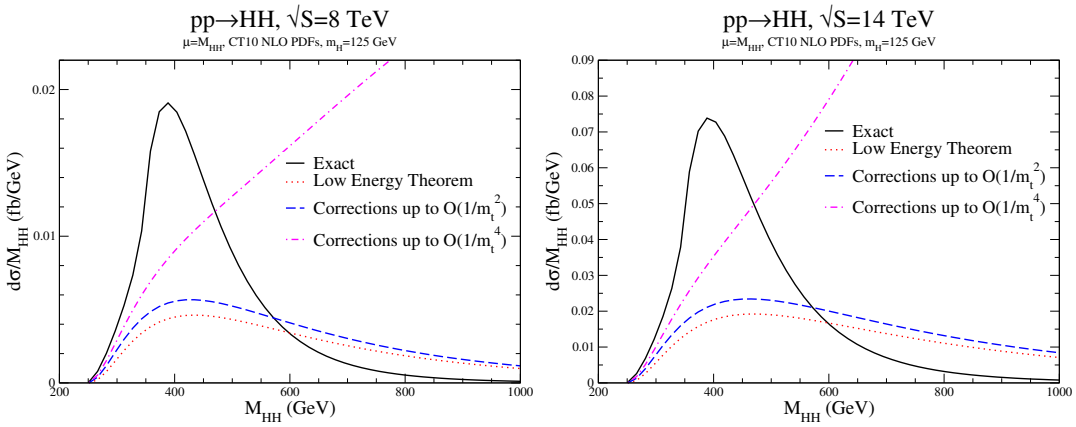

Figure 1.6: Invariant mass distributions for LO Higgs pair-production at $\sqrt{s} = 8$ TeV and $\sqrt{s} = 14$ TeV, for terms in the large mass expansion up to $\mathcal{O}(m_t^{-4})$ (dashed lines), with the LET (dotted red line) and with the exact cross section (solid line).

tion at low scale Q_0 respect to the Bjorken variable x, and using the DGLAP equations they are obtained at any scale and any x. Since the PDFs are fitted from the data, they depend on the choice of the data sets and the treatment of the errors on the data, as well as on the parametrization. Also the α_s are fitted from data, in general togheter with the PDF.

3. the error due to the heavy quark mass approximation for the calculation of the higher order corrections.

The central value of the scales are now fixed [36] to $\mu_0 = M_{hh}^2/2$ with the restriction $1/2 < \mu_R/\mu_F < 2$. This choice has numerical importance in order to minimize the threshold resummation. The scale uncertainties are $\sim 4 - 6\%$.
The parametrization of the parton distribution functions is another source of theoretical uncertainty. A possibility might be to compare different parameter sets. In particular the PDF4LHC15 [37] combine this sets: CT10 [38], MMHT14 [39] and NNPDF3.0 [40]. In addition to the PDF uncertainties, there is also an uncertainty due to the errors on the value of the strong coupling constant α_s. In ref. [37], both at NLO and NNLO, is being used the following value of $\alpha_s(m_Z^2)$ and its associated uncertainty:

$$\alpha_s(m_Z^2) \;=\; 0.1180 \pm 0.0015\,. \tag{1.5.1}$$

The PDF + α_s uncertainties are determined by first computing the PDF uncertainty for the central α_s then computing predictions for the upper and lower values of α_s,

consistently using the corresponding PDF sets, and finally adding results in quadrature. The NNLL threshold resummed cross sections are combined consistently with the fixed order NNLO results in Table 1.1, with the rate being weighted by the exact LO finite m_t result normalized to the $m_t \to \infty$ LO result. This is the HEFT approximation. For all the predictions we use the `PDF4LHC15_nnlo_mc` proton PDF set that is recommended by the PDF4LHC group [37]. The inclusion of the mass effects reduces the NLO rate by an energy dependent factor which can be parametrized as

$$\sigma(gg \to hh)^{exact}_{NLO} = \sigma(gg \to hh)^{HEFT}_{NLO}(1 + \delta_t)\,, \tag{1.5.2}$$

where, using $m_t = 173$ GeV,

$$\begin{aligned}
\delta_t(7\ )\text{TeV} &= -9.94\% && (1.5.3)\\
\delta_t(8\ )\text{TeV} &= -10.88\% && (1.5.4)\\
\delta_t(13\ )\text{TeV} &= -13.72\% && (1.5.5)\\
\delta_t(14\ )\text{TeV} &= -14.11\%\,. && (1.5.6)
\end{aligned}$$

The top mass effects can be included consistently by writing our final result as

$$\sigma'_{NNLL} = \sigma_{NNLL} + \delta_t \sigma^{HEFT}_{NLO}\,, \tag{1.5.7}$$

where σ_{NNLL} is given in Table 1.1. This prescription amounts to subtracting 5.49 fb from the 14 TeV, 4.50 fb from the 13 TeV, 1.02 fb from the 8 TeV and 0.64 fb from the 7 TeV numbers of Table 1.1 . (We note that Table 1.1 uses $m_t = 172.5$ GeV, so there is a slight mis-match in the m_t values.) Furthermore, we neglect any possible m_h dependence of δ_t. The results are given in Table 1.2 and correspond to the convention of Eq. 1.5.7. We arbitrarily assume a top mass uncertainty of $\pm 5\%$ from unknown top quark mass effects at NNLO, and do not include a theoretical error on δ_t.

Table 1.1: NNLL matched to NNLO cross sections for $gg \to hh$ with a central scale $\mu_0 = M_{hh}^2/2$ with $m_h = 124.5$ GeV, $m_h = 125$ GeV, $m_h = 125.09$ GeV and $m_h = 125.5$ GeV [33] computed in the HEFT approximation. The uncertainties from top quark mass effects are not included in this table. Uncertainties are evaluated using the PDF4LHC recommendation and are based on the `PDF4LHC15_nnlo_mc` set.

$m_h = 124.5$ GeV	σ_{NNLL}(fb)	Scale Unc. (%)	PDF Unc. (%)	α_s Unc. (%)
$\sqrt{s} = 7$ TeV	7.772	$+4.0 - 5.7$	± 3.4	± 2.8
$\sqrt{s} = 8$ TeV	11.26	$+4.1 - 5.7$	± 3.0	± 2.6
$\sqrt{s} = 13$ TeV	38.20	$+4.3 - 6.0$	± 2.1	± 2.3
$\sqrt{s} = 14$ TeV	45.34	$+4.4 - 6.0$	± 2.1	± 2.2
$m_h = 125$ GeV	σ_{NNLL}(fb)	Scale Unc. (%)	PDF Unc. (%)	α_s Unc. (%)
$\sqrt{s} = 7$ TeV	7.718	$+4.0 - 5.7$	± 3.4	± 2.8
$\sqrt{s} = 8$ TeV	11.18	$+4.1 - 5.7$	± 3.1	± 2.6
$\sqrt{s} = 13$ TeV	37.95	$+4.3 - 6.0$	± 2.1	± 2.3
$\sqrt{s} = 14$ TeV	45.05	$+4.4 - 6.0$	± 2.1	± 2.2
$m_h = 125.09$ GeV	σ_{NNLL}(fb)	Scale Unc. (%)	PDF Unc. (%)	α_s Unc. (%)
$\sqrt{s} = 7$ TeV	7.708	$+4.0 - 5.7$	± 3.4	± 2.8
$\sqrt{s} = 8$ TeV	11.17	$+4.1 - 5.7$	± 3.1	± 2.6
$\sqrt{s} = 13$ TeV	37.91	$+4.3 - 6.0$	± 2.1	± 2.3
$\sqrt{s} = 14$ TeV	45.00	$+4.4 - 6.0$	± 2.1	± 2.2
$m_h = 125.5$ GeV	σ_{NNLL}(fb)	Scale Unc. (%)	PDF Unc. (%)	α_s Unc. (%)
$\sqrt{s} = 7$ TeV	7.663	$+4.0 - 5.7$	± 3.4	± 2.8
$\sqrt{s} = 8$ TeV	11.11	$+4.1 - 5.7$	± 3.1	± 2.6
$\sqrt{s} = 13$ TeV	37.71	$+4.3 - 6.0$	± 2.1	± 2.3
$\sqrt{s} = 14$ TeV	44.76	$+4.4 - 5.9$	± 2.1	± 2.2

Table 1.2: NNLL matched to NNLO cross sections for $gg \to hh$ including top quark mass effects to NLO [31] with a central scale $\mu_0 = M_{hh}^2/2$ with $m_h = 124.5$ GeV, $m_h = 125$ GeV, $m_h = 125.09$ GeV and $m_h = 125.5$ GeV [33]. Uncertainties are evaluated using the PDF4LHC15 recommendation and are based on the `PDF4LHC15_nnlo_mc` set.

$m_h = 124.5$ GeV	σ'_{NNLL}(fb)	Scale Unc. (%)	PDF Unc. (%)	α_s Unc. (%)
$\sqrt{s} = 7$ TeV	7.132	$+4.0 - 5.7$	± 3.4	± 2.8
$\sqrt{s} = 8$ TeV	10.24	$+4.1 - 5.7$	± 3.0	± 2.6
$\sqrt{s} = 13$ TeV	33.78	$+4.3 - 6.0$	± 2.1	± 2.3
$\sqrt{s} = 14$ TeV	39.93	$+4.4 - 6.0$	± 2.1	± 2.2
$m_h = 125$ GeV	σ'_{NNLL}(fb)	Scale Unc. (%)	PDF Unc. (%)	α_s Unc. (%)
$\sqrt{s} = 7$ TeV	7.078	$+4.0 - 5.7$	± 3.4	± 2.8
$\sqrt{s} = 8$ TeV	10.16	$+4.1 - 5.7$	± 3.1	± 2.6
$\sqrt{s} = 13$ TeV	33.53	$+4.3 - 6.0$	± 2.1	± 2.3
$\sqrt{s} = 14$ TeV	39.64	$+4.4 - 6.0$	± 2.1	± 2.2
$m_h = 125.09$ GeV	σ'_{NNLL}(fb)	Scale Unc. (%)	PDF Unc. (%)	α_s Unc. (%)
$\sqrt{s} = 7$ TeV	7.068	$+4.0 - 5.7$	± 3.4	± 2.8
$\sqrt{s} = 8$ TeV	10.15	$+4.1 - 5.7$	± 3.1	± 2.6
$\sqrt{s} = 13$ TeV	33.49	$+4.3 - 6.0$	± 2.1	± 2.3
$\sqrt{s} = 14$ TeV	39.59	$+4.4 - 6.0$	± 2.1	± 2.2
$m_h = 125.5$ GeV	σ'_{NNLL}(fb)	Scale Unc. (%)	PDF Unc. (%)	α_s Unc. (%)
$\sqrt{s} = 7$ TeV	7.023	$+4.0 - 5.7$	± 3.4	± 2.8
$\sqrt{s} = 8$ TeV	10.09	$+4.1 - 5.7$	± 3.1	± 2.6
$\sqrt{s} = 13$ TeV	33.29	$+4.3 - 6.0$	± 2.1	± 2.3
$\sqrt{s} = 14$ TeV	39.35	$+4.4 - 5.9$	± 2.1	± 2.2

Chapter 2

Double Higgs production at NLO in the MSSM

In SUSY, single particle states are included in irreducible representations of the super algebra. These representations contain both fermionic and bosonic degrees of freedom. Supersymmetric transformations convert fermions into bosons and vice versa. The SUSY generators commute with gauge transformations, which make the bosons and the fermions in one supersymmetric multiplet identical in quantum numbers and mass. In addition to symmetry considerations, SUSY is motivated by the fact that many shortcomings of the SM can be solved.

For instance, one of the main motivations for low-energy SUSY is, that the quadratic dependence of the Higgs boson mass on the cut-off is cured. In a supersymmetric theory, bosonic loops exactly cancel all fermionic loop contributions in the Higgs boson mass. In contrast to the prediction of degenerate masses for the members of one supermultiplet, none of the superpartners have been observed yet. Hence, SUSY must be broken. If SUSY is broken softly, meaning that no SUSY breaking operators of dimension four or higher are added in the SUSY breaking part, the Higgs mass corrections are only logarithmically divergent, and not quadratically as in the SM. A moderate amount of fine-tuning will, however, be introduced due to the current bounds from direct searches for SUSY particles. In order to break SUSY, the Lagrangian has to be extended by terms parameterizing this breaking. The coefficients of the soft-SUSY breaking operators in the Lagrangian are in general treated as unknown parameters. This means, that many new parameters are introduced into the theory. The number of parameters can be reduced by assumptions on the SUSY breaking mechanism.

In supersymmetric extensions of the SM new renormalizable operators can arise leading

to proton decay, which has not been observed so far. Such operators can be forbidden if a discrete symmetry, called R-parity, is introduced. Superpartners get different charges under R-parity. If R-parity is indeed preserved, the lightest SUSY particle (LSP) is stable. In case the LSP is uncharged and colourless, it provides a natural candidate for Dark Matter. Additional benefits of SUSY are the successful unification of the gauge couplings and a dynamical mechanism for electroweak symmetry breaking. In most SUSY models, the sign of the Higgs boson mass squared parameter is driven to negative values by renormalization group running, whereas the signs of the other mass parameters stay positive.

In the minimal supersymmetric extension of the SM (MSSM) the Higgs sector consists of two SU(2) doublets, H_1 and H_2, whose relative contribution to electroweak (EW) symmetry breaking is determined by the ratio of vacuum expectation values (VEVs) of their neutral components, $\tan\beta \equiv v_2/v_1$. The spectrum of physical Higgs bosons is richer than in the SM, consisting of two neutral scalars, h and H, one neutral pseudoscalar, A, and two charged scalars, $H^{\pm}$. The couplings of the scalars to matter fermions and gauge bosons, as well as their self-couplings, differ in general from the SM ones. However, in the so-called decoupling limit of the MSSM Higgs sector, $m_A \gg m_Z$, the lightest scalar h has SM-like couplings and can be identified with the particle discovered at the LHC, with $m_h \approx 125$ GeV [41].

In the contest of the Higgs physics, the SUSY effects could be discovery for example in Higgs production as indirect signal. The dominant mechanism for Higgs pair production in the MSSM is gluon fusion, like in the SM, mediated by loops involving the top and bottom quarks and in this case also their superpartners, the stop and sbottom squarks. The triangle form factor[1] that contributes to the production of a scalar pair at the NLO can again be borrowed from the calculation of single-scalar production. In particular, the contributions of two-loop diagrams involving only quarks and gluons can be adapted from the corresponding SM results [42–45] via a rescaling of the Higgs-quark couplings. The contributions of two-loop diagrams involving only squarks and gluons are fully known [44–47]. In contrast, an exact calculation of the two-loop diagrams involving quarks, squarks and gluinos – which can involve up to five different masses – is still missing. Calculations based on a combination of numerical and analytic methods were presented in refs. [48, 49], but neither explicit formulae nor computer codes implementing the results of those calculations have been made available so far. Approximate results

[1] In the MSSM, loop topologies other than triangle and box contribute to scalar pair production, due to the existence of quartic interactions involving squarks. With a slight abuse of language, in the following we denote as "triangle" all diagrams that involve the s-channel exchange of a single scalar, and as "box" all of the remaining diagrams.

for the quark-squark-gluino contributions can however be obtained in the presence of some hierarchy between the relevant masses. The top-stop-gluino contributions were computed in the vanishing Higgs-mass limit (VHML) in refs. [50–52], and both the top-stop-gluino and bottom-sbottom-gluino contributions were computed in the limit of heavy superparticles – but without assuming a hierarchy between the Higgs mass and the quark mass – in refs. [53–55]. In particular, the calculation in ref. [52] relied on a low-energy theorem (LET) to provide explicit and compact analytic formulae for the top-stop-gluino contributions to the triangle form factor in the VHML. For what concerns the box form factor, in the MSSM the contributions of one-loop diagrams involving quarks differ from their SM counterparts by a rescaling of the Higgs-quark couplings, and their calculation must be extended to account for the possibility of two different scalars in the final state [29]. The contributions of one-loop diagrams involving squarks have been computed in refs. [56, 57] (see also ref. [58]). Going beyond the LO calculation, the contributions of two-loop diagrams involving top quarks and gluons in the heavy-top limit can be adapted from the corresponding SM results via a rescaling of the Higgs-top couplings [23]. On the other hand, the diagrams involving bottom quarks – whose effect is negligible in the SM, but can become relevant in the MSSM where at least one of the scalars has $\tan\beta$-enhanced couplings to down-type quarks – are known only at one loop, because the heavy-quark limit adopted in the existing NLO calculations cannot, of course, be applied to them. Finally, no calculation of the contributions to the box form factor from two-loop diagrams involving squarks has, to our knowledge, been presented so far.

This chapter is organised as follows: we present in 2.1 and in 2.2 the complete NLO-QCD determination of the production of a pair of Higgs scalars in the MSSM, evaluated with the LET, taking a step towards a complete NLO-QCD determination, based on our work [59]. Finally in the section 2.3 we show the numerical results of our calculation, pointing out that the two-loop squark contributions can have non-negligible effects in MSSM scenarios with stop masses below the TeV scale. We also show in appendix C how our results can be adapted to the case of Higgs pair production in the NMSSM.

2.1 Higgs pair production via gluon fusion at NLO in the MSSM

In this section we recapitulate some general results on the gluon-fusion production of a pair of neutral Higgs scalars, denoted as ϕ and χ (each of them can be either h or H). Some equations are similar respect to sections 1.3, but now are generalized for the MSSM, then for clarity we repeat some relations. The hadronic cross section for the process $h_1 + h_2 \to \phi + \chi + X$ at center-of-mass energy $\sqrt{s}$ can be written as

$$M^2_{\phi\chi} \frac{d\sigma}{dM^2_{\phi\chi}} = \sum_{a,b} \int_0^1 dx_1 dx_2 \; f_{a,h_1}(x_1,\mu_F)\, f_{b,h_2}(x_2,\mu_F) \int_0^1 dz \; \delta\left(z - \frac{M^2_{\phi\chi}}{\hat{s}}\right) M^2_{\phi\chi} \frac{d\hat{\sigma}_{ab}}{dM^2_{\phi\chi}} \;, \tag{2.1.1}$$

where: $M^2_{\phi\chi}$ is the invariant mass of the $\phi + \chi$ system; $f_{a,h_i}(x,\mu_F)$ is the density for the parton of type a (with $a = g, q, \overline{q}$) in the colliding hadron h_i; μ_F is the factorization scale; $\hat{s} = s\, x_1\, x_2$ is the partonic center-of-mass energy; $\hat{\sigma}_{ab}$ is the cross section for the partonic subprocess $ab \to \phi + \chi + X$. The partonic cross section can be written in terms of the LO contribution $\sigma^{(0)}_{\phi\chi}$ as

$$M^2_{\phi\chi} \frac{d\hat{\sigma}_{ab}}{dM^2_{\phi\chi}} \;=\; \sigma^{(0)}_{\phi\chi}\, z\, G_{ab}(z) \;. \tag{2.1.2}$$

The LO cross section is

$$\sigma^{(0)}_{\phi\chi} = \frac{1}{1+\delta_{\phi\chi}} \frac{G_F^2\, \alpha_s^2(\mu_R)}{256\,(2\pi)^3} \int_{\hat{t}_-}^{\hat{t}_+} d\hat{t} \left(\left| \mathcal{F}^{\phi\chi,\,1\ell} \right|^2 + \left| \mathcal{G}^{\phi\chi,\,1\ell} \right|^2 \right) \;, \tag{2.1.3}$$

where: G_F is the Fermi constant; $\alpha_s(\mu_R)$ is the strong gauge coupling expressed in the $\overline{\rm MS}$ renormalization scheme at the scale μ_R; the Mandelstam variables of the partonic process, $\hat{t}$ and (for later convenience) $\hat{u}$, are defined as

$$\hat{t} \;=\; -\frac{1}{2}\left(M^2_{\phi\chi} - m^2_\phi - m^2_\chi - \cos\theta \sqrt{\lambda(M^2_{\phi\chi}, m^2_\phi, m^2_\chi)} \right) \;, \tag{2.1.4}$$

$$\hat{u} \;=\; -\frac{1}{2}\left(M^2_{\phi\chi} - m^2_\phi - m^2_\chi + \cos\theta \sqrt{\lambda(M^2_{\phi\chi}, m^2_\phi, m^2_\chi)} \right) \;, \tag{2.1.5}$$

with θ the scattering angle in the partonic center-of-mass system, and

$$\lambda(x,y,z) = (x-y-z)^2 - 4yz \;. \tag{2.1.6}$$

The integration limits in eq. (2.1.3) are given by

$$\hat{t}_\pm = -\frac{1}{2}\left(M_{\phi\chi}^2 - m_\phi^2 - m_\chi^2 \mp \sqrt{\lambda(M_{\phi\chi}^2, m_\phi^2, m_\chi^2)}\right) \,, \tag{2.1.7}$$

corresponding to $\cos\theta = \pm 1$. Finally, in eq. (2.1.3), where obviously we obtain the same structure like in the SM in eq. 1.3.11, indeed $\mathcal{F}^{\phi\chi,\,1\ell}$ and $\mathcal{G}^{\phi\chi,\,1\ell}$ represent the one-loop parts of the spin-zero and spin-two form factors for the process $gg \to \phi\chi$, respectively. While the spin-two form factor $\mathcal{G}^{\phi\chi}$ receives only contributions from box diagrams, the spin-zero form factor $\mathcal{F}^{\phi\chi}$ can be decomposed in box and triangle contributions as:

$$\mathcal{F}^{\phi\chi} \;=\; F_\Box^{\phi\chi} \;+\; C_\Delta^{h\phi\chi}\, F_\Delta^h \;+\; C_\Delta^{H\phi\chi}\, F_\Delta^H \,. \tag{2.1.8}$$

In particular, $F_\Box^{\phi\chi}$ contains the spin-zero part of the box diagrams, while F_Δ^h (F_Δ^H) contains the contribution of the triangle diagrams for the production of an off-shell scalar h (H) which subsequently decays into the pair $\phi\chi$ through the factor $C_\Delta^{h\phi\chi}$ ($C_\Delta^{H\phi\chi}$), defined as

$$C_\Delta^{h\phi\chi} \;=\; \lambda_{h\phi\chi}\,\frac{m_Z^2}{M_{\phi\chi}^2 - m_h^2 + i\,m_h\,\Gamma_h} \,, \tag{2.1.9}$$

where $\lambda_{h\phi\chi}$ is the trilinear scalar coupling [2] and Γ_h is the width of the scalar h (in turn, $C_\Delta^{H\phi\chi}$ is obtained from eq. (2.1.9) with the replacement $h \to H$). The form factor F_Δ^ϕ is decomposed in one- and two-loop parts as

$$F_\Delta^\phi \;=\; F_\Delta^{\phi,\,1\ell} \;+\; \frac{\alpha_s}{\pi}\,F_\Delta^{\phi,\,2\ell} \;+\; \mathcal{O}(\alpha_s^2) \,, \tag{2.1.10}$$

and analogous decompositions hold for $F_\Box^{\phi\chi}$, $\mathcal{F}^{\phi\chi}$ and $\mathcal{G}^{\phi\chi}$.
The coefficient function $G_{ab}(z)$ in eq. (2.1.2) can in turn be decomposed, up to NLO terms, as

$$G_{ab}(z) \;=\; G_{ab}^{(0)}(z) \;+\; \frac{\alpha_s}{\pi}\,G_{ab}^{(1)}(z) \;+\; \mathcal{O}(\alpha_s^2) \,, \tag{2.1.11}$$

with the LO contribution given only by the gluon-fusion channel:

$$G_{ab}^{(0)}(z) \;=\; \delta(1-z)\,\delta_{ag}\,\delta_{bg} \,. \tag{2.1.12}$$

The NLO terms include, besides the gg channel, also the one-loop induced processes $gq \to q\phi\chi$ and $q\overline{q} \to g\phi\chi$. The gg-channel contribution, involving two-loop virtual

[2] We normalize all trilinear Higgs couplings to $\lambda_0 = m_Z^2/v$, with $v = (\sqrt{2}G_F)^{-1/2} \approx 246$ GeV.

corrections to $gg \to \phi\chi$ and one-loop real corrections from $gg \to \phi\chi g$, can be written as

$$G_{gg}^{(1)}(z) = \delta(1-z)\left[C_A\,\frac{\pi^2}{3} + \beta_0\,\ln\left(\frac{\mu_R^2}{\mu_F^2}\right) + \frac{\int_{t_-}^{t_+} d\hat{t}\,\left(\mathcal{C}_{\rm NLO}^{\phi\chi} + \text{h.c.}\right)}{\int_{\hat{t}_-}^{\hat{t}_+} d\hat{t}\,\left(|\mathcal{F}^{\phi\chi,\,1\ell}|^2 + |\mathcal{G}^{\phi\chi,\,1\ell}|^2\right)}\right] + P_{gg}(z)\,\ln\left(\frac{\hat{s}}{\mu_F^2}\right) + C_A\,\frac{4}{z}\,(1-z+z^2)^2\,\mathcal{D}_1(z) + C_A\,\mathcal{R}_{gg}\,, \tag{2.1.13}$$

where

$$\mathcal{C}_{\rm NLO}^{\phi\chi} = \left(\mathcal{F}^{\phi\chi,\,1\ell}\right)^*\left(\mathcal{F}^{\phi\chi,\,2\ell} + \mathcal{F}_{\Delta\Delta}^{\phi\chi}\right) + \left(\mathcal{G}^{\phi\chi,\,1\ell}\right)^*\left(\mathcal{G}^{\phi\chi,\,2\ell} + \mathcal{G}_{\Delta\Delta}^{\phi\chi}\right)\,. \tag{2.1.14}$$

The first line of eq. (2.1.13) displays the two-loop virtual contribution regularized by the infrared singular part of the real-emission cross section. The second line contains the non-singular contribution from the real gluon emission in the gluon-fusion process. The function $\mathcal{R}_{gg}$ is obtained from one-loop diagrams where only quarks or squarks circulate into the loop, and in the limit of vanishing external momenta it becomes $\mathcal{R}_{gg} \to -11(1-z)^3/(6z)$. The form factors $\mathcal{F}_{\Delta\Delta}^{\phi\chi}$ and $\mathcal{G}_{\Delta\Delta}^{\phi\chi}$ in eq. (2.1.14) represent the contributions of two-loop double-triangle diagrams with t/u-channel gluon exchange. In the limit of vanishing external momenta, the double-triangle form factors can be expressed in terms of the one-loop triangle form factors:

$$\mathcal{F}_{\Delta\Delta}^{\phi\chi} \underset{p_i=0}{\longrightarrow} \frac{1}{2}\,F_\Delta^{\phi,1\ell}\,F_\Delta^{\chi,1\ell}\,, \qquad \mathcal{G}_{\Delta\Delta}^{\phi\chi} \underset{p_i=0}{\longrightarrow} -\frac{p_T^2}{4\,\hat{t}\hat{u}}\,(M_{\phi\chi}^2 - m_\phi^2 - m_\chi^2)\,F_\Delta^{\phi,1\ell}\,F_\Delta^{\chi,1\ell}\,, \tag{2.1.15}$$

with

$$p_T^2 = \frac{\left(\hat{t}-m_\phi^2\right)\left(\hat{u}-m_\phi^2\right)}{M_{\phi\chi}^2} - m_\phi^2\,. \tag{2.1.16}$$

Finally, the contributions of the $gq \to q\phi\chi$ and $q\bar{q} \to g\phi\chi$ channels are given by:

$$G_{q\bar{q}}^{(1)}(z) = \mathcal{R}_{q\bar{q}}\,, \qquad G_{qg}^{(1)}(z) = P_{gq}(z)\left[\ln(1-z) + \frac{1}{2}\ln\left(\frac{\hat{s}}{\mu_F^2}\right)\right] + \mathcal{R}_{qg}\,, \tag{2.1.17}$$

where

$$P_{gq}(z) = C_F\,\frac{1+(1-z)^2}{z}\,. \tag{2.1.18}$$

The functions $\mathcal{R}_{q\bar{q}}$ and $\mathcal{R}_{qg}$ in (2.1.17) are obtained from one-loop quark and squark diagrams, and in the limit of vanishing external momenta become $\mathcal{R}_{q\bar{q}} \to 32\,(1-z)^3/(27z)$, $\mathcal{R}_{qg} \to 2\,z/3 - (1-z)^2/z$.

Finally, a brief comment in order to illustrate the differences between SM and MSSM cross section. As just mentioned in the introduction, the big difference between SM and MSSM, for the double Higgs production, is the presence in the loop of top and bottom superpartners. In the next sections we calculate the form factors with LET, then the form factors in eq. (2.1.3) will be very more complicated respect to the SM, eq. (1.3.11). This is true at LO and NLO but in the latter case we must consider also the contributions of the gluino. Indeed in eq. (2.1.13) have the same structure of eq. (1.3.12) but in the function $\mathcal{C}_{\rm NLO}^{\phi\chi}$ are now presents the stop,sbottom and gluino contributions. Whereas for the real channel the functions $\mathcal{R}_{gg}$, $\mathcal{R}_{q\bar{q}}$ and $\mathcal{R}_{qg}$ present the same dependence to z.

2.2 Box form factors in the limit of vanishing external momenta

As already mentioned, exact results for the one-loop form factors $\mathcal{F}^{\phi\chi,\,1\ell}$ and $\mathcal{G}^{\phi\chi,\,1\ell}$ which determine the cross section for Higgs pair production at the LO have been known for a long time, both for the SM [22] and for the MSSM [29, 56, 57]. At two loops, the triangle contributions to the form factors can be borrowed from the calculation of the cross section for single Higgs production. However, explicit formulae for the contributions of triangle diagrams involving quarks, squarks and gluinos are available only in approximate form, assuming the existence of some hierarchy among the relevant masses and momenta [50–55]. Two-loop results for the box contributions to the form factors are known only for the diagrams involving top quarks and gluons, and only in the heavy-top limit [23].

In this section we present a novel calculation of the contributions of diagrams involving top quarks and stop squarks to the box component $F_{\Box}^{\phi\chi}$ of the spin-zero form factor $\mathcal{F}^{\phi\chi}$, up to the two-loop order. We restrict our calculation to the limit of vanishing external momenta, which, for the top-gluon contribution alone, corresponds to the heavy-top limit. Note that the corresponding triangle component F_{Δ}^{ϕ} can be extracted from ref. [52], and that the spin-two form factor $\mathcal{G}^{\phi\chi}$ vanishes in the zero-momentum limit. We also present results for the contributions of the diagrams involving sbottom squarks, under the additional approximation of vanishing bottom mass. Finally, we show how the formulae for the two-loop part of the form factors are affected by a change in the renormalization scheme of the parameters entering the one-loop part.

It is convenient to decompose the triangle and box form factors for the production

of scalar mass eigenstates as

$$F_{\Delta}^{h} = -T_F \left[-\sin\alpha\,\mathcal{H}_1 + \cos\alpha\,\mathcal{H}_2\right] , \tag{2.2.1}$$

$$F_{\Delta}^{H} = -T_F \left[\cos\alpha\,\mathcal{H}_1 + \sin\alpha\,\mathcal{H}_2\right] , \tag{2.2.2}$$

$$F_{\Box}^{hh} = -T_F \left[\sin^2\alpha\,\mathcal{H}_{11} + \cos^2\alpha\,\mathcal{H}_{22} - 2\,\sin\alpha\,\cos\alpha\,\mathcal{H}_{12}\right] , \tag{2.2.3}$$

$$F_{\Box}^{HH} = -T_F \left[\cos^2\alpha\,\mathcal{H}_{11} + \sin^2\alpha\,\mathcal{H}_{22} + 2\,\sin\alpha\,\cos\alpha\,\mathcal{H}_{12}\right] , \tag{2.2.4}$$

$$F_{\Box}^{hH} = -T_F \left[(\cos^2\alpha - \sin^2\alpha)\,\mathcal{H}_{12} - \sin\alpha\,\cos\alpha\,(\mathcal{H}_{11} - \mathcal{H}_{22})\right] , \tag{2.2.5}$$

where $T_F = 1/2$ is a color factor (we make it explicit to follow the notation of ref. [52]), the angle α relates the scalar mass eigenstates, h and H, to the real parts of the neutral components of the two MSSM Higgs doublets, S_1 and S_2,

$$\begin{pmatrix} H \\ h \end{pmatrix} = \begin{pmatrix} \cos\alpha & \sin\alpha \\ -\sin\alpha & \cos\alpha \end{pmatrix} \begin{pmatrix} S_1 \\ S_2 \end{pmatrix} , \tag{2.2.6}$$

and $\mathcal{H}_i$ and $\mathcal{H}_{ij}$, with $i, j = (1, 2)$, are form factors in the interaction basis. As mentioned above, the form factors $\mathcal{H}_i$ were computed in refs. [52, 53, 55] for single Higgs production. Finally, we further decompose the form factors $\mathcal{H}_{ij}$ into top/stop and bottom/sbottom contributions, $\mathcal{H}_{ij} = \mathcal{H}_{ij}^{t} + \mathcal{H}_{ij}^{b}$.

2.2.1 Top/stop contributions via the low-energy theorem

In our derivation of the top/stop contributions to the box form factors we rely on the same LET for Higgs interactions [25–27] that was employed in ref. [52] for the calculation of the top/stop contribution to the triangle form factors. We have just discussed the LET in 1.2 simply in the case of single production in SM, where we make a single derivative respect to the Higgs field. In our case, the LET connects the form factor for the interactions of two gluons with two Higgs scalars at vanishing external momenta to the second derivatives of the gluon self-energy with respect to the Higgs scalars. In particular, we can write the top/stop contributions to the form factors in the interaction basis as

$$\mathcal{H}_{ij}^{t} = \frac{2\pi\,v^2}{\alpha_s\,T_F}\,\frac{\partial\Pi^{t}(0)}{\partial S_i\,\partial S_j} , \tag{2.2.7}$$

where $\Pi^{t}(q^2)$ denotes the top/stop contribution to the transverse part of the dimensionless (i.e., divided by q^2) self-energy of the gluon. In analogy with the effective-potential

calculation of the MSSM Higgs masses in ref. [60] and with the LET calculation of single Higgs production in ref. [52], the dependence of the gluon self-energy on the Higgs fields S_i can be identified through the field dependence of the top mass m_t, the stop masses $m^2_{\tilde{t}_1}$ and $m^2_{\tilde{t}_2}$ and the stop mixing angle θ_t, defined as

$$\begin{pmatrix} \tilde{t}_1 \\ \tilde{t}_2 \end{pmatrix} = \begin{pmatrix} \cos\theta_t & \sin\theta_t \\ -\sin\theta_t & \cos\theta_t \end{pmatrix} \begin{pmatrix} \tilde{t}_L \\ \tilde{t}_R \end{pmatrix} . \tag{2.2.8}$$

A lengthy but straightforward application of the chain rule for the derivatives allows us to express the form factors as

$$\begin{aligned} \mathcal{H}^t_{11} &= \frac{2\,m_t^2}{\sin^2\beta}\left[\frac{1}{2}\,\mu^2\,s^2_{2\theta_t}\,F_3 \;+\; \frac{\mu^2}{m^2_{\tilde{t}_1}-m^2_{\tilde{t}_2}}\,F\right] \\ &+ 4\,m_Z^2\left[m_t\,\mu\,\cot\beta\,s_{2\theta_t}\,\widetilde{F}_2 \;+\; m_Z^2\,\cos^2\beta\,\widetilde{F}_3 \;+\; \frac{1}{2}\,D\right], \end{aligned} \tag{2.2.9}$$

$$\begin{aligned} \mathcal{H}^t_{12} &= \frac{2\,m_t^2}{\sin^2\beta}\left[\mu\,m_t\,s_{2\theta_t}\,F_2 \;+\; \frac{1}{2}\,\mu\,A_t\,s^2_{2\theta_t}\,F_3 \;+\; \frac{\mu\,A_t}{m^2_{\tilde{t}_1}-m^2_{\tilde{t}_2}}\,F\right] \\ &+ 4\,m_Z^2\left[m_t^2\,\cot\beta\,\widetilde{F}_1 \;+\; \frac{1}{2}\,m_t\,(A_t\,\cot\beta-\mu)\,s_{2\theta_t}\,\widetilde{F}_2 \;-\; m_Z^2\,\sin\beta\,\cos\beta\,\widetilde{F}_3\right], \end{aligned} \tag{2.2.10}$$

$$\begin{aligned} \mathcal{H}^t_{22} &= \frac{2\,m_t^2}{\sin^2\beta}\left[2\,m_t^2\,F_1 \;+\; 2\,m_t\,A_t\,s_{2\theta_t}\,F_2 \;+\; \frac{1}{2}\,A_t^2\,s^2_{2\theta_t}\,F_3 \;+\; \frac{A_t^2}{m^2_{\tilde{t}_1}-m^2_{\tilde{t}_2}}\,F \;+\; G\right] \\ &+ 4\,m_Z^2\left[-\,2\,m_t^2\,\widetilde{F}_1 - m_t\,A_t\,s_{2\theta_t}\,\widetilde{F}_2 \;+\; m_Z^2\,\sin^2\beta\,\widetilde{F}_3 \;-\; \frac{1}{2}\,D\right], \end{aligned} \tag{2.2.11}$$

where A_t is the trilinear soft-SUSY breaking Higgs-stop coupling, μ is the Higgs/higgsino mass term in the superpotential (with the sign convention of refs. [52, 60]), and we define $s_{2\theta_t} \equiv \sin 2\theta_t$ and, for later convenience, $c_{2\theta_t} \equiv \cos 2\theta_t$. We note that the first line of each equation contains contributions from diagrams in which the Higgs scalars interact only via the top Yukawa coupling, whereas the second line contains sub-dominant contributions from diagrams in which one or both Higgs scalars interact with the squarks via a D-term induced EW coupling. The functions F_i, F, G, $\widetilde{F}_i$ and D are combinations of the first and second derivatives of the gluon self-energy with respect to the parameters m_t^2, $m^2_{\tilde{t}_1}$,

$m^2_{\tilde{t}_2}$ and $c^2_{2\theta_t}$. At one loop, the functions in the first lines of eqs. (2.2.9)–(2.2.11) read

$$\begin{aligned} F_1^{1\ell} &= \frac{1}{6}\left(\frac{1}{m^4_{\tilde{t}_1}}+\frac{1}{m^4_{\tilde{t}_2}}+\frac{4}{m^4_t}\right), \quad F_2^{1\ell}=\frac{1}{6}\left(\frac{1}{m^4_{\tilde{t}_1}}-\frac{1}{m^4_{\tilde{t}_2}}\right), \\ F_3^{1\ell} &= \frac{1}{6}\left(\frac{1}{m^4_{\tilde{t}_1}}+\frac{1}{m^4_{\tilde{t}_2}}-\frac{2}{m^2_{\tilde{t}_1}\,m^2_{\tilde{t}_2}}\right), \end{aligned} \tag{2.2.12}$$

$$F^{1\ell} = -\frac{1}{6}\left(\frac{1}{m^2_{\tilde{t}_1}}-\frac{1}{m^2_{\tilde{t}_2}}\right), \qquad G^{1\ell} = -\frac{1}{6}\left(\frac{1}{m^2_{\tilde{t}_1}}+\frac{1}{m^2_{\tilde{t}_2}}+\frac{4}{m^2_t}\right), \tag{2.2.13}$$

and those in the second lines read

$$\widetilde{F}_1^{1\ell} = \frac{d^t_L+d^t_R}{12}\left(\frac{1}{m^4_{\tilde{t}_1}}+\frac{1}{m^4_{\tilde{t}_2}}\right) + c_{2\theta_t}\,\frac{d^t_L-d^t_R}{12}\left(\frac{1}{m^4_{\tilde{t}_1}}-\frac{1}{m^4_{\tilde{t}_2}}\right), \tag{2.2.14}$$

$$\widetilde{F}_2^{1\ell} = \frac{d^t_L+d^t_R}{12}\left(\frac{1}{m^4_{\tilde{t}_1}}-\frac{1}{m^4_{\tilde{t}_2}}\right) + c_{2\theta_t}\,\frac{d^t_L-d^t_R}{12}\,\frac{(m^2_{\tilde{t}_1}-m^2_{\tilde{t}_2})^2}{m^4_{\tilde{t}_1}\,m^4_{\tilde{t}_2}}, \tag{2.2.15}$$

$$\begin{aligned} \widetilde{F}_3^{1\ell} &= \frac{(d^t_L)^2+(d^t_R)^2}{12}\left(\frac{1}{m^4_{\tilde{t}_1}}+\frac{1}{m^4_{\tilde{t}_2}}\right) - s^2_{2\theta_t}\,\frac{(d^t_L-d^t_R)^2}{24}\,\frac{(m^2_{\tilde{t}_1}-m^2_{\tilde{t}_2})^2}{m^4_{\tilde{t}_1}\,m^4_{\tilde{t}_2}} \\ &\quad + c_{2\theta_t}\,\frac{(d^t_L)^2-(d^t_R)^2}{12}\left(\frac{1}{m^4_{\tilde{t}_1}}-\frac{1}{m^4_{\tilde{t}_2}}\right), \end{aligned} \tag{2.2.16}$$

$$D^{1\ell} = -\frac{d^t_L+d^t_R}{12}\left(\frac{1}{m^2_{\tilde{t}_1}}+\frac{1}{m^2_{\tilde{t}_2}}\right) - c_{2\theta_t}\,\frac{d^t_L-d^t_R}{12}\left(\frac{1}{m^2_{\tilde{t}_1}}-\frac{1}{m^2_{\tilde{t}_2}}\right), \tag{2.2.17}$$

where

$$d^t_L = \frac{1}{2}-\frac{2}{3}\sin^2\theta_W\,, \qquad d^t_R = \frac{2}{3}\sin^2\theta_W\,, \tag{2.2.18}$$

θ_W being the Weinberg angle.
It's evident, for the box form factor, that the SM contribution is only presents in the form factor in 2.2.11, in particular in the functions F_1 in eq. (2.2.12) and G in eq. (2.2.13). The triangle SM contribution, indeed, is located in eq. (2.2.1) in the form factor $\mathcal{H}_2$.

In appendix A we provide the explicit definitions of the two-loop functions $F_i^{2\ell}$, $F^{2\ell}$, $G^{2\ell}$, $\widetilde{F}_i^{2\ell}$ and $D^{2\ell}$ in terms of the derivatives of the gluon self-energy. For the latter, we define the shortcut $Z \equiv (2/T_F)\,\Pi^{2\ell,\,t}(0)$, after decomposing the gluon self-energy in one-

and two-loop parts as

$$\Pi(q^2) \;=\; \frac{\alpha_s}{\pi}\,\Pi^{1\ell}(q^2) \;+\; \left(\frac{\alpha_s}{\pi}\right)^2 \Pi^{2\ell}(q^2) \;+\; \mathcal{O}(\alpha_s^3)\;. \tag{2.2.19}$$

Analytic formulae for the first derivatives of Z, computed under the assumption that the one-loop part of the gluon self-energy is expressed in terms of $\overline{\rm DR}$-renormalized top/stop parameters, were given in ref. [52]. Indeed, the functions F, G and D entering eqs. (2.2.9)–(2.2.11) coincide with those defined in that paper for the case of single Higgs production. Analytic formulae for the second derivatives of Z, which enter the functions F_i and $\widetilde{F}_i$, can be easily obtained from those for the first derivatives, using the recursive relations for the derivatives of the two-loop function $\Phi(m_1^2, m_2^2, m_3^2)$ given e.g. in appendix A of ref. [61]. However, those formulae are too lengthy to be given explicitly in print, thus we make our results available upon request as a Fortran routine.

2.2.2 Bottom/sbottom contributions for vanishing bottom mass

The LET employed in the previous section to compute the top/stop contributions to the box form factors relies on the assumption that the external momenta are negligible with respect to the masses of all particles running in the loops. Obviously, this assumption cannot hold for the contributions involving bottom quarks, nor for those involving quarks of the first two generations. In ref. [53] the bottom/sbottom contributions to single Higgs production were computed with an asymptotic expansion in the heavy supersymmetric masses (which we collectively denote by M), up to terms that induce $\mathcal{O}(m_b^2/m_\phi^2)$, $\mathcal{O}(m_b/M)$ and $\mathcal{O}(m_Z^2/M^2)$ contributions to the triangle form factors. In the calculation of the bottom/sbottom contributions to the box form factors we follow the same approach as in ref. [53], but we make the further approximation that the bottom mass and the left-right mixing in the sbottom mass matrix are set to zero (i.e., $m_b = \theta_b = 0$), effectively killing the Yukawa-induced interactions between Higgs bosons and bottom (s)quarks.[3] This leaves us with the contributions of diagrams in which the Higgs bosons interact with the squarks $\tilde{b}_L$ and $\tilde{b}_R$ only via D-term induced EW couplings, which are parametrically of the same order as the terms involving the functions $\widetilde{F}_3$ and

[3] Since the sbottom mixing contains a $\tan\beta$-enhanced term, this might not be a good approximation at large $\tan\beta$.

D in the top/stop contributions, eqs. (2.2.9)–(2.2.11). In particular, we find

$$\mathcal{H}^b_{11}\Big|_{D\text{-term}} = 4\,m_Z^4\,\cos^2\beta\,\widetilde{F}_{3\,b} + 2\,m_Z^2\,D_b\,, \tag{2.2.20}$$

$$\mathcal{H}^b_{12}\Big|_{D\text{-term}} = -\,4\,m_Z^4\,\sin\beta\,\cos\beta\,\widetilde{F}_{3\,b}\,, \tag{2.2.21}$$

$$\mathcal{H}^b_{22}\Big|_{D\text{-term}} = 4\,m_Z^4\,\sin^2\beta\,\widetilde{F}_{3\,b} - 2\,m_Z^2\,D_b\,. \tag{2.2.22}$$

The one-loop parts of the functions $\widetilde{F}_{3\,b}$ and D_b read, in this approximation,

$$\widetilde{F}^{1\ell}_{3\,b} = \frac{(d^b_{\scriptscriptstyle L})^2}{6\,m^4_{\tilde{b}_L}} + \frac{(d^b_{\scriptscriptstyle R})^2}{6\,m^4_{\tilde{b}_R}}\,, \qquad D^{1\ell}_b = -\frac{d^b_{\scriptscriptstyle L}}{6\,m^2_{\tilde{b}_L}} - \frac{d^b_{\scriptscriptstyle R}}{6\,m^2_{\tilde{b}_R}}\,, \tag{2.2.23}$$

where

$$d^b_{\scriptscriptstyle L} = -\frac{1}{2} + \frac{1}{3}\,\sin^2\theta_W\,, \qquad d^b_{\scriptscriptstyle R} = -\frac{1}{3}\,\sin^2\theta_W\,. \tag{2.2.24}$$

We obtained the two-loop parts of the functions $\widetilde{F}_{3\,b}$ and D_b by explicit computation of the relevant two-loop diagrams, setting $m_b = \theta_b = 0$ from the start and taking the first non-vanishing term of an asymptotic expansion in the heavy superparticle masses (for an outline of this approach, see section 3 of ref. [53]). Under the assumption that the one-loop parts of the form factors are expressed in terms of $\overline{\rm DR}$-renormalized sbottom masses at the scale Q, we get

$$\begin{aligned}\widetilde{F}^{2\ell}_{3\,b} &= (d^b_{\scriptscriptstyle L})^2\left[\frac{C_F}{12\,m^4_{\tilde{g}}}\left(\frac{-4+17\,x_{\scriptscriptstyle L}-29\,x_{\scriptscriptstyle L}^2+19\,x_{\scriptscriptstyle L}^3-3\,x_{\scriptscriptstyle L}^4}{(1-x_{\scriptscriptstyle L})^3\,x_{\scriptscriptstyle L}^3}+\frac{4}{x_{\scriptscriptstyle L}^3}\ln\frac{m^2_{\tilde{g}}}{Q^2}x_{\scriptscriptstyle L}\right)\right.\\ &\quad\left. -\,\frac{4}{(1-x_{\scriptscriptstyle L})^3}\ln x_{\scriptscriptstyle L}+\frac{C_A}{12\,m^4_{\tilde{g}}}\left(\frac{1-3\,x_{\scriptscriptstyle L}}{(1-x_{\scriptscriptstyle L})^2\,x_{\scriptscriptstyle L}^2}-\frac{2}{(1-x_{\scriptscriptstyle L})^3}\ln x_{\scriptscriptstyle L}\right)\right] + (L\to R)\,,\end{aligned} \tag{2.2.25}$$

$$\begin{aligned}D^{2\ell}_b &= d^b_{\scriptscriptstyle L}\left[-\frac{C_F}{12\,m^2_{\tilde{g}}}\left(\frac{-2+9\,x_{\scriptscriptstyle L}-10\,x_{\scriptscriptstyle L}^2+3\,x_{\scriptscriptstyle L}^3}{(1-x_{\scriptscriptstyle L})^2\,x_{\scriptscriptstyle L}^2}+\frac{2}{x_{\scriptscriptstyle L}^2}\ln\frac{m^2_{\tilde{g}}}{Q^2}+\frac{2}{(1-x_{\scriptscriptstyle L})^2}\ln x_{\scriptscriptstyle L}\right)\right.\\ &\quad\left. -\,\frac{C_A}{12\,m^2_{\tilde{g}}}\left(\frac{1}{(1-x_{\scriptscriptstyle L})\,x_{\scriptscriptstyle L}}+\frac{1}{(1-x_{\scriptscriptstyle L})^2}\ln x_{\scriptscriptstyle L}\right)\right] + (L\to R)\,,\end{aligned} \tag{2.2.26}$$

with $x_{L,R} = m^2_{\tilde{b}_{L,R}}/m^2_{\tilde{g}}$ and the notation $(L\to R)$ means a term that is obtained from the previous one with the exchanges $x_{\scriptscriptstyle L}\to x_{\scriptscriptstyle R}$ and $d^b_{\scriptscriptstyle L}\to d^b_{\scriptscriptstyle R}$. We find that, when $m_b = \theta_b = 0$, there are no infrared-divergent parts in the two-loop bottom/sbottom diagrams, therefore our results could also be obtained as the first non-vanishing term of

a Taylor expansion of those diagrams in the external momenta. On the other hand, we stress that our results cannot be obtained by setting $m_t = \theta_t = 0$ in the LET results for the top/stop contributions, because the latter rely on the assumption that the external momenta are much smaller than the quark mass. Finally, the contributions of the first two generations of quarks and squarks can be obtained, by means of trivial substitutions, from eqs. (2.2.9)–(2.2.11) and from the results presented in this section.

2.2.3 Change of renormalization scheme

The results presented in sections 2.2.1 and 2.2.2 were obtained under the assumption that the parameters entering the one-loop part of the form factors are expressed in the $\overline{\rm DR}$ renormalization scheme. If a different scheme is used, the two-loop part of the form factor receives a shift

$$\mathcal{H}_{ij}^{2\ell} \;\longrightarrow\; \mathcal{H}_{ij}^{2\ell} \;+\; \frac{\pi}{\alpha_s}\,\delta\mathcal{H}_{ij}\;, \tag{2.2.27}$$

where $\delta\mathcal{H}_{ij}$ is a function of the shifts of all the parameters in the one-loop part of the form factor that are subject to $\mathcal{O}(\alpha_s)$ corrections.[4]

In the top/stop sector, the parameters that need shifting are the top mass, the stop masses, the stop mixing angle and the trilinear coupling A_t. In particular, the shifts of those parameters to the on-shell (OS) scheme adopted in our numerical discussion can be found in appendix B of ref. [60]. The shifts $\delta\mathcal{H}_{ij}^t$ can then be written as

$$\begin{aligned}\delta\mathcal{H}_{11}^t \;&=\; \frac{2\,m_t^2}{\sin^2\beta}\left[\frac{1}{2}\,\mu^2\,s_{2\theta_t}^2\,\delta F_3 \;+\; \frac{\mu^2}{m_{\tilde t_1}^2 - m_{\tilde t_2}^2}\,\delta F\right] \\ &+\; 4\,m_Z^2\left[m_t\,\mu\,\cot\beta\,s_{2\theta_t}\,\delta\widetilde{F}_2 \;+\; m_Z^2\,\cos^2\beta\,\delta\widetilde{F}_3 \;+\; \frac{1}{2}\,\delta D\right]\;,\end{aligned} \tag{2.2.28}$$

[4] For a generic parameter x, we define the shift from the $\overline{\rm DR}$ scheme to a generic scheme R as $x^{\overline{\rm DR}} = x^R + \delta x$.

$$
\begin{aligned}
\delta\mathcal{H}^t_{12} &= \frac{2\,m_t^2}{\sin^2\beta}\left[\mu\,m_t\,s_{2\theta_t}\,\delta F_2 \;+\; \frac{1}{2}\,\mu\,A_t\,s^2_{2\theta_t}\,\delta F_3 \;+\; \frac{\mu\,A_t}{m^2_{\tilde t_1}-m^2_{\tilde t_2}}\,\delta F\right.\\
&\qquad\left. +\,\frac{1}{2}\,\mu\,\delta A_t\,s^2_{2\theta_t}\,F_3^{1\ell} \;+\; \frac{\mu\,\delta A_t}{m^2_{\tilde t_1}-m^2_{\tilde t_2}}\,F^{1\ell}\right]\\
&+\; 4\,m_Z^2\left[m_t^2\,\cot\beta\,\delta\widetilde F_1 \;+\; \frac{1}{2}\,m_t\,(A_t\,\cot\beta-\mu)\,s_{2\theta_t}\,\delta\widetilde F_2 \;-\; m_Z^2\,\sin\beta\,\cos\beta\,\delta\widetilde F_3\right.\\
&\qquad\left. +\frac{1}{2}\,m_t\,\delta A_t\,\cot\beta\,s_{2\theta_t}\,\widetilde F_2^{1\ell}\right]\,, \qquad (2.2.29)
\end{aligned}
$$

$$
\begin{aligned}
\delta\mathcal{H}^t_{22} &= \frac{2\,m_t^2}{\sin^2\beta}\left[2\,m_t^2\,\delta F_1 \;+\; 2\,m_t\,A_t\,s_{2\theta_t}\,\delta F_2 \;+\; \frac{1}{2}\,A_t^2\,s^2_{2\theta_t}\,\delta F_3 \;+\; \frac{A_t^2}{m^2_{\tilde t_1}-m^2_{\tilde t_2}}\,\delta F \;+\right.\\
&\qquad\left. \delta G+\; 2\,m_t\,\delta A_t\,s_{2\theta_t}\,F_2^{1\ell} \;+\; A_t\,\delta A_t\,s^2_{2\theta_t}\,F_3^{1\ell} \;+\; \frac{2\,A_t\,\delta A_t}{m^2_{\tilde t_1}-m^2_{\tilde t_2}}\,F^{1\ell}\right]\\
&+\; 4\,m_Z^2\left[-\,2\,m_t^2\,\delta\widetilde F_1 \;-\; m_t\,A_t\,s_{2\theta_t}\,\delta\widetilde F_2 \;+\; m_Z^2\,\sin^2\beta\,\delta\widetilde F_3 \;-\; \frac{1}{2}\,\delta D\right.\\
&\qquad\left. -m_t\,\delta A_t\,s_{2\theta_t}\,\widetilde F_2^{1\ell}\right]\,, \qquad (2.2.30)
\end{aligned}
$$

where the one-loop parts of the functions F_2, F_3, F and $\widetilde F_2$ are given in eqs. (2.2.12), (2.2.13) and (2.2.15), and explicit expressions for the shifts δF_i, δF, δG, $\delta\widetilde F_i$ and δD are given in appendix B.

For what concerns the bottom/sbottom contributions, under the approximation $m_b=\theta_b=0$ employed in section 2.2.2 the shifts to the form factors reduce to

$$
\delta\mathcal{H}^b_{11}\Big|_{D\text{-term}} \;=\; 4\,m_Z^4\,\cos^2\beta\,\delta\widetilde F_{3\,b} \;+\; 2\,m_Z^2\,\delta D_b\,, \qquad (2.2.31)
$$

$$
\delta\mathcal{H}^b_{12}\Big|_{D\text{-term}} \;=\; -\,4\,m_Z^4\,\sin\beta\,\cos\beta\,\delta\widetilde F_{3\,b}\,, \qquad (2.2.32)
$$

$$
\delta\mathcal{H}^b_{22}\Big|_{D\text{-term}} \;=\; 4\,m_Z^4\,\sin^2\beta\,\delta\widetilde F_{3\,b} \;-\; 2\,m_Z^2\,\delta D_b\,, \qquad (2.2.33)
$$

where

$$
\delta\widetilde F_{3\,b} \;=\; -\frac{(d^b_L)^2}{3\,m^6_{\tilde b_L}}\,\delta m^2_{\tilde b_L} \;-\; \frac{(d^b_R)^2}{3\,m^6_{\tilde b_R}}\,\delta m^2_{\tilde b_R}\,, \qquad \delta D_b \;=\; \frac{d^b_L}{6\,m^4_{\tilde b_L}}\,\delta m^2_{\tilde b_L} \;+\; \frac{d^b_R}{6\,m^4_{\tilde b_R}}\,\delta m^2_{\tilde b_R}\,. \qquad (2.2.34)
$$

If the sbottom masses in the one-loop part of the form factors are expressed in the OS

scheme, the shift $\delta m^2_{\tilde{b}_L}$ reads, for $m_b = \theta_b = 0$,

$$\frac{\delta m^2_{\tilde{b}_L}}{m^2_{\tilde{b}_L}} = \frac{\alpha_s\, C_F}{2\pi}\left[\ln x_{_L} - 1 + \frac{1}{x_{_L}}\left(2\,\ln\frac{m^2_{\tilde{g}}}{Q^2} - 3\right) - \left(1 - \frac{1}{x_{_L}}\right)^2 \ln|1 - x_{_L}|\right], \tag{2.2.35}$$

and the shift $\delta m^2_{\tilde{b}_R}/m^2_{\tilde{b}_R}$ can be obtained from eq. (2.2.35) with the replacement $x_{_L} \to x_{_R}$.

2.3 The effect of SUSY contributions to Higgs pair production

In this section we present numerical results for the newly-computed SUSY contributions to the box form factors, and for their effect on the Higgs-production cross section. We focus on the process that is most interesting from the point of view of LHC phenomenology, i.e. the production of a pair of light MSSM scalars hh with mass $m_h \approx 125$ GeV.

2.3.1 Implementation in `HPAIR`

For the numerical evaluation of the cross section, we added the contributions of loops involving superparticles to the code `HPAIR` [62], whose public version includes by default the one-loop top- and bottom-quark contributions with full mass dependence [29] and the QCD corrections to the top-quark contributions in the heavy-top limit [23].

For the LO cross section, we added the one-loop squark contributions to the spin-zero and spin-two form factors, borrowing from ref. [56] the results with full mass dependence. At NLO, we included our results for the two-loop stop and (partial) sbottom contributions in the approximation of vanishing external momenta, derived in section 2.2. In order to improve on that approximation, the LO cross section factored out of the coefficient function $G_{ab}(z)$ in eq. (2.1.2) is computed with full dependence on the top and bottom quark and squark masses. In analogy with the implementation of the top quark loops in `HPAIR`, the gg-channel contribution to the NLO coefficient function in eqs. (1.3.12) and

(1.3.13) – specialized to the production of a hh pair – becomes

$$
\begin{aligned}
G_{gg}^{(1)}(z) \;=\; & \delta(1-z)\left\{ C_A\,\frac{\pi^2}{3} \;+\; \beta_0\,\ln\left(\frac{\mu_R^2}{\mu_F^2}\right) \;+\; 2\,\mathrm{Re}\left(\frac{\mathcal{F}^{hh,\,2\ell}_{\mathrm{LET}}}{\mathcal{F}^{hh,\,1\ell}_{\mathrm{LET}}}\right)\right. \\
& \left. +\; \frac{\int_{t_-}^{t_+} d\hat{t}\;\mathrm{Re}\left[\left(\left(\mathcal{F}^{hh,\,1\ell}\right)^* \;-\; \frac{p_T^2}{2\hat{t}\hat{u}}(M_{hh}^2-2\,m_h^2)\,\left(\mathcal{G}^{hh,\,1\ell}\right)^*\right)\left(F^{h,\,1\ell}_{\Delta\,\mathrm{LET}}\right)^2\right]}{\int_{\hat{t}_-}^{\hat{t}_+} d\hat{t}\,\left(|\mathcal{F}^{hh,\,1\ell}|^2+|\mathcal{G}^{hh,\,1\ell}|^2\right)}\right\} \\
& +\; P_{gg}(z)\,\ln\left(\frac{\hat{s}}{\mu_F^2}\right) + C_A\,\frac{4}{z}\,(1-z+z^2)^2\,\mathcal{D}_1(z) + C_A\,\mathcal{R}_{gg}\,, \qquad (2.3.1)
\end{aligned}
$$

where the subscript "LET" denotes form factors computed in the limit of vanishing external momenta after setting $m_b = \theta_b = 0$. The two-loop SUSY contributions enter the last term in the first line of eq. (2.3.1), which, if only the top-quark contributions were considered as in ref. [23], would reduce to a simple coefficient $c_1 = 11/2$. The second line of eq. (2.3.1) contains the contributions of diagrams with t/u-channel gluon exchange. Following ref. [23], in those contributions we retain the full momentum dependence in the one-loop form factors that stem from the LO matrix element, but take the limit of vanishing external momenta, see eq. (2.1.15), in the double-triangle form factors. We also remark that in the NLO coefficient of eq. (2.3.1) all form factors – including those with full momentum dependence – are obtained for $m_b = \theta_b = 0$.

For a precise prediction of the cross section for the production of a pair of MSSM Higgs bosons, it is essential to include the corrections to the trilinear Higgs couplings, which can be as significant as the corresponding corrections to the MSSM Higgs masses and mixing. Indeed, to properly reproduce the decoupling limit in which the lightest scalar h has a SM-like self-coupling, $\lambda_{hhh}^{SM} = 3\,m_h^2/m_Z^2$, the corrections to the coupling should be computed at the same level of accuracy as the corrections to the mass m_h. The trilinear couplings are known at one loop [63–67], but at two loops only the $\mathcal{O}(\alpha_s\alpha_t)$ corrections have been computed, in the effective-potential approximation, for both the MSSM [68] and the NMSSM [69]. In contrast, in this analysis we compute the MSSM Higgs masses and mixing using the code `FeynHiggs` [70–74], which includes two-loop corrections beyond the $\mathcal{O}(\alpha_s\alpha_t)$ effective-potential ones. Since we are anyway focusing on the effects of the SUSY contributions to the gluon-fusion loop, we bypass the calculation of the corrections to the trilinear couplings by relying on a simplifying approach, known as "hMSSM", which was recently proposed in refs. [75–78]. In this approximation one assumes that the corrections to the elements other than $(2,2)$ of the Higgs mass matrix are negligible, i.e. $\Delta\mathcal{M}^2_{1j} \approx 0$ with $j = 1, 2$. In that case the remaining correction $\Delta\mathcal{M}^2_{22}$,

which includes potentially large logarithmic effects from top/stop loops, can be expressed in terms of the parameters that determine the tree-level mass matrix (i.e. $\tan\beta$, m_Z and the pseudoscalar mass m_A) plus the lightest eigenvalue m_h, treated as an input parameter:

$$\Delta\mathcal{M}^2_{22} = \frac{m_h^2\,(m_A^2+m_Z^2-m_h^2) - m_A^2 m_Z^2\cos^2 2\beta}{m_Z^2\cos^2\beta + m_A^2\sin^2\beta - m_h^2}\,. \tag{2.3.2}$$

In this approximation the trilinear couplings relevant to the production of an hh pair become

$$\lambda_{hhh} = 3\cos 2\alpha\,\sin(\alpha+\beta) + 3\,\frac{\Delta\mathcal{M}^2_{22}}{m_Z^2}\,\frac{\cos^3\alpha}{\sin\beta}\,, \tag{2.3.3}$$

$$\lambda_{Hhh} = 2\sin 2\alpha\,\sin(\alpha+\beta) - \cos 2\alpha\cos(\alpha+\beta) + 3\,\frac{\Delta\mathcal{M}^2_{22}}{m_Z^2}\,\frac{\cos^2\alpha\sin\alpha}{\sin\beta} \tag{2.3.4}$$

Combining eqs. (2.3.2) and (2.3.3) one can see that in the decoupling limit $m_A \gg m_Z$, when $\alpha \to \beta - \pi/2$, the coupling λ_{hhh} does indeed tend to its SM limit. As discussed e.g. in refs. [79, 80], the approximation of neglecting the corrections $\Delta\mathcal{M}^2_{1j}$ might not prove accurate for small m_A and rather large μ and $\tan\beta$. We will therefore avoid those choices of parameters in our numerical example.

2.3.2 A numerical example

The SM parameters entering our computation of the cross section for Higgs pair production are the Z boson mass $m_Z = 91.1876$ GeV, the W boson mass $m_W = 80.398$ GeV, the Fermi constant $G_F = 1.16637\cdot 10^{-5}$ GeV^{-2}, the pole top-quark mass $m_t = 173.2$ GeV and the strong coupling $\alpha_s(m_Z) = 0.119$. For the parton distribution functions we use the MSTW08 set [81–83] with its default LO and NLO values of α_s. The hadronic center-of-mass energy is set to $\sqrt{s} = 14$ TeV. The factorization and renormalization scales are set to the invariant mass M_{hh} of the Higgs boson pair.

We use the code `FeynHiggs` [70–74] to compute the masses and mixing angle of the Higgs scalars. We consider an MSSM scenario characterized by the following parameters in the OS renormalization scheme:

$$\begin{aligned}\tan\beta = 10,\quad m_A = 500\text{ GeV},\quad \mu = -400\text{ GeV},\quad M_3 = 1500\text{ GeV},\\ X_t = 2\,M_S\ ,\quad m_{\tilde{t}_L} = m_{\tilde{t}_R} = m_{\tilde{b}_R} = M_S,\end{aligned} \tag{2.3.5}$$

where M_3 denotes the soft SUSY-breaking gluino mass, we define $X_t \equiv A_t + \mu\cot\beta$,

and $m_{\tilde{t}_L}$, $m_{\tilde{t}_R}$, and $m_{\tilde{b}_R}$ denote the soft SUSY-breaking masses of the third-generation squarks. We remark that in the OS scheme, where all of the squark masses are considered as pole masses, the soft SUSY-breaking parameter $m_{\tilde{b}_L}$ differs from its stop counterpart $m_{\tilde{t}_L}$ by a finite shift [84, 85].

The parameters in eq. (2.3.5) – as well as the remaining soft SUSY-breaking parameters, which are not relevant to our discussion – were chosen in such a way that, for $M_S = 500$ GeV, they reproduce the *light-stop* benchmark scenario proposed in ref. [86] and studied in the context of single-Higgs production in ref. [87]. Our choices of m_A and $\tan\beta$ ensure that the lightest Higgs scalar h has essentially SM-like couplings to the top and bottom quarks, and that the contribution of triangle diagrams with s-channel exchange of the heaviest scalar H is significantly suppressed, allowing us to focus on the effects of the SUSY contributions to the box form factor. We then vary the squark mass parameter M_S between 500 GeV and 1500 GeV, which results in a lightest stop mass $m_{\tilde{t}_1}$ ranging between 324 GeV and 1326 GeV, and in a prediction by `FeynHiggs` for m_h ranging between 122.3 GeV and 130.7 GeV.

In figure 2.1 we plot the box form factor $F_{\square}^{hh}$ – computed in the vanishing-momentum limit as described in section 2.2 – as a function of the squark-mass scale M_S. The solid lines correspond to the one-loop (dark blue) and two-loop (light blue) part of the form factor, including both the top-quark contribution and the squark contributions. The dashed lines correspond to the one- and two-loop form factors including only the top contributions. The plot shows that the squark contributions can be relevant for small squark masses, and they are significantly larger in the two-loop form factor than in the one-loop form factor. Moreover, the decoupling behaviour of the squark contributions for large M_S appears to be slower at two loops than at one loop. This can be explained by the occurrence of two-loop terms proportional to $m_t^2/M^2 \ln(M^2/m_t^2)$ (with M denoting generically a SUSY mass parameter), whereas at one loop all terms decouple at least as fast as m_t^2/M^2.

In figure 2.2 we plot the cross section for the production of a hh pair as a function of M_S, computed as described in section 2.3.1. The dark-blue lines correspond to the LO cross section, the light-blue lines to the NLO cross section, and again the solid (dashed) lines correspond to form factors including (not including) the SUSY contributions.[5] In addition, the dotted light-blue line corresponds to the NLO cross section computed by omitting the SUSY contributions in the two-loop part of the box form factor. The plot shows that, for the considered choices of MSSM parameters, the squark loops can significantly contribute to the cross section for relatively small M_S, although their effect

[5] The mild M_S dependence of the dashed lines reflects the dependence of m_h on the stop masses.

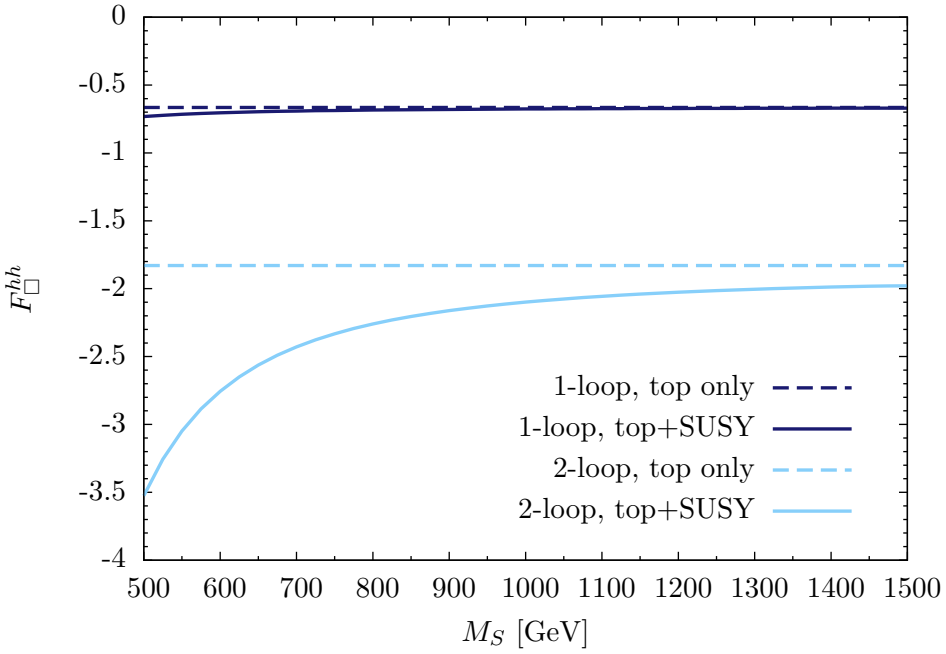

Figure 2.1: Box form factor $F_{\Box}^{hh}$ in the vanishing-momentum limit, as a function of the squark-mass scale M_S. Dark-blue lines show the one-loop form factor, light-blue lines show the two-loop form factor. The dashed lines correspond to the top-quark contributions alone, whereas the solid lines include also the SUSY contributions.

gets quickly suppressed when $M_S \gtrsim 1$ TeV. In particular, in the *light-stop* scenario – corresponding to the left edge of the plot – for our choices of m_A and $\tan\beta$ the SUSY contributions increase the NLO cross section for h pair production by more than 30% (in contrast, ref. [87] showed that they reduce the cross section for the production of a single SM-like scalar by about 20%). Finally, the comparison between the solid and dotted light-blue lines shows that the newly-computed two-loop SUSY contributions to the box form factor account for a non-negligible part of the increase in the pair-production cross section.

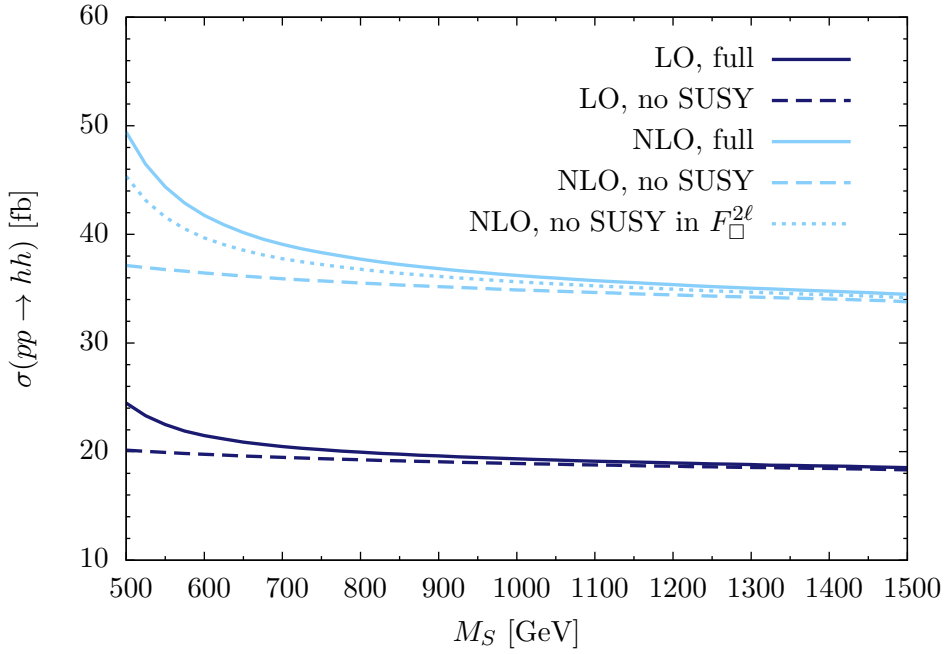

Figure 2.2: Higgs pair-production cross section $\sigma(pp \to hh)$ as a function of the squark-mass scale M_S. Dark-blue lines show the LO cross section, light-blue lines show the NLO cross section. The dashed lines correspond to the quark contributions alone, whereas the solid lines include also the SUSY contributions. The dotted light-blue line omits the SUSY contributions to the two-loop box form factor.

2.4 Discussion

Relying on a low-energy theorem that connects the Higgs-gluon interactions to the derivatives of the gluon self-energy, we obtained analytic results for the contributions to Higgs pair production from one- and two-loop box diagrams involving top quarks and stop squarks in the limit of vanishing external momenta. We also obtained, by direct calculation of the relevant two-loop diagrams, the subset of bottom/sbottom contributions that involve the D-term-induced EW Higgs-squark coupling and survive in the limit of vanishing bottom mass. Combined with the existing results for the triangle diagrams in the same approximations [52, 53], our calculation allows for a consistent NLO determination of the SUSY contributions to Higgs pair production in the MSSM. We incorporated our results in a private version of the code `HPAIR`, and found that the two-loop SUSY contributions to the production of a light-scalar pair can have a non-negligible effect in scenarios with stop masses below the TeV scale.

To conclude, a discussion is in order of the approximation of vanishing external momenta that we employed in our calculation. Our results can be viewed as the first

term of an asymptotic expansion of the form factor $\mathcal{F}^{\phi\chi,\,2\ell}$ in the heavy masses of all particles running in the loops. Such expansion is in principle valid only for partonic center-of-mass energies up to the lowest threshold encountered in the relevant diagrams, which for the contributions considered in this paper corresponds to $\sqrt{\hat{s}} = 2\,m_t$.

In the SM, the vanishing-momentum approximation is known to work rather well for the top-quark contributions to the production of a single scalar h with $m_h \approx 125$ GeV, because the region in the partonic phase space with $\sqrt{\hat{s}} > 2\,m_t$ gives only a small contribution to the hadronic cross section. In contrast, the same approximation is less reliable for pair production, where it is always $\sqrt{\hat{s}} > 2\,m_h$ and the whole region up to $\sqrt{\hat{s}} \sim 600$ GeV gives a significant contribution to the cross section [88]. The factorization of the LO cross section with full momentum dependence is expected to reduce the uncertainty of the NLO result due to the dominance of soft and collinear gluon effects [23]. Nevertheless, a NLO determination of the top-quark contributions to Higgs pair production going beyond the vanishing-momentum – or, equivalently, infinite-top-mass – approximation would be desirable. Of the necessary ingredients, the contribution to $\mathcal{F}_{\Delta}^{h,\,2\ell}$ of two-loop triangle diagrams involving top quarks and gluons is known with full top-mass dependence from single-Higgs production; the contribution of one-loop top diagrams to $\mathcal{R}_{gg}$, $\mathcal{R}_{q\bar{q}}$ and $\mathcal{R}_{qg}$ is known exactly from ref. [89]; the contribution of two-loop, one-particle-reducible top diagrams to $\mathcal{F}_{\Delta\Delta}^{\phi\chi}$ and $\mathcal{G}_{\Delta\Delta}^{\phi\chi}$ is relatively easy to compute. However, an exact evaluation of the two-loop box diagrams involving top quarks and gluons is currently not available, and represents the bottleneck in the quest for an exact NLO determination of the pair-production cross section. Attempts to go beyond the limit of infinite top mass for the two-loop box diagrams were made in refs. [88, 90], where several terms in a heavy-top asymptotic expansion of the cross section, i.e. terms proportional to powers of $\hat{s}/m_t^2$ or m_h^2/m_t^2, were obtained. However, as shown explicitly for the LO result in refs. [34, 35], the inclusion of additional terms in the large-mass expansion does not necessarily improve the evaluation of the cross section. Indeed, by including additional terms one is improving the evaluation of the region with $\sqrt{\hat{s}} < 2\,m_t$ at the price of worsening the evaluation of the complementary region with $\sqrt{\hat{s}} > 2\,m_t$, which is approximated by a function that has the wrong behavior as $\hat{s}$ increases. In fact, the appropriate expansion in the region with $\sqrt{\hat{s}} > 2\,m_t$ would be a large-momentum expansion as opposed to a large-mass expansion.

In the MSSM, the NLO cross section for the production of a pair of SM-like scalars hh suffers from the same uncertainty as in the SM, stemming from the incomplete knowledge of the two-loop diagrams with top quarks and gluons. For what concerns the SUSY contributions, those from two-loop diagrams involving squarks and gluons or quartic

squark couplings should be sufficiently well approximated, in realistic MSSM scenarios, by the results obtained in the vanishing-momentum limit. In contrast, some two-loop diagrams involving top, stop and gluino do have thresholds at $\sqrt{\hat{s}} = 2\,m_t$, thus their contributions are in principle subject to uncertainties comparable to those of the SM contributions. The knowledge of those contributions could however be improved following the same strategy employed in ref. [55] for single scalar production, namely evaluating the top-stop-gluino box diagrams via a large-mass expansion in the SUSY masses while treating the top quark as a light particle.

Finally, another feature specific to the MSSM calculation of hh production is the possibility of large resonant contributions from triangle diagrams with s-channel exchange of the heaviest scalar H. In such a scenario, the determination of the NLO cross section could be improved by using for $F_\Delta^{H,\,2\ell}$ the quark-gluon contributions with full momentum dependence combined with the heavy-SUSY results of refs. [53, 55], while retaining the vanishing-momentum approximation in $F_\Delta^{h,\,2\ell}$ to avoid spoiling potential cancellations with the box form factor.

Chapter 3

Real corrections in the double Higgs production

As we have said in the first chapter the NLO corrections in the double Higgs production (as in the single Higgs production) are very important, the K factor being about 2. In particular the real corrections, basically at the parton level the processes $gg \to hhg$, $q\bar{q} \to hhg$ and $gq \to qhh$, are important.
As we have been discussed in 1.5 the dominant uncertainty is given by the unknown top-quark mass effects at NLO in the corrections. The top-quark mass effects have been included in various approximations in the literature:

1. The "Born-improved HEFT (Higgs Effective Field Theory)" approximation, which is the one employed in the program Hpair [62]. It uses the heavy top-quark limit throughout the NLO calculation, in combination with a re-weighting factor B/B_{HEFT}, where B denotes the leading order result in the full theory.

2. The "FT approx" result of [88], [24], [89] contains the full top-quark mass dependence in the real radiation, while the virtual part is rescaled by the re-weighting factor mentioned above. It was found that this approximation leads to a total cross section which is about 10% smaller than the one obtained using Born-improved HEFT.

3. The "FT' approx" is [89] as in (2) for the real radiation part, while it uses partial NLO results for the virtual part, specifically, the exact results for the two-loop triangle diagrams as far as they are known from single Higgs boson production.

The last two results were obtained via a full numerical approach and no analytic results with respect to the real radiation were presented. All these results suggest that the

uncertainty on the cross section due to top-quark mass effects is $\pm 10\%$ at NLO. In [31] was observed that the total cross section including the full top-quark mass dependence is about 14% smaller than the one obtained within the Born-improved HEFT approximation. These results have been however obtained totally numerical.
It is clear that the calculation of the full top-quark mass dependence is vital in order to get reliable predictions for Higgs boson pair production over the full invariant mass range.

In this chapter we calculate the real NLO corrections at the double Higgs production, in particular the process $gg \to hhg$. We re-evaluated the amplitude in heavy top limit and we will present for the first time, the result up to and including $\mathcal{O}(1/m_t^2)$. Going in order in the first section, starting from the general amplitude, we construct the projectors of the process. In the second one we describe the kinematics and the phase space for a process with three body final states. Finally we show the analytic result of our calculation.

3.1 General Lorentz structure of the process

We begin describing the general Lorentz structure of the process $gg \to hhg$ and constructing the orthogonal projectors. First of all, we fix the momenta and the Lorentz indices in this way:

$$g(q_1^\mu) + g(q_2^\nu) \longrightarrow g(q_3^\rho) + h(q_4) + h(q_5)\,. \tag{3.1.1}$$

The most general amplitude $T^{\mu\nu\rho}$ of the process presents only two forms $g^{\mu\nu}q_i^\rho$ and $q_i^\mu q_j^\nu q_k^\rho$ with all possible index permutations without repetitions and without terms with q_1^μ, q_2^ν and q_3^ρ. We can write:

$$\begin{aligned}
T^{\mu\nu\rho} &= a_1 g^{\mu\nu}q_1^\rho + a_2 g^{\mu\nu}q_2^\rho + a_3 g^{\mu\nu}q_4^\rho + a_4 g^{\mu\rho}q_1^\nu + a_5 g^{\mu\rho}q_3^\nu + a_6 g^{\mu\rho}q_4^\nu + a_7 g^{\nu\rho}q_2^\mu \\
&+ a_8 g^{\nu\rho}q_3^\mu + a_9 g^{\nu\rho}q_4^\mu + a_{10} q_1^\nu q_1^\rho q_2^\mu + a_{11} q_1^\nu q_1^\rho q_3^\mu + a_{12} q_1^\nu q_1^\rho q_4^\mu + a_{13} q_1^\nu q_2^\mu q_2^\rho \\
&+ a_{14} q_1^\nu q_2^\mu q_4^\rho + a_{15} q_1^\nu q_2^\rho q_3^\mu + a_{16} q_1^\nu q_2^\rho q_4^\mu + a_{17} q_1^\nu q_3^\mu q_4^\rho + a_{18} q_1^\nu q_4^\mu q_4^\rho + a_{19} q_1^\rho q_2^\mu q_3^\nu \\
&+ a_{20} q_1^\rho q_2^\mu q_4^\nu + a_{21} q_1^\rho q_3^\mu q_3^\nu + a_{22} q_1^\rho q_3^\mu q_4^\nu + a_{23} q_1^\rho q_3^\nu q_4^\mu + a_{24} q_1^\rho q_4^\mu q_4^\nu + a_{25} q_2^\mu q_2^\rho q_3^\nu \\
&+ a_{26} q_2^\mu q_2^\rho q_4^\nu + a_{27} q_2^\mu q_3^\nu q_4^\rho + a_{28} q_2^\mu q_4^\nu q_4^\rho + a_{29} q_2^\rho q_3^\mu q_3^\nu + a_{30} q_2^\rho q_3^\mu q_4^\nu + a_{31} q_2^\rho q_3^\nu q_4^\mu \\
&+ a_{32} q_2^\rho q_4^\mu q_4^\nu + a_{33} q_3^\mu q_3^\nu q_4^\rho + a_{34} q_3^\mu q_4^\nu q_4^\rho + a_{35} q_3^\nu q_4^\mu q_4^\rho + a_{36} q_4^\mu q_4^\nu q_4^\rho\,,
\end{aligned} \tag{3.1.2}$$

where the coefficients a_i stand for remaining of the amplitude, i.e. contains propagators and so on.
In a gauge invariant theory, the total amplitude $\mathcal{M}^{\mu\,\nu\,\rho}$ [1] of a process which contains one or more external gluons (3 in our case), has the properties:

$$q_{\mu\,(\nu,\,\rho)}\,\mathcal{M}^{\mu\,\nu\,\rho} = 0\,. \tag{3.1.3}$$

In our process we have three conditions, like 3.1.3, one for each external gluon, and using them we obtain some relations for the coefficients a_i in 3.1.2. In particular for each of 3.1.3 we obtain 10 relations and finally a linear system 30×36. Solving it we have achieved 14 linear independent Lorentz structure that are not orthogonal. Now we are able to rewrite the amplitude as

$$T^{\mu\,\nu\,\rho} = \sum_{i=1}^{14} F_i\,P_i^{\mu\,\nu\,\rho}\,, \tag{3.1.4}$$

[1] For total amplitude, obviously, we consider the sum of all possible Feynamn diagram for a generic process. The amplitude of the single diagram is in general not gauge-invariant.

where F_i are the form factors and P_i are the orthogonal projectors that can be constructed from the 14 Lorentz structures found. The Lorentz structures, $L_i^{\mu\nu\rho}$, have the form:

$$L_1^{\mu\nu\rho} = \frac{(q_1q_2)\,(q_2q_3)}{(q_1q_3)}\left(g^{\,\mu\nu} - \frac{q_1^{\,\nu}q_2^{\,\mu}}{(q_1q_2)}\right)\left(q_1^{\,\rho} - \frac{(q_1q_3)}{(q_2q_3)}\,q_2^{\,\rho}\right), \tag{3.1.5}$$

$$L_2^{\mu\nu\rho} = \frac{(q_1q_2)\,(q_3q_4)}{(q_1q_3)}\left(g^{\,\mu\nu} - \frac{q_1^{\,\nu}q_2^{\,\mu}}{(q_1q_2)}\right)\left(q_1^{\,\rho} - \frac{(q_1q_3)}{(q_3q_4)}\,q_4^{\,\rho}\right), \tag{3.1.6}$$

$$L_3^{\mu\nu\rho} = L_1^{\mu\nu\rho}\,(\nu \to \rho, q_2 \leftrightarrow q_3)\,, \tag{3.1.7}$$

$$L_4^{\mu\nu\rho} = L_2^{\mu\nu\rho}\,(\nu \to \rho, q_2 \leftrightarrow q_3)\,, \tag{3.1.8}$$

$$L_5^{\mu\nu\rho} = L_3^{\mu\nu\rho}\,(\mu \to \nu, q_1 \leftrightarrow q_2)\,, \tag{3.1.9}$$

$$L_6^{\mu\nu\rho} = L_4^{\mu\nu\rho}\,(\mu \to \nu,\, q_1 \leftrightarrow q_2)\,, \tag{3.1.10}$$

$$\begin{aligned} L_7^{\mu\nu\rho} &= -\,(q_2q_3)\,g^{\,\mu\nu}\left(q_1^{\,\rho} - \frac{(q_1q_3)}{(q_2q_3)}\,q_2^{\,\rho}\right) - (q_1q_3)\,g^{\,\nu\rho}\left(q_2^{\,\mu} - \frac{(q_1q_2)}{(q_1q_3)}\,q_3^{\,\mu}\right) \\ &+ (q_2q_3)\,g^{\,\mu\rho}\left(q_1^{\,\nu} - \frac{(q_1q_2)}{(q_2q_3)}\,q_3^{\,\nu}\right) - q_1^{\,\nu}\,q_2^{\,\rho}\,q_3^{\,\mu} + q_1^{\,\rho}\,q_2^{\,\mu}\,q_3^{\,\nu}\,, \end{aligned} \tag{3.1.11}$$

$$\begin{aligned} L_8^{\mu\nu\rho} &= \frac{(q_2q_3)\,(q_2q_4)}{(q_1q_2)}\left[\left(g^{\,\mu\rho} - \frac{q_2^{\,\rho}q_3^{\,\mu}}{(q_2q_3)}\right)\left(q_1^{\,\nu} - \frac{(q_1q_2)}{(q_2q_4)}\,q_4^{\,\nu}\right)\right. \\ &- \left.\left(g^{\,\mu\nu} - \frac{q_2^{\,\mu}q_4^{\,\nu}}{(q_2q_4)}\right)\left(q_1^{\,\rho} - \frac{(q_1q_3)}{(q_2q_3)}\,q_2^{\,\rho}\right)\right], \end{aligned} \tag{3.1.12}$$

$$\begin{aligned} L_9^{\mu\nu\rho} &= \frac{(q_2q_4)\,(q_3q_4)}{(q_1q_2)}\left[\left(g^{\mu\rho} - \frac{q_3^{\,\mu}\,q_4^{\,\rho}}{(q_3q_4)}\right)\left(q_1^{\,\nu} - \frac{(q_1q_2)}{(q_2q_4)}\,q_4^{\,\nu}\right)\right. \\ &- \left.\left(g^{\mu\nu} - \frac{q_2^{\,\mu}q_4^{\,\nu}}{(q_2q_4)}\right)\left(q_1^{\,\rho} - \frac{(q_1q_3)}{(q_3q_4)}\,q_4^{\,\rho}\right)\right], \end{aligned} \tag{3.1.13}$$

$$L_{10}^{\mu\nu\rho} = L_9^{\mu\nu\rho}\,(\mu \to \nu, q_1 \leftrightarrow q_2)\,, \tag{3.1.14}$$

$$\begin{aligned} L_{11}^{\mu\nu\rho} &= \frac{(q_1q_3)\,(q_3q_4)}{(q_1q_2)}\left[\left(g^{\nu\rho} - \frac{q_3^{\,\nu}q_4^{\,\rho}}{(q_3q_4)}\right)\left(q_2^{\,\mu} - \frac{(q_1q_2)}{(q_1q_3)}q_3^{\,\mu}\right)\right. \\ &- \left.\left(g^{\mu\nu} - \frac{q_1^{\,\nu}q_3^{\,\mu}}{(q_1q_3)}\right)\left(q_2^{\,\rho} - \frac{(q_2q_3)}{(q_3q_4)}q_4^{\,\rho}\right)\right], \end{aligned} \tag{3.1.15}$$

$$\begin{aligned} L_{12}^{\mu\nu\rho} &= \frac{(q_1q_4)(q_2q_3)}{(q_1q_2)}\left(g^{\mu\rho} - \frac{q_1^{\,\rho}q_4^{\,\mu}}{(q_1q_4)}\right)\left(q_1^{\,\nu} - \frac{(q_1q_2)}{(q_2q_3)}q_3^{\,\nu}\right) \\ &+ (q_1q_4)\left(g^{\nu\rho} - \frac{q_1^{\,\nu}q_2^{\,\rho}}{(q_1q_2)}\right)\left(q_3^{\,\mu} - \frac{(q_1q_3)}{(q_1q_4)}q_4^{\,\mu}\right), \end{aligned} \tag{3.1.16}$$

$$
\begin{aligned}
L_{13}^{\mu\nu\rho} &= -\frac{(q_1q_4)(q_2q_3)(q_2q_4)}{(q_1q_2)(q_1q_3)}\left(g^{\mu\nu}-\frac{q_1^\nu q_4^\mu}{(q_1q_4)}-\frac{q_2^\mu q_4^\nu}{(q_2q_4)}\right)\left(q_1^\rho-\frac{(q_1q_3)}{(q_2q_3)}q_2^\rho\right)\\
&- \frac{(q_2q_3)}{(q_1q_3)}q_4^\mu q_4^\nu\left(q_1^\rho-\frac{(q_1q_3)}{(q_2q_3)}q_2^\rho\right), \qquad (3.1.17)\\
L_{14}^{\mu\nu\rho} &= -\frac{(q_1q_4)(q_2q_4)(q_3q_4)}{(q_1q_2)(q_1q_3)}\left(g^{\mu\nu}-\frac{q_1^\nu q_4^\mu}{(q_1q_4)}-\frac{q_2^\mu q_4^\nu}{(q_2q_4)}\right)\left(q_1^\rho-\frac{(q_1q_3)}{(q_3q_4)}q_4^\rho\right)\\
&- \frac{(q_3q_4)}{(q_1q_3)}q_4^\mu q_4^\nu\left(q_1^\rho-\frac{(q_1q_3)}{(q_3q_4)}q_4^\rho\right), \qquad (3.1.18)
\end{aligned}
$$

The orthogonal projectors ($P_i \cdot P_j = 0$) are written as a linear combinations of the $L_i^{\mu\nu\rho}$ as follows:

$$
\begin{aligned}
P_1^{\mu\nu\rho} &= -\frac{L_1^{\mu\nu\rho}}{(q_1q_2)^2(q_2q_3)}-\frac{L_7^{\mu\nu\rho}}{2(q_1q_2)(q_2q_3)(q_1q_3)}, \qquad (3.1.19)\\
P_2^{\mu\nu\rho} &= -\frac{L_5^{\mu\nu\rho}}{(q_2q_3)^2(q_1q_3)}-\frac{L_7^{\mu\nu\rho}}{2(q_1q_2)(q_2q_3)(q_1q_3)}, \qquad (3.1.20)\\
P_3^{\mu\nu\rho} &= \frac{L_3^{\mu\nu\rho}}{(q_1q_3)^2(q_2q_3)}-\frac{L_7^{\mu\nu\rho}}{2(q_1q_2)(q_2q_3)(q_1q_3)}, \qquad (3.1.21)\\
P_4^{\mu\nu\rho} &= \frac{L_7^{\mu\nu\rho}}{2(q_1q_2)(q_2q_3)(q_1q_3)}, \qquad (3.1.22)\\
P_5^{\mu\nu\rho} &= -\frac{K_1}{2(q_1q_2)(q_2q_3)}L_1^{\mu\nu\rho}+L_2^{\mu\nu\rho}, \qquad (3.1.23)\\
P_6^{\mu\nu\rho} &= -L_6^{\mu\nu\rho}+L_8^{\mu\nu\rho}-\frac{K_2}{2(q_1q_2)^2}L_1^{\mu\nu\rho}-\frac{K_3}{2(q_1q_2)(q_1q_3)}L_7^{\mu\nu\rho}, \qquad (3.1.24)\\
P_7^{\mu\nu\rho} &= L_4^{\mu\nu\rho}+\frac{K_3}{2(q_2q_3)^2}L_5^{\mu\nu\rho}-\frac{(q_1q_3)}{(q_2q_3)}L_6^{\mu\nu\rho}-\frac{K_3}{2(q_1q_3)(q_2q_3)}L_3^{\mu\nu\rho}, \qquad (3.1.25)\\
P_8^{\mu\nu\rho} &= L_8^{\mu\nu\rho}+\frac{(q_3q_4)}{(q_1q_2)}-\frac{K_3}{2(q_1q_3)^2}L_3^{\mu\nu\rho}-\frac{K_3}{2(q_1q_2)(q_1q_3)}L_7^{\mu\nu\rho}\\
&- \frac{K_3}{2(q_1q_3)(q_2q_3)}L_5^{\mu\nu\rho}-\frac{(q_2q_3)}{(q_1q_2)}L_2^{\mu\nu\rho}+\frac{(q_2q_3)}{(q_1q_3)}L_4^{\mu\nu\rho}, \qquad (3.1.26)
\end{aligned}
$$

with

$$
\begin{aligned}
K_1 &= (q_1q_4)(q_2q_3)-(q_1q_3)(q_2q_4)+(q_1q_2)(q_3q_4),\\
K_2 &= (q_1q_4)(q_2q_3)-(q_1q_3)(q_2q_4)-(q_1q_2)(q_3q_4),
\end{aligned}
$$

$$K_3 \;=\; (q_1q_4)(q_2q_3) + (q_1q_3)(q_2q_4) - (q_1q_2)(q_3q_4)\,. \tag{3.1.27}$$

We have chosen the first four projectors like those of the process $gg \to hg$ [91] and this is convenient as we will illustrate. We have showed only the first eight projectors because the remaining six have norm equal to zero, namely $P_i \cdot P_i = 0$ for $9 \leq i \leq 14$, so the index i in 3.1.4 is restricted to $1 \leq i \leq 8$.

3.2 Kinematics and phase space of the process

In general it is possible to describe the kinematics of a three-body proces by using five independent scalar quantities [92]. In our case, keeping the notation of 3.1.1 for the momenta, we define[2]:

$$\begin{aligned} s &= (q_1 + q_2)^2\,, \\ t &= (q_1 - q_3)^2\,, \\ u &= (q_2 - q_3)^2\,, \\ g_1 &= (q_1 - q_4)^2\,, \\ g_2 &= (q_2 - q_5)^2\,. \end{aligned} \tag{3.2.1}$$

Another important invariant is the invariant mass of the Higgs system, $M_{hh}^2 = s + t + u$. It will be convenient to introduce variables z and v, where $z = M_{hh}^2/s$ and v is related at the cosine of the angle θ between q_1 and q_3 in the gg center of mass system, $\cos\theta = 2v - 1$. Defining $\tau = 4m_h^2/s$, we have

$$\tau \;\leq\; z \;\leq\; 1, \qquad 0 \;\leq\; v \;\leq\; 1\;, \tag{3.2.2}$$

and

$$\begin{aligned} t &= -s\,(1-z)\,(1-v)\;, \\ u &= -s\,(1-z)\,v\,. \end{aligned} \tag{3.2.3}$$

[2]In this chapter the partonic c.m. energy will be indicated as s and not $\hat{s}$ as in the previous chapters.

In the center of mass frame of the Higgs system, our four-momenta are given by

$$\begin{aligned}
q_1 &= q_1^0\,(1,0,0,1)\ , \\
q_2 &= q_2^0\,(1,0,\sin\psi,\cos\psi)\ , \\
q_3 &= q_3^0\,\left(1,0,\sin\psi',\cos\psi'\right)\ , \\
q_4 &= \frac{\sqrt{M_{hh}^2}}{2}\,(1,\beta_z\sin\theta_2\sin\theta_1,\beta_z\cos\theta_2\sin\theta_1,\beta_z\cos\theta_1)\ , \\
q_5 &= \frac{\sqrt{M_{hh}^2}}{2}\,(1,-\beta_z\sin\theta_2\sin\theta_1,-\beta_z\cos\theta_2\sin\theta_1,-\beta_z\cos\theta_1)\ ,
\end{aligned} \tag{3.2.4}$$

where

$$\begin{aligned}
q_1^0 = \frac{s+t}{2\sqrt{M_{hh}^2}}\,, \quad q_2^0 &= \frac{s+u}{2\sqrt{M_{hh}^2}}\,, \quad q_3^0 = -\frac{t+u}{2\sqrt{M_{hh}^2}}\,, \\
\cos\psi &= 1-\frac{s}{2\,q_1^0\,q_2^0}\,, \\
\cos\psi' &= 1+\frac{t}{2\,q_1^0\,q_3^0}\,, \\
\beta_z &= \sqrt{1-\frac{4\,m_h^2}{z\,s}}\,.
\end{aligned} \tag{3.2.5}$$

The two remaining independent invariants g_1, g_2 can be written as

$$\begin{aligned}
g_1 &= m_h^2-\frac{s+t}{2}\,(1-\beta_z\cos\theta_1)\ , \\
g_2 &= m_h^2-\frac{s+u}{2}\,(1+\beta_z\cos\theta_2\sin\theta_1\sin\psi+\beta_z\cos\theta_1\cos\psi)\ .
\end{aligned} \tag{3.2.6}$$

Now all invariants are expressed in terms of z, v, θ_1, θ_2 and s through the equations 3.2.3, 3.2.4, 3.2.5 and 3.2.6.
For what concerns the three-body phase space, dPS_3, we can factorize it into two decays, then the products of two two-body phase-space:

$$dPS_3 = \frac{d\vec{p}_{hh}^{\,2}}{2\pi}dPS_2\,(q,q_3,p_{hh})\,dPS_2\,(p_{hh},q_4,q_5)\ , \tag{3.2.7}$$

where q is the momentum of the initial gluon system and $p_{hh}=q_4+q_5$ the momentum of the Higgs system. Fundamentally, we are considering two decays: the first one has

as initial state, the initial gluons system q and as final states, the final gluon (q_3) and a intermediate state with momentum p_{hh}; the second is the decay of the state p_{hh} into the two Higgs (q_4, q_5).
For the first decay we can write

$$\begin{aligned}\frac{d\vec{p}_{hh}^{\,2}}{2\pi} dPS_2\left(q, q_3, p_{hh}\right) &= \frac{2E_{hh}dE_{hh}}{2\pi}\frac{d^3\vec{p}_{hh}}{\left(2\pi\right)^3 2E_{hh}}\frac{d^3\vec{q}_3}{\left(2\pi\right)^3 2E_{q_3}}\left(2\pi\right)^4\delta^4\left(q-p_{hh}-q_3\right)\\ &= \frac{d^4p_{hh}}{\left(2\pi\right)^3}\frac{dE_{q_3}}{2}\,d\cos\theta\,d\phi\,\delta^4\left(q-p_{hh}-q_3\right)\left|\vec{q_3}\right|, \qquad (3.2.8)\end{aligned}$$

where the angle θ is just the same discuss previously instead ϕ can be integrated out, there is not dependence in our amplitude with respect to this angle. The second phase space of 3.2.7 reads

$$\begin{aligned}dPS_2\left(p_{hh}, q_4, q_5\right) &= \frac{d^3\vec{q}_4}{\left(2\pi\right)^3 2E_{q_4}}\frac{d^3\vec{q}_5}{\left(2\pi\right)^3 2E_{q_5}}\left(2\pi\right)^4\delta^4\left(p_{hh}-q_4-q_5\right)\\ &= \frac{d^4q_4}{8\pi^2}\,\delta\left(q_4^2-m_h^2\right)\left|\vec{q_5}\right|dE_{q_5}\,\delta^4\left(p_{hh}-q_4-q_5\right)d\cos\theta_1\,d\theta_2\,.\end{aligned} \qquad (3.2.9)$$

where

$$\delta\left(q_4^2-m_h^2\right) = \delta\left(\left(p_{hh}-q_5\right)^2-m_h^2\right) = \delta\left(E_{q_5}-\frac{\sqrt{M_{hh}^2}}{2}\right)\frac{1}{2\sqrt{M_{hh}^2}}\,. \qquad (3.2.10)$$

With $|\vec{q_3}|^2 = \frac{\sqrt{s}}{2}(1-z)$, $|\vec{q_5}|^2 = \frac{\sqrt{M_{hh}^2}}{2}\beta_z$ and $dE_{q_3} = -\frac{dM_{hh}^2}{2\sqrt{s}}$, we are now able to rewrite dPS_3 as

$$\begin{aligned}dPS_3 &= \frac{d^4p_{hh}}{\left(2\pi\right)^2}\frac{dE_{q_3}}{2}\,d\cos\theta\,\delta^4\left(q-p_{hh}-q_3\right)\left(1-z\right)\frac{\sqrt{s}}{2}\cdot\frac{d^4q_4}{8\pi^2}\\ &\quad\frac{\delta\left(E_{q_5}-\frac{\sqrt{M_{hh}^2}}{2}\right)}{2\sqrt{M_{hh}^2}}\frac{\sqrt{M_{hh}^2}}{2}\,\beta_z\,dE_{q_5}\,\delta^4\left(p_{hh}-q_4-q_5\right)d\cos\theta_1\,d\theta_2\\ &= \frac{1}{2^6\left(2\pi\right)^4}\left(1-z\right)\beta_z\,d\cos\theta\,d\cos\theta_1\,d\theta_2\,dM_{hh}^2\,. \qquad (3.2.11)\end{aligned}$$

where θ_1 range between 0 and π instead θ_2 between 0 and 2π.

3.3 Outline of calculation of amplitude

Now we have all ingredients to evaluate the amplitude of the process $gg \to hhg$ and the first step is to contract the eight orthogonal projectors with the amplitude. To improve the CPU memory resource instead of projectors we have contracted the amplitude with the Lorentz structure (LS) eq. 3.1.5 – 3.1.12 and then we reconstructed the eight projectors. We have generated the amplitude and the Feynman diagrams by using the Mathematica package `FeynArts` [93]. The relevant diagram, with amplitude different to zero, are 54 divided into 3 topologies: 6 triangles, 24 boxes and 24 pentagons with a fermionic loop, as it showed in the figure 3.1.
We manipulate the amplitude with `Mathematica` [94] private routines and we make the trace of the gamma matrices with `Tracer` [95]. The next steps are the sum over the color and finally the reduction of the loop integrals in 2-point (B0), 3-point (C0), 4-point (D0) and 5-point (E0) scalar functions.
All calculations were made in $n = 4 - 2\epsilon$ dimension and the first check on our calculation is respect to the $\frac{1}{\epsilon}$ poles, which are obviously absent. The second simple check is to obtain the result of [91] for $gg \to hg$ starting by our results and excluding the pentagon diagrams and box diagrams without Higgs propagator. In this way we get the same structure and symmetries for the form factors of [91].
At this stage the 8 Lorentz structure contracted with the amplitude[3], have the same set of scalar integrals, in total 4 B0, 25 C0, 30 D0 and 12 E0. In order to test the numerical stability of our results we performed, in a private Fortran code, the phase-space integration of the amplitude squared with `Vegas` evaluating the scalar integrals using `LoopTools` [96].
We found that only LS 1, 2, 7 and 8 were numerically stable, this implies that these LS were reduced to a integral basis. At the contrary the remaining LS presented a numerical instability. However for the unstable LS one can use the transformations described in eq. (3.1.7–3.1.10) in order to obtain the correct integral basis and then a good numerical stability.

[3]For simplicity, in this discussion, we will refer to Lorentz structure as the contraction of LS with the amplitude.

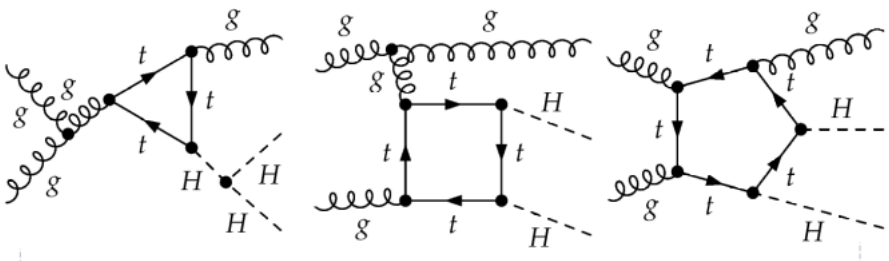

Figure 3.1: *The diagram topologies for the process $gg \to hhg$.*

3.4 Heavy top limit results

In this section we present for the first time the large top-mass-expansion evaluation of the amplitude, by reporting the analytic expressions that we obtained via a Taylor expansion for $s, t, u, M_{hh}^2, m_h^2 \ll m_t^2$ up to and including $\mathcal{O}(1/m_t^2)$.
First of all we show the expressions for the Lorentz structure, contracted with the amplitude, $C_i = L_i^{\mu\nu\rho} T_{\mu\nu\rho}$, at order zero in the expansion. Defining $\omega = \frac{(4m_h^2 - M_{hh}^2)}{(m_h^2 - M_{hh}^2)}$, we have:

$$C_1 = -\frac{s}{6\,t}\,\omega\,\left(M_{hh}^4 + s^2\right)\,, \tag{3.4.1}$$

$$C_2 = \frac{\omega}{12\,t\,u}\left(M_{hh}^4 + s^2\right)\left(g_1(u-s) + g_2(s+t) + m_h^2(s - M_{hh}^2) + tu\right)\,, \tag{3.4.2}$$

$$C_3 = \frac{t}{6\,s}\,\omega\,\left(M_{hh}^4 + t^2\right)\,, \tag{3.4.3}$$

$$C_4 = \frac{\omega}{12\,s\,u}\left(M_{hh}^4 + t^2\right)\left(g_1(M_{hh}^2 - t) - g_2(s+t) + m_h^2(t-u) - tu\right)\,, \tag{3.4.4}$$

$$C_5 = -\frac{u}{6\,s}\,\omega\,\left(M_{hh}^4 + u^2\right)\,, \tag{3.4.5}$$

$$C_6 = \frac{\omega}{12\,s\,t}\left(M_{hh}^4 + u^2\right)\left(g_1(t - M_{hh}^2) + g_2(s+t) + m_h^2(t+u) + tu\right)\,, \tag{3.4.6}$$

$$C_7 = -\frac{\omega}{3}\,M_{hh}^4\,, \tag{3.4.7}$$

$$
\begin{aligned}
C_8 &= \frac{\omega}{12\,s\,t}\Big(-\left(M_{hh}^4 - 2M_{hh}^2 s + 2s^2\right)\left(g_1 M_{hh}^2 - g_2 s + m_h^2(s - M_{hh}^2)\right) \\
&+ t\left(M_{hh}^4(3g_1 - g_2 - 2m_h^2 - M_{hh}^2) + 2s^2(g_1 + g_2 - 2m_h^2 + M_{hh}^2)\right. \\
&- M_{hh}^2 s(4(g_1 + g_2 - 2m_h^2) + 3M_{hh}^2) - 2s^3\Big) - t^2\left(-s(2g_1 + 3g_2 - 5m_h^2 + 6M_{hh}^2)\right. \\
&+ \left. M_{hh}^2(3g_1 + 2g_2 - 5m_h^2 + M_{hh}^2) + 2s^2\right) + t^3(g_1 + g_2 - 2m_h^2 + 3M - 3s) - t^4\Big)\,,
\end{aligned}
\tag{3.4.8}
$$

the C_i are in units $\frac{8}{\sqrt{2}}\,G_\mu\,g_s^3\,\frac{1}{(16\pi)^2}\,f^{abc}$, where $g_s^2 = \alpha_s\,(4\pi)$ is the strong coupling costant, G_μ is the muon decay constant, the factor $1/(16\pi)^2$ arises from the integral loop and f^{abc} is the structure constant of the Lie algebra of SU(3).
The symmetries for the L_3 and L_5 showed in 3.1.7, 3.1.9, which now are shifted in $L_1 \overset{s\leftrightarrow t}{\longrightarrow} -L_3$ and $L_3 \overset{t\leftrightarrow u}{\longrightarrow} -L_5$, are evident, whereas for L_4 and L_6 the symmetries are not manifest, but however present, because of the dependence of g_1 and g_2 by t and u. Taking into account that $P_i P_i = 16/(stu)$, for $i = 1, ..., 4$, the first four form factor read[4]

$$
\begin{aligned}
\frac{16}{s\,t\,u}\,F_1 &= \frac{8}{s^2 u}\,C_1 - \frac{4}{stu}\,C_7 \;=\; -\frac{4\,\omega}{3}\,\frac{s^2}{s\,t\,u}\,, \\
\frac{16}{s\,t\,u}\,F_2 &= \frac{8}{u^2 t}\,C_5 - \frac{4}{stu}\,C_7 \;=\; -\frac{4\,\omega}{3}\,\frac{u^2}{s\,t\,u}\,, \\
\frac{16}{s\,t\,u}\,F_3 &= -\frac{8}{t^2 u}\,C_3 - \frac{4}{stu}\,C_7 \;=\; -\frac{4\,\omega}{3}\,\frac{t^2}{s\,t\,u}\,, \\
\frac{16}{s\,t\,u}\,F_4 &= \frac{4}{stu}\,C_7 \;=\; \frac{4\,\omega}{3}\frac{M_{hh}^4}{s\,t\,u}\,,
\end{aligned}
\tag{3.4.9}
$$

while the remaining form factors are egual to zero, this representing a remarkable result. Now we can write the amplitude:

$$
|\mathcal{A}_{hhg}^{(0)}|^2 = \left(F_1^2 + F_2^2 + F_3^2 + F_4^2\right)\,\frac{16}{s\,t\,u} \;=\; \frac{\omega^2}{9}\,\frac{\left(M_{hh}^8 + s^4 + t^4 + u^4\right)}{s\,t\,u}\,. \tag{3.4.10}
$$

If we look the amplitude of $gg \to hg$, $|\mathcal{A}_{hg}|^2 = m_h^8 + s^4 + t^4 + u^4/(stu)$, we have found the same structure apart the ratio in front of 3.4.10.
The process that we are analysing presents soft and collinear divergences, due to the emission of the gluon in the final state, as it's clear in the amplitudes 3.4.10 with the

[4]The contraction of the amplitude with the projectors is:

$$P_i^{\mu\nu\rho} T_{\mu\nu\rho} = |P_i|^2\,F_i\,.$$

denominator of the form $s\,t\,u$. The soft divergence are cancelled out with the virtual contribution whereas collinear divergences can be removed thanks to the factorization theorem: the t and u singularities (respectively $v = 1$ and $v = 0$) must factorize in terms of the LO cross section of the process without the outgoing gluon, i.e. $gg \to hh$, times the Altarelli-Parisi splitting function. Then we have to know the LO process, the double Higgs production, in the heavy top limit, see eq. (1.3.11):

$$M_{hh}^2 \frac{d\hat{\sigma}_{hh}^{(0)}}{dM_{hh}^2} = \frac{G_\mu^2 \alpha_s^2(\mu_R)}{512\,(2\,\pi)^3}\,\beta_z\,z\,M_{hh}^2\,|\mathcal{A}_{hh}^{(0)}|^2\,, \tag{3.4.11}$$

where

$$|\mathcal{A}_{hh}^{(0)}|^2 = \frac{4}{9}\,\omega^2\,. \tag{3.4.12}$$

For the process $gg \to hhg$, the differential partonic cross section in heavy top limit will be:

$$\frac{d\,\hat{\sigma}_{hhg}^{(0)}}{d\cos\theta\,dM_{hh}^2} = C_A\,\frac{G_\mu^2 \alpha_s^2(\mu_R)}{512\,(2\,\pi)^4}\,\frac{\alpha_s(\mu_R)}{\pi}\,\beta_z\,(1-z)\,\frac{4\,\pi}{2\,s}\,\frac{\omega^2}{9}\,\frac{\left(M_{hh}^8 + s^4 + t^4 + u^4\right)}{s\,t\,u}\,, \tag{3.4.13}$$

where the numerical factor $1/512$ in the above comes from averaging over the initial gluon helicities $1/2^2$, from color averaging $1/8^2$ and from the identical final state particles the factor $1/2!$, the ratio $\frac{1}{2s}$ is the flux factor, 4π arises from the trivial integration of the angles θ_1 and θ_2 and finally μ_R is the renormalization scale.
We want to write our results in terms of the function R_{gg}, known at the moment only in heavy top limit, that appears in eq. (1.3.12) and in eq. (2.1.13). In order to regulate the collinear singularities we have to introduce the contour term *c.t.*:

$$c.t. = \frac{1}{2}\,\frac{1}{v(1-v)}\,\frac{\alpha_s(\mu_R)}{2\pi}\,P_{gg}(z)\,, \tag{3.4.14}$$

where the $P_{gg}(z)$ is the Altarelli-Parisi splitting function defined in eq. (1.3.14).
Performing the Altarelli-Parisi subtraction, the R_{gg} function reads

$$R_{gg}^{(0)} = \left(\frac{d\hat{\sigma}_{hh}^{(0)}}{dM_{hh}^2}\right)^{-1} 2\int_0^1 dv\,\left[\frac{d\,\hat{\sigma}_{hhg}^{(0)}}{dM_{hh}^2} - c.t.\frac{d\hat{\sigma}_{hh}^{(0)}}{dM_{hh}^2}\right], \tag{3.4.15}$$

where we have substituted $d\cos\theta$ with $2\,dv$ in the integral. Inserting the eq. (3.4.11), eq. (3.4.13) and eq. (3.4.14) into eq. (3.4.15), and rearranging all terms we obtain

$$R_{gg}^{(0)} \;=\; \frac{2}{z\,|\mathcal{A}_{hh}^{(0)}|^2}\int_0^1 dv\left[\frac{(1-z)}{2\,s}\,2\,|\mathcal{A}_{hhg}^{(0)}|^2 - \frac{(1-z+z^2)^2}{2\,(1-z)\,v\,(1-v)}\,|\mathcal{A}_{hh}^{(0)}|^2\right], \qquad (3.4.16)$$

where we don't have write the common coefficient of eq. (3.4.13) and eq. (3.4.11) because the LO contribution is factorized out as is defined in eq. (1.3.2). Noticing that ω^2 not depends by t and u, we have

$$R_{gg}^{(0)} \;=\; \frac{1}{z(1-z)}\int_0^1 \frac{dv}{v(1-v)}\left[\frac{M_{hh}^8+s^4+t^4+u^4}{2\,s^4} \;-\; \left(1-z+z^2\right)^2\right], \qquad (3.4.17)$$

where in the denominator we insert the relations of eq. (3.2.3). We perform the integration respect to v, by using a cut-off Λ and after the integration we restore the cross section making the limit $\Lambda \to 0$. If we use the trick $\frac{1}{v(1-v)} = \frac{1}{v} + \frac{1}{1-v}$, we can integrate separately the singularities: in particular for $v = 0$ the divergent interval is $[\Lambda,\, 1]$ and for $v = 1$ the divergent interval is $[0,\, 1-\Lambda]$. With the relations in eq. (3.2.3) we are now ready to integrate eq. (3.4.17), obtaining the well-known results, just mentioned in the previous chapters, mainly $R_{gg}^{(0)} = -11\,(1-z)^3/(6z)$.

Now we present the result for R_{gg} at the first order of the expansion in the top mass. At the zero order of the top mass expansion we have $F_5^{(0)} = F_6^{(0)} = F_7^{(0)} = F_8^{(0)} = 0$ whereas for $F_5^{(1)}$, $F_6^{(1)}$, $F_7^{(1)}$, $F_8^{(1)}$ we have checked numerically that they are zero. Therefore we present the analytic expressions of the expansion only for the $F_1^{(1)}$ and $F_7^{(1)}$, by using the symmetries is simple to obtain the remaining $F_i^{(1)}$. Defining $\omega_1 = \frac{(2\,m_h^2 - M_{hh}^2)}{(m_h^2 - M_{hh}^2)}$, we obtain:

$$\begin{aligned}
\frac{16}{s\,t\,u}\,F_1^{(1)} \;&=\; \frac{1}{180\,m_t^2\,s\,t\,u}\Bigg[11\,(4m_h^2 - M_{hh}^2)(M_{hh}^4 - 2M_{hh}^2 s) \\
&+\; \frac{s^2}{(m_h^2 - M_{hh}^2)}\,\left(11\,M_{hh}^4 - 40\,m_h^4 - 13\,m_h^2 M_{hh}^2\right) \\
&+\; \frac{11 M_{hh}^2}{(M_{hh}^2 - u^2)}\Big(4\,G_1\,G_2\,\sqrt{M_{hh}^2\,s\,t\,u}\,(s\,u - M_{hh}^2\,t) + 2\,G_2^2\,(M_{hh}^4\,t^2 + s^2\,u^2) \\
&+\; G_1^2\,(M_{hh}^4\,t^2 + 6\,M_{hh}^2\,s\,t\,u + s^2\,u^2)\Big)\Bigg],
\end{aligned}$$

$$
\begin{aligned}
\frac{16}{s\,t\,u}\,F_2^{(1)} &= F_1^{(1)}(s\to t, t\to s)\,,\\
\frac{16}{s\,t\,u}\,F_3^{(1)} &= F_2^{(1)}(t\to u, u\to t)\,,\\
\frac{16}{s\,t\,u}\,F_4^{(1)} &= -\frac{\omega_1}{30\,m_t^2\,s\,t\,u}\,\left(7\,m_h^2\,M_{hh}^4 - 6\,s\,t\,u\right)\,,
\end{aligned}
\tag{3.4.18}
$$

where we have substituted the invariants g_1 and g_2, writing the dependence on the angles θ_1 and θ_2 in G_1 and G_2, $G_1 = \beta_z\,\cos\theta_1$, $G_2 = \beta_z\,\cos\theta_2\,\sin\theta_1$. In this way we have cancelled the apparent poles of the type $1/t^2$ and $1/u^2$.
Now we are able to evaluated the amplitude at order $\mathcal{O}(1/m_t^2)$. After the integration in θ_1 and θ_2 we have:

$$
|\mathcal{A}'^{(1)}_{hhg}|^2 = \pi\,|\mathcal{A}^{(1)}_{hhg}|^2 = \pi\,\frac{m_h^2}{m_t^2}\,\frac{7}{45}\,\omega\,\omega_1\left[\frac{6\,M_{hh}^4}{7\,m_h^2} - \frac{\left(M_{hh}^8 + s^4 + t^4 + u^4\right)}{s\,t\,u}\right],
\tag{3.4.19}
$$

whereas for the LO process[5] we have

$$
|\mathcal{A}^{(1)}_{hh}|^2 = \frac{m_h^2}{m_t^2}\,\frac{7}{45}\,\omega\,\omega_1\,.
\tag{3.4.20}
$$

In order to calculate $R_{gg}^{(1)}$ we have to consider all orders $\mathcal{O}(1/m_t^2)$ of this expression:

$$
R_{gg}^{(0,1)} = \left(\frac{d\hat{\sigma}^{(0,1)}_{hh}}{dM^2_{hh}}\right)^{-1} 2\int_0^1 dv\,\left[\frac{d\,\hat{\sigma}^{(0,1)}_{hhg}}{dM^2_{hh}} - c.t.\,\frac{d\hat{\sigma}^{(0,1)}_{hh}}{dM^2_{hh}}\right],
\tag{3.4.21}
$$

where

$$
\frac{d\hat{\sigma}^{(0,1)}_{hh}}{dM^2_{hh}} = \frac{G_\mu^2\alpha_s^2(\mu_R)}{512\,(2\,\pi)^3}\,\beta_z\,z\left(|\mathcal{A}^{(0)}_{hh}|^2 + |\mathcal{A}^{(1)}_{hh}|^2\right)\,,
\tag{3.4.22}
$$

$$
\frac{d\hat{\sigma}^{(0,1)}_{hhg}}{dM^2_{hh}\,d\cos\theta} = C_A\,\frac{G_\mu^2\alpha_s^2(\mu_R)}{512\,(2\,\pi)^4}\,\frac{\alpha_s(\mu_R)}{\pi}\,\beta_z\,(1-z)\,\frac{2\,\pi}{2\,s}\left(2|\mathcal{A}^{(0)}_{hhg}|^2 + \frac{1}{2}\,|\mathcal{A}^{(1)}_{hhg}|^2\right).
\tag{3.4.23}
$$

[5] From eq. 19-20 of [28] we have that, $F_\Delta^{1\ell}(\hat{s}) = \frac{4}{3} + \frac{7}{90}\frac{\hat{s}}{m_t^2}$ and $F_\Box^{1\ell}(\hat{s}) = -\frac{4}{3} - \frac{7}{15}\frac{m_h^2}{m_t^2}$. From eq. (1.3.11) and since the form factor of spin-2 case not contribute at $\mathcal{O}(1/m_t^2)$ we obtain eq. (3.4.20)

If we insert in eq. (3.4.22) the eq. (3.4.12) and eq. (3.4.20) and in eq. (3.4.23) insert the eq. (3.4.10) and eq. (3.4.19) and expand the denominator[6] we have (also in this case we don't write the prefactor of the cross section according to what made previously for the zero order)

$$\begin{aligned} R_{gg}^{(0,1)} &= R_{gg}^{(0)} + \frac{2}{z\,|\mathcal{A}_{hh}^{(0)}|^2}\int_0^1 dv\,\left[\frac{1-z}{2\,s}\,\frac{|\mathcal{A}_{hhg}^{(1)}|^2}{2} - \frac{(1-z+z^2)^2}{2\,v\,(1-v)}\,\frac{|\mathcal{A}_{hh}^{(1)}|^2}{1-z}\right] \\ &- \frac{2}{z}\,\frac{|\mathcal{A}_{hh}^{(1)}|^2}{|\mathcal{A}_{hh}^{(0)}|^4}\int_0^1 dv\,\left[\frac{1-z}{2\,s}\,2\,|\mathcal{A}_{hhg}^{(0)}|^2 - \frac{(1-z+z^2)^2}{2\,v\,(1-v)}\,\frac{|\mathcal{A}_{hh}^{(0)}|^2}{1-z}\right]. \end{aligned} \tag{3.4.24}$$

The amplitude $|\mathcal{A}_{hhg}^{(1)}|^2$, eq. (3.4.19), in the first part do not depend on v meanwhile the second part have the same dependence to s, t and u of zero order, eq. (3.4.10). Therefore we perform the integration in v, by using the cut-off tecnique, the result is obviously divergence-safe. In eq. (3.4.24) the second term of $|\mathcal{A}_{hhg}^{(1)}|^2$, eq. (3.4.19), cancels with the last term of eq. (3.4.24), so that we find[7]

$$R_{gg}^{(0,1)} = R_{gg}^{(0)} + R_{gg}^{(1)} = -\frac{11}{6}\frac{(1-z)^3}{z} + \frac{1}{20}\,\frac{s}{m_t^2}\,\frac{\omega_1}{\omega}\,(3\,z\,(1-z))\,. \tag{3.4.25}$$

The result in eq. (3.4.25) represents the correction at the first order of the expansion in top mass, evaluated for the first time in this work. We note that the correction is proportional to s/m_t^2 and confirm the discussion made in 1.4 about the validity of the LET and of the expansion in top mass.

[6] If we consider the denominator, mainly the amplitudes in the bracket in eq. (3.4.22), as $a + b/m_t^2$, the expansion, for $m_t^2 \to \infty$ will be:

$$\frac{1}{a+b/m_t^2} \sim \frac{1}{a} - \frac{b}{a^2}\frac{1}{m_t^2} + \mathcal{O}(1/m_t^4)\,.$$

[7] The second term of eq. (3.4.24) is proportional to $\frac{|\mathcal{A}_{hh}^{(1)}|^2}{|\mathcal{A}_{hh}^{(0)}|^2}\,\frac{-6\,M_{hh}^4}{7\,m_h^2}$ plus $\frac{|\mathcal{A}_{hh}^{(1)}|^2}{|\mathcal{A}_{hh}^{(0)}|^2}\,R_{gg}^{(0)}$, the third term of eq. (3.4.24) is proportional to $-\frac{|\mathcal{A}_{hh}^{(1)}|^2}{|\mathcal{A}_{hh}^{(0)}|^2}\,R_{gg}^{(0)}$, then the result in eq. (3.4.25) will depend only from $\frac{|\mathcal{A}_{hh}^{(1)}|^2}{|\mathcal{A}_{hh}^{(0)}|^2}\,\frac{-6\,M_{hh}^4}{7\,m_h^2}$.

Conclusions

Determination of the Higgs self-interaction through the double Higgs production from gluon fusion is a major goal of current and future collider experiments. The double Higgs production is a process that proceed via fermionic loop, quark top fundamentally in the SM, already at leading order. Therefore the NLO QCD corrections are very difficult to compute. At moment an exact analytic evaluation of the two-loop QCD virtual corrections is presently not available. At the analytic level explicit results for the two-loop virtual corrections in Higgs pair production were presented in [28], where the double-triangle contribution was computed exactly while the spin-0 and spin-2 two-loop form factors in the amplitude were computed via an asymptotic expansion in the top mass up to and including terms $\mathcal{O}(1/m_t^8)$.

For what concern the real corrections, at present we have analytic results only obtained via LET approximation, and numerical results that include the top mass effects, as just discuss extensively. The numerical analysis have estimated this effects to be of the order of 10%, then they are very important in order to have a good estimate of the double Higgs production cross section.

In this thesis we have showed, for the first time, the analytic results for the real correction in the double Higgs production (focusing in particular on the process $gg \to hhg$) in the SM up to and including $\mathcal{O}(1/m_t^2)$. We have presented the result in terms of the R_{gg} function, and by eq. (3.4.25) one can see that the new terms are proportional to s/m_t^2, as expected.

To obtain the first term of the expansion in heavy top we started from the exact amplitude. Then in the near future we will be able to present the exact result for the amplitude $gg \to hhg$. At moment we have not a good cancellation of the divergences in the numerical integration. This is due to the presence of apparent poles in the amplitude of the type $1/t^2$ and $1/u^2$, as already happened for the $1/m_t^2$ term of the expansion showed in this work. We must manipulate the amplitude in order to eliminate the apparent poles and therefore go forward with the numerical integration and obtain the exact result.

In this thesis we have also considered the double Higgs production in the MSSM, the minimal supersymmetric extension of the SM. In this model we have an Higgs spectrum more reach than the SM and the Higgs production can be mediated by loops involving the top and bottom quarks and their superpartners, the stop and sbottom squarks.
We take a step towards a complete NLO-QCD determination of the production of a pair of Higgs scalars in the MSSM. Exploiting a low-energy theorem that connects the Higgs-gluon interactions to the derivatives of the gluon self-energy, we obtain analytic results for the one- and two-loop squark contributions to Higgs pair production in the limit of vanishing external momenta. To assess the importance of the newly-computed corrections, we include the squark contributions to both triangle and box form factors in a private version of the public code HPAIR, which computes the NLO- QCD cross section for Higgs pair production in the SM and in the MSSM. We find that the two-loop squark contributions can have a non-negligible effect in scenarios with stop masses below the TeV scale.

Appendix

Appendix A

Functions entering the box form factors

In this appendix we provide the definitions of the functions entering the form factors in eqs. (2.2.9)–(2.2.11) in terms of the derivatives of the gluon self-energy. Focusing on the two-loop part of the form factors, and defining the shortcut $Z \equiv (2/T_F)\,\Pi^{2\ell,\,t}(0)$, the functions that represent the contributions of diagrams involving only the top Yukawa coupling read

$$F_1^{2\ell} = \frac{\partial^2 Z}{(\partial m_t^2)^2} + \frac{\partial^2 Z}{(\partial m_{\tilde{t}_1}^2)^2} + \frac{\partial^2 Z}{(\partial m_{\tilde{t}_2}^2)^2} + 2\,\frac{\partial^2 Z}{\partial m_t^2 \partial m_{\tilde{t}_1}^2} + 2\,\frac{\partial^2 Z}{\partial m_t^2 \partial m_{\tilde{t}_2}^2} + 2\,\frac{\partial^2 Z}{\partial m_{\tilde{t}_1}^2\,\partial m_{\tilde{t}_2}^2}\ , \tag{A.0.1}$$

$$\begin{aligned} F_2^{2\ell} = {} & \frac{\partial^2 Z}{(\partial m_{\tilde{t}_1}^2)^2} - \frac{\partial^2 Z}{(\partial m_{\tilde{t}_2}^2)^2} + \frac{\partial^2 Z}{\partial m_t^2 \partial m_{\tilde{t}_1}^2} - \frac{\partial^2 Z}{\partial m_t^2 \partial m_{\tilde{t}_2}^2} \\ & - \frac{4\,c_{2\theta_t}^2}{m_{\tilde{t}_1}^2 - m_{\tilde{t}_2}^2}\left(\frac{\partial^2 Z}{\partial c_{2\theta_t}^2 \partial m_t^2} + \frac{\partial^2 Z}{\partial c_{2\theta_t}^2 \partial m_{\tilde{t}_1}^2} + \frac{\partial^2 Z}{\partial c_{2\theta_t}^2 \partial m_{\tilde{t}_2}^2}\right)\ , \end{aligned} \tag{A.0.2}$$

$$
\begin{aligned}
F_3^{2\ell} &= \frac{\partial^2 Z}{(\partial m^2_{\tilde{t}_1})^2} + \frac{\partial^2 Z}{(\partial m^2_{\tilde{t}_2})^2} - 2\,\frac{\partial^2 Z}{\partial m^2_{\tilde{t}_1}\partial m^2_{\tilde{t}_2}} - \frac{2}{m^2_{\tilde{t}_1} - m^2_{\tilde{t}_2}}\left(\frac{\partial Z}{\partial m^2_{\tilde{t}_1}} - \frac{\partial Z}{\partial m^2_{\tilde{t}_2}}\right) \\
&\quad + \frac{16\,c^2_{2\theta_t}}{(m^2_{\tilde{t}_1} - m^2_{\tilde{t}_2})^2}\left(c^2_{2\theta_t}\,\frac{\partial^2 Z}{(\partial c^2_{2\theta_t})^2} + 2\,\frac{\partial Z}{\partial c^2_{2\theta_t}}\right) \\
&\quad - \frac{8\,c^2_{2\theta_t}}{m^2_{\tilde{t}_1} - m^2_{\tilde{t}_2}}\left(\frac{\partial^2 Z}{\partial c^2_{2\theta_t}\partial m^2_{\tilde{t}_1}} - \frac{\partial^2 Z}{\partial c^2_{2\theta_t}\partial m^2_{\tilde{t}_2}}\right), \qquad \text{(A.0.3)}
\end{aligned}
$$

$$
F^{2\ell} = \frac{\partial Z}{\partial m^2_{\tilde{t}_1}} - \frac{\partial Z}{\partial m^2_{\tilde{t}_2}} - \frac{4\,c^2_{2\theta_t}}{m^2_{\tilde{t}_1} - m^2_{\tilde{t}_2}}\,\frac{\partial Z}{\partial c^2_{2\theta_t}}\,, \qquad \text{(A.0.4)}
$$

$$
G^{2\ell} = \frac{\partial Z}{\partial m^2_{\tilde{t}_1}} + \frac{\partial Z}{\partial m^2_{\tilde{t}_2}} + \frac{\partial Z}{\partial m^2_t}\,. \qquad \text{(A.0.5)}
$$

The functions that represent the sub-dominant contributions of diagrams involving D-term induced EW couplings read

$$
\widetilde{F}_1^{2\ell} = d^t_{11}\,\tilde{f}_1 \;+\; d^t_{22}\,\tilde{f}_2 \;-\; 4\,c_{2\theta_t}\,s_{2\theta_t}\,d^t_{12}\,\tilde{f}_3\,, \qquad \text{(A.0.6)}
$$

$$
\widetilde{F}_2^{2\ell} = d^t_{11}\,\tilde{f}_4 \;-\; d^t_{22}\,\tilde{f}_5 \;+\; 2\,\frac{c_{2\theta_t}}{s_{2\theta_t}}\,d^t_{12}\,\tilde{f}_6\,, \qquad \text{(A.0.7)}
$$

$$
\begin{aligned}
\widetilde{F}_3^{2\ell} &= (d^t_{11})^2\,\frac{\partial^2 Z}{(\partial m^2_{\tilde{t}_1})^2} \;+\; (d^t_{22})^2\,\frac{\partial^2 Z}{(\partial m^2_{\tilde{t}_2})^2} \;+\; 2\,d^t_{11}\,d^t_{22}\,\frac{\partial^2 Z}{\partial m^2_{\tilde{t}_1}\partial m^2_{\tilde{t}_2}} \;+\; 2\,(d^t_{12})^2\,\tilde{f}_7 \\
&\quad - 8\,c_{2\theta_t}\,s_{2\theta_t}\,\frac{d^t_{12}}{m^2_{\tilde{t}_1} - m^2_{\tilde{t}_2}}\left(d^t_{11}\,\frac{\partial^2 Z}{\partial c^2_{2\theta_t}\partial m^2_{\tilde{t}_1}} \;+\; d^t_{22}\,\frac{\partial^2 Z}{\partial c^2_{2\theta_t}\partial m^2_{\tilde{t}_2}}\right), \qquad \text{(A.0.8)}
\end{aligned}
$$

$$
D^{2\ell} = d^t_{11}\,\frac{\partial Z}{\partial m^2_{\tilde{t}_1}} \;+\; d^t_{22}\,\frac{\partial Z}{\partial m^2_{\tilde{t}_2}} \;-\; 4\,c_{2\theta_t}\,s_{2\theta_t}\,\frac{d^t_{12}}{m^2_{\tilde{t}_1} - m^2_{\tilde{t}_2}}\,\frac{\partial Z}{\partial c^2_{2\theta_t}}\,, \qquad \text{(A.0.9)}
$$

where

$$
d^t_{11} = \frac{d^t_L + d^t_R}{2} + c_{2\theta_t}\,\frac{d^t_L - d^t_R}{2}\,, \quad d^t_{22} = \frac{d^t_L + d^t_R}{2} - c_{2\theta_t}\,\frac{d^t_L - d^t_R}{2}\,, \quad d^t_{12} = -s_{2\theta_t}\,\frac{d^t_L - d^t_R}{2}\,, \qquad \text{(A.0.10)}
$$

and

$$
\tilde{f}_1 = \frac{\partial^2 Z}{(\partial m^2_{\tilde{t}_1})^2} \;+\; \frac{\partial^2 Z}{\partial m^2_{\tilde{t}_1}\partial m^2_{\tilde{t}_2}} \;+\; \frac{\partial^2 Z}{\partial m^2_t\partial m^2_{\tilde{t}_1}}\,, \qquad \text{(A.0.11)}
$$

$$\tilde{f}_1 = \frac{\partial^2 Z}{(\partial m^2_{\tilde{t}_1})^2} + \frac{\partial^2 Z}{\partial m^2_{\tilde{t}_1}\partial m^2_{\tilde{t}_2}} + \frac{\partial^2 Z}{\partial m^2_t \partial m^2_{\tilde{t}_1}} , \tag{A.0.12}$$

$$\tilde{f}_2 = \frac{\partial^2 Z}{(\partial m^2_{\tilde{t}_2})^2} + \frac{\partial^2 Z}{\partial m^2_{\tilde{t}_1}\partial m^2_{\tilde{t}_2}} + \frac{\partial^2 Z}{\partial m^2_t \partial m^2_{\tilde{t}_2}} , \tag{A.0.13}$$

$$\tilde{f}_3 = \frac{1}{m^2_{\tilde{t}_1} - m^2_{\tilde{t}_2}} \left(\frac{\partial^2 Z}{\partial c^2_{2\theta_t}\partial m^2_{\tilde{t}_1}} + \frac{\partial^2 Z}{\partial c^2_{2\theta_t}\partial m^2_{\tilde{t}_2}} + \frac{\partial^2 Z}{\partial c^2_{2\theta_t}\partial m^2_t} \right) , \tag{A.0.14}$$

$$\tilde{f}_4 = \frac{\partial^2 Z}{(\partial m^2_{\tilde{t}_1})^2} - \frac{\partial^2 Z}{\partial m^2_{\tilde{t}_1}\partial m^2_{\tilde{t}_2}} - \frac{4\, c^2_{2\theta_t}}{m^2_{\tilde{t}_1} - m^2_{\tilde{t}_2}} \frac{\partial^2 Z}{\partial c^2_{2\theta_t}\partial m^2_{\tilde{t}_1}} , \tag{A.0.15}$$

$$\tilde{f}_5 = \frac{\partial^2 Z}{(\partial m^2_{\tilde{t}_2})^2} - \frac{\partial^2 Z}{\partial m^2_{\tilde{t}_1}\partial m^2_{\tilde{t}_2}} + \frac{4\, c^2_{2\theta_t}}{m^2_{\tilde{t}_1} - m^2_{\tilde{t}_2}} \frac{\partial^2 Z}{\partial c^2_{2\theta_t}\partial m^2_{\tilde{t}_2}} , \tag{A.0.16}$$

$$\begin{aligned} \tilde{f}_6 = {} & \frac{1}{m^2_{\tilde{t}_1} - m^2_{\tilde{t}_2}} \left(\frac{\partial Z}{\partial m^2_{\tilde{t}_1}} - \frac{\partial Z}{\partial m^2_{\tilde{t}_2}} \right) - \frac{2\, s^2_{2\theta_t}}{m^2_{\tilde{t}_1} - m^2_{\tilde{t}_2}} \left(\frac{\partial^2 Z}{\partial c^2_{2\theta_t}\partial m^2_{\tilde{t}_1}} - \frac{\partial^2 Z}{\partial c^2_{2\theta_t}\partial m^2_{\tilde{t}_2}} \right) \\ & + \frac{8}{(m^2_{\tilde{t}_1} - m^2_{\tilde{t}_2})^2} \left[(1 - 2\, c^2_{2\theta_t}) \frac{\partial Z}{\partial c^2_{2\theta_t}} + c^2_{2\theta_t}\, s^2_{2\theta_t} \frac{\partial^2 Z}{(\partial c^2_{2\theta_t})^2} \right] , \end{aligned} \tag{A.0.17}$$

$$\begin{aligned} \tilde{f}_7 = {} & \frac{1}{m^2_{\tilde{t}_1} - m^2_{\tilde{t}_2}} \left(\frac{\partial Z}{\partial m^2_{\tilde{t}_1}} - \frac{\partial Z}{\partial m^2_{\tilde{t}_2}} \right) \\ & + \frac{4}{(m^2_{\tilde{t}_1} - m^2_{\tilde{t}_2})^2} \left[(1 - 4\, c^2_{2\theta_t}) \frac{\partial Z}{\partial c^2_{2\theta_t}} + 2\, c^2_{2\theta_t}\, , s^2_{2\theta_t} \frac{\partial^2 Z}{(\partial c^2_{2\theta_t})^2} \right] . \end{aligned} \tag{A.0.18}$$

Appendix B

Shifts to a different renormalization scheme

In this appendix we list the shifts to the functions F_i, F, G, $\widetilde{F}_i$ and D arising when the parameters m_t, $m^2_{\tilde{t}_i}$, θ_t and A_t in the top/stop contributions to the one-loop part of the form factors are expressed in a renormalization scheme R other than $\overline{\rm DR}$. Recalling the definition $x^{\overline{\rm DR}} = x^R + \delta x$, the shifts to the functions read

$$\delta F_1 = -\frac{1}{3}\left(\frac{\delta m^2_{\tilde{t}_1}}{m^6_{\tilde{t}_1}} + \frac{\delta m^2_{\tilde{t}_2}}{m^6_{\tilde{t}_2}} + 8\,\frac{\delta m_t}{m^5_t}\right) + 4\,\frac{\delta m_t}{m_t}\,F_1^{1\ell}\,, \tag{B.0.1}$$

$$\delta F_2 = -\frac{1}{3}\left(\frac{\delta m^2_{\tilde{t}_1}}{m^6_{\tilde{t}_1}} - \frac{\delta m^2_{\tilde{t}_2}}{m^6_{\tilde{t}_2}}\right) + \left(3\,\frac{\delta m_t}{m_t} + \frac{\delta s_{2\theta_t}}{s_{2\theta_t}}\right) F_2^{1\ell}\,, \tag{B.0.2}$$

$$\begin{aligned}\delta F_3 = {} & -\frac{1}{3}\left(\frac{\delta m^2_{\tilde{t}_1}}{m^6_{\tilde{t}_1}} + \frac{\delta m^2_{\tilde{t}_2}}{m^6_{\tilde{t}_2}} - \frac{\delta m^2_{\tilde{t}_1}}{m^4_{\tilde{t}_1}\,m^2_{\tilde{t}_2}} - \frac{\delta m^2_{\tilde{t}_2}}{m^4_{\tilde{t}_2}\,m^2_{\tilde{t}_1}}\right) \\ & + \left(2\,\frac{\delta m_t}{m_t} + 2\,\frac{\delta s_{2\theta_t}}{s_{2\theta_t}}\right) F_3^{1\ell}\,,\end{aligned} \tag{B.0.3}$$

$$\delta F = \frac{1}{6}\left(\frac{\delta m^2_{\tilde{t}_1}}{m^4_{\tilde{t}_1}} - \frac{\delta m^2_{\tilde{t}_2}}{m^4_{\tilde{t}_2}}\right) + \left(2\,\frac{\delta m_t}{m_t} - \frac{\delta m^2_{\tilde{t}_1} - \delta m^2_{\tilde{t}_2}}{m^2_{\tilde{t}_1} - m^2_{\tilde{t}_2}}\right) F^{1\ell}\,, \tag{B.0.4}$$

$$\delta G = \frac{1}{6}\left(\frac{\delta m^2_{\tilde{t}_1}}{m^4_{\tilde{t}_1}} + \frac{\delta m^2_{\tilde{t}_2}}{m^4_{\tilde{t}_2}} + 8\,\frac{\delta m_t}{m^3_t}\right) + 2\,\frac{\delta m_t}{m_t}\,G^{1\ell}\,, \tag{B.0.5}$$

and

$$\delta\widetilde{F}_1 = -\frac{d_L^t + d_R^t}{6}\left(\frac{\delta m^2_{\tilde{t}_1}}{m^6_{\tilde{t}_1}} + \frac{\delta m^2_{\tilde{t}_2}}{m^6_{\tilde{t}_2}}\right) - \frac{d_L^t - d_R^t}{12}\left[2\,c_{2\theta_t}\left(\frac{\delta m^2_{\tilde{t}_1}}{m^6_{\tilde{t}_1}} - \frac{\delta m^2_{\tilde{t}_2}}{m^6_{\tilde{t}_2}}\right) - \delta c_{2\theta_t}\left(\frac{1}{m^4_{\tilde{t}_1}} - \frac{1}{m^4_{\tilde{t}_2}}\right)\right] + 2\,\frac{\delta m_t}{m_t}\,\widetilde{F}_1^{1\ell}\,, \tag{B.0.6}$$

$$\delta\widetilde{F}_2 = -\frac{d_L^t + d_R^t}{6}\left(\frac{\delta m^2_{\tilde{t}_1}}{m^6_{\tilde{t}_1}} - \frac{\delta m^2_{\tilde{t}_2}}{m^6_{\tilde{t}_2}}\right) - \frac{d_L^t - d_R^t}{12}\left[2\,c_{2\theta_t}\left(\frac{1}{m^2_{\tilde{t}_1}} - \frac{1}{m^2_{\tilde{t}_2}}\right)\left(\frac{\delta m^2_{\tilde{t}_1}}{m^4_{\tilde{t}_1}} - \frac{\delta m^2_{\tilde{t}_2}}{m^4_{\tilde{t}_2}}\right) - \delta c_{2\theta_t}\,\frac{(m^2_{\tilde{t}_1} - m^2_{\tilde{t}_2})^2}{m^4_{\tilde{t}_1}\,m^4_{\tilde{t}_2}}\right] + \left(\frac{\delta m_t}{m_t} + \frac{\delta s_{2\theta_t}}{s_{2\theta_t}}\right)\widetilde{F}_2^{1\ell}\,, \tag{B.0.7}$$

$$\delta\widetilde{F}_3 = -\frac{(d_L^t)^2 + (d_R^t)^2}{6}\left(\frac{\delta m^2_{\tilde{t}_1}}{m^6_{\tilde{t}_1}} + \frac{\delta m^2_{\tilde{t}_2}}{m^6_{\tilde{t}_2}}\right) - \frac{(d_L^t)^2 - (d_R^t)^2}{12}\left[2\,c_{2\theta_t}\left(\frac{\delta m^2_{\tilde{t}_1}}{m^6_{\tilde{t}_1}} - \frac{\delta m^2_{\tilde{t}_2}}{m^6_{\tilde{t}_2}}\right) - \delta c_{2\theta_t}\left(\frac{1}{m^4_{\tilde{t}_1}} - \frac{1}{m^4_{\tilde{t}_2}}\right)\right] + \frac{(d_L^t - d_R^t)^2}{12}\left[s^2_{2\theta_t}\left(\frac{1}{m^2_{\tilde{t}_1}} - \frac{1}{m^2_{\tilde{t}_2}}\right)\left(\frac{\delta m^2_{\tilde{t}_1}}{m^4_{\tilde{t}_1}} - \frac{\delta m^2_{\tilde{t}_2}}{m^4_{\tilde{t}_2}}\right) + c_{2\theta_t}\,\delta c_{2\theta_t}\,\frac{(m^2_{\tilde{t}_1} - m^2_{\tilde{t}_2})^2}{m^4_{\tilde{t}_1}\,m^4_{\tilde{t}_2}}\right], \tag{B.0.8}$$

$$\delta D = \frac{d_L^t + d_R^t}{12}\left(\frac{\delta m^2_{\tilde{t}_1}}{m^4_{\tilde{t}_1}} + \frac{\delta m^2_{\tilde{t}_2}}{m^4_{\tilde{t}_2}}\right) + \frac{d_L^t - d_R^t}{12}\left[c_{2\theta_t}\left(\frac{\delta m^2_{\tilde{t}_1}}{m^4_{\tilde{t}_1}} - \frac{\delta m^2_{\tilde{t}_2}}{m^4_{\tilde{t}_2}}\right) - \delta c_{2\theta_t}\left(\frac{1}{m^2_{\tilde{t}_1}} - \frac{1}{m^2_{\tilde{t}_2}}\right)\right], \tag{B.0.9}$$

where $\delta s_{2\theta_t} = 2\,c_{2\theta_t}\,\delta\theta_t$ and $\delta c_{2\theta_t} = -2\,s_{2\theta_t}\,\delta\theta_t$. If the parameters in the top/stop sector are renormalized in the OS scheme, the shifts δm_t, $\delta m^2_{\tilde{t}_i}$, $\delta\theta_t$ and δA_t can be found in appendix B of ref. [60].

Appendix C

Extension to the NMSSM

In this appendix we describe how our results for the box form factor for Higgs pair production in the MSSM can be extended to the case of the NMSSM. Instead of the Higgs mass term $\mu\, H_1 H_2$, which in the simplest realization of the NMSSM is forbidden by a Z_3 symmetry, the superpotential contains [1]

$$W \;\supset\; \lambda\, S H_1 H_2 \;+\; \frac{\kappa}{3}\, S^3 \;, \tag{C.0.1}$$

where S is an additional gauge-singlet superfield. An effective μ term is generated by the singlet VEV as $\mu = \lambda \langle S \rangle$, and the CP-even parts S_i of the neutral component of the three Higgs fields – ordered as (H_1, H_2, S) – mix into three mass eigenstates which we denote as h_a,

$$h_a \;=\; R^S_{ai}\, S_i \;, \tag{C.0.2}$$

where R^S is an orthogonal matrix. The decompositions of the triangle and box form factors in eqs. (2.2.1)–(2.2.5) generalize to

$$F_\Delta^{h_a} \;=\; -T_F\, R^S_{ai}\, \mathcal{H}_i \;, \qquad\qquad F_\Box^{h_a h_b} \;=\; -T_F\, R^S_{ai}\, R^S_{bj}\, \mathcal{H}_{ij} \;. \tag{C.0.3}$$

The extension to the NMSSM of the results of refs. [52, 53, 55] for the triangle form factors of the MSSM has been presented, in the context of single Higgs production, in ref. [98]. Concerning the box form factors, the terms $\mathcal{H}_{11}$, $\mathcal{H}_{12}$ and $\mathcal{H}_{22}$ coincide with those obtained for the MSSM in section 2.2. The top/stop contributions to the remaining

[1] For consistency with the definition of μ in our MSSM results, here we adopt for the sign of λ the opposite convention with respect to ref. [97] and most public codes for NMSSM calculations. We also note that our normalization of the EW parameter, $v \approx 246$ GeV, differs by a factor $\sqrt{2}$ from the one in ref. [97].

terms read

$$\mathcal{H}^t_{13} = \frac{\sqrt{2}\,\lambda\,v\,m_t}{\sin\beta}\left[\frac{1}{2}\,m_t\,\mu\,\cot\beta\,s^2_{2\theta_t}\,F_3 + \frac{m_t\,(A_t+2\,\mu\,\cot\beta)}{m^2_{\tilde{t}_1}-m^2_{\tilde{t}_2}}\,F + m_Z^2\,\cos^2\beta\,s_{2\theta_t}\,\widetilde{F}_2\right], \tag{C.0.4}$$

$$\mathcal{H}^t_{23} = \frac{\sqrt{2}\,\lambda\,v\,m_t}{\sin\beta}\left[m_t^2\,\cot\beta\,s_{2\theta_t}\,F_2 + \frac{1}{2}\,m_t\,A_t\,\cot\beta\,s^2_{2\theta_t}\,F_3 + \frac{m_t\,A_t\,\cot\beta}{m^2_{\tilde{t}_1}-m^2_{\tilde{t}_2}}\,F - m_Z^2\,\sin\beta\cos\beta\,s_{2\theta_t}\,\widetilde{F}_2\right], \tag{C.0.5}$$

$$\mathcal{H}^t_{33} = \lambda^2\,v^2\left[\frac{1}{2}\,m_t^2\,\cot^2\beta\,s^2_{2\theta_t}\,F_3 + \frac{m_t^2\,\cot^2\beta}{m^2_{\tilde{t}_1}-m^2_{\tilde{t}_2}}\,F\right], \tag{C.0.6}$$

where the functions F_2, F_3, F and $\widetilde{F}_2$ coincide with those entering the MSSM results, see section 2.2 and appendix A. In the limit $m_b = \theta_b = 0$ there are no contributions to $\mathcal{H}_{13}$, $\mathcal{H}_{23}$ and $\mathcal{H}_{33}$ from bottom/sbottom loops.

Finally, when the parameters entering the top/stop contributions to the one-loop part of the form factors are expressed in a renormalization scheme other than $\overline{\rm DR}$, the shifts to the form factors that were not already given in section 2.2.3 read

$$\delta\mathcal{H}^t_{13} = \frac{\sqrt{2}\,\lambda\,v\,m_t}{\sin\beta}\left[\frac{1}{2}\,m_t\,\mu\,\cot\beta\,s^2_{2\theta_t}\,\delta F_3 + \frac{m_t\,(A_t+2\,\mu\,\cot\beta)}{m^2_{\tilde{t}_1}-m^2_{\tilde{t}_2}}\,\delta F + m_Z^2\,\cos^2\beta\,s_{2\theta_t}\,\delta\widetilde{F}_2 + \frac{m_t\,\delta A_t}{m^2_{\tilde{t}_1}-m^2_{\tilde{t}_2}}\,F^{1\ell}\right], \tag{C.0.7}$$

$$\delta\mathcal{H}^t_{23} = \frac{\sqrt{2}\,\lambda\,v\,m_t}{\sin\beta}\left[m_t^2\,\cot\beta\,s_{2\theta_t}\,\delta F_2 + \frac{1}{2}\,m_t\,A_t\,\cot\beta\,s^2_{2\theta_t}\,\delta F_3 + \frac{m_t\,A_t\,\cot\beta}{m^2_{\tilde{t}_1}-m^2_{\tilde{t}_2}}\,\delta F - m_Z^2\,\sin\beta\cos\beta\,s_{2\theta_t}\,\delta\widetilde{F}_2 + \frac{1}{2}\,m_t\,\delta A_t\,\cot\beta\,s^2_{2\theta_t}\,F_3^{1\ell} + \frac{m_t\,\delta A_t\,\cot\beta}{m^2_{\tilde{t}_1}-m^2_{\tilde{t}_2}}\,F^{1\ell}\right], \tag{C.0.8}$$

$$\delta\mathcal{H}^t_{33} = \lambda^2\,v^2\left[\frac{1}{2}\,m_t^2\,\cot^2\beta\,s^2_{2\theta_t}\,\delta F_3 + \frac{m_t^2\,\cot^2\beta}{m^2_{\tilde{t}_1}-m^2_{\tilde{t}_2}}\,\delta F\right], \tag{C.0.9}$$

where the shifts δF_2, δF_3, δF and $\delta\widetilde{F}_2$ coincide with those defined in appendix B.

Bibliography

[1] **ATLAS** Collaboration, G. Aad *et al.*, *Observation of a new particle in the search for the Standard Model Higgs boson with the ATLAS detector at the LHC*. Phys. Lett. **B716** (2012) 1–29, arXiv:1207.7214 [hep-ex].

[2] **CMS** Collaboration, S. Chatrchyan *et al.*, *Observation of a new boson at a mass of 125 GeV with the CMS experiment at the LHC*. Phys. Lett. **B716** (2012) 30–61, arXiv:1207.7235 [hep-ex].

[3] P. W. Higgs, *Broken Symmetries and the Masses of Gauge Bosons*. Phys. Rev. Lett. **13** (1964) 508.

[4] P. W. Higgs, *Broken symmetries, massless particles and gauge fields*. Phys. Lett. **12** (1964) 132.

[5] Englert, F. and Brout, R. *Broken symmetry and the mass of gauge vector mesons*. Phys. Rev. Lett. **13** (1964) 321.

[6] Guralnik, G. S. and Hagen, C. R. and Kibble, T. W. B. *Global conservation laws and massless particles*. Phys. Rev. Lett. **13** (1964) 585.

[7] Kibble, T. W. B. *Symmetry breaking in non-Abelian gauge theories*. Phys. Rev. **155** (1967) 1554.

[8] **ATLAS and CMS** Collaboration, *Measurements of the Higgs boson production and decay rates and constraints on its couplings from a combined ATLAS and CMS analysis of the LHC pp collision data at* $\sqrt{s} = 7$ *and 8 TeV*. ATLAS-CONF-2015-044 and CMS-PAS-HIG-15-002.

[9] T. Plehn and M. Rauch, *The quartic higgs coupling at hadron colliders*. Phys. Rev. **D72** (2005) 053008, arXiv:hep-ph/0507321 [hep-ph].

[10] T. Binoth, S. Karg, N. Kauer, and R. Ruckl, *Multi-Higgs boson production in the Standard Model and beyond*. Phys. Rev. **D74** (2006) 113008, arXiv:hep-ph/0608057 [hep-ph].

[11] U. Baur, T. Plehn, and D. L. Rainwater, *Probing the Higgs selfcoupling at hadron colliders using rare decays*. Phys. Rev. **D69** (2004) 053004, arXiv:hep-ph/0310056 [hep-ph].

[12] J. Baglio, A. Djouadi, R. Gröber, M. M. Mühlleitner, J. Quevillon, and M. Spira, *The measurement of the Higgs self-coupling at the LHC: theoretical status*. JHEP **04** (2013) 151, arXiv:1212.5581 [hep-ph].

[13] W. Yao, "Studies of measuring Higgs self-coupling with $HH \to b\bar{b}\gamma\gamma$ at the future hadron colliders," in *Community Summer Study 2013: Snowmass on the Mississippi (CSS2013) Minneapolis, MN, USA, July 29-August 6, 2013*. 2013. arXiv:1308.6302 [hep-ph].

[14] V. Barger, L. L. Everett, C. B. Jackson, and G. Shaughnessy, *Higgs-Pair Production and Measurement of the Triscalar Coupling at LHC(8,14)*. Phys. Lett. **B728** (2014) 433–436, arXiv:1311.2931 [hep-ph].

[15] A. Azatov, R. Contino, G. Panico, and M. Son, *Effective field theory analysis of double Higgs boson production via gluon fusion*. Phys. Rev. **D92** (2015) no. 3, 035001, arXiv:1502.00539 [hep-ph].

[16] C.-T. Lu, J. Chang, K. Cheung, and J. S. Lee, *An exploratory study of Higgs-boson pair production*. JHEP **08** (2015) 133, arXiv:1505.00957 [hep-ph].

[17] M. J. Dolan, C. Englert, and M. Spannowsky, *Higgs self-coupling measurements at the LHC*. JHEP **10** (2012) 112, arXiv:1206.5001 [hep-ph].

[18] A. Papaefstathiou, L. L. Yang, and J. Zurita, *Higgs boson pair production at the LHC in the $b\bar{b}W^+W^-$ channel*. Phys. Rev. **D87** (2013) no. 1, 011301, arXiv:1209.1489 [hep-ph].

[19] D. E. Ferreira de Lima, A. Papaefstathiou, and M. Spannowsky, *Standard model Higgs boson pair production in the ($b\bar{b}$)($b\bar{b}$) final state*. JHEP **08** (2014) 030, arXiv:1404.7139 [hep-ph].

[20] D. Wardrope, E. Jansen, N. Konstantinidis, B. Cooper, R. Falla, and N. Norjoharuddeen, *Non-resonant Higgs-pair production in the $b\bar{b}$ $b\bar{b}$ final state at the LHC*. Eur. Phys. J. **C75** (2015) no. 5, 219, arXiv:1410.2794 [hep-ph].

[21] J. K. Behr, D. Bortoletto, J. A. Frost, N. P. Hartland, C. Issever, and J. Rojo, *Boosting Higgs pair production in the $b\bar{b}b\bar{b}$ final state with multivariate techniques*. arXiv:1512.08928 [hep-ph].

[22] E. W. N. Glover and J. J. van der Bij, *Higgs boson pair production via gluon fusion*. Nucl. Phys. **B309** (1988) 282.

[23] S. Dawson, S. Dittmaier, and M. Spira, *Neutral Higgs boson pair production at hadron colliders: QCD corrections*. Phys. Rev. **D58** (1998) 115012, arXiv:hep-ph/9805244 [hep-ph].

[24] R. Frederix, S. Frixione, V. Hirschi, F. Maltoni, O. Mattelaer, P. Torrielli, E. Vryonidou, and M. Zaro, *Higgs pair production at the LHC with NLO and parton-shower effects*. Phys. Lett. **B732** (2014) 142–149, arXiv:1401.7340 [hep-ph].

[25] M. A. Shifman, A. I. Vainshtein, M. B. Voloshin, and V. I. Zakharov, *Low-Energy Theorems for Higgs Boson Couplings to Photons*. Sov. J. Nucl. Phys. **30** (1979) 711–716. [Yad. Fiz.30,1368(1979)].

[26] B. A. Kniehl and M. Spira, *Low-energy theorems in Higgs physics*. Z. Phys. **C69** (1995) 77–88, arXiv:hep-ph/9505225 [hep-ph].

[27] J. R. Ellis, M. K. Gaillard, and D. V. Nanopoulos, *A Phenomenological Profile of the Higgs Boson*. Nucl. Phys. **B106** (1976) 292.

[28] G. Degrassi, P. P. Giardino and R. Gröber, *On the two-loop virtual QCD corrections to Higgs boson pair production in the Standard Model*. Eur. Phys. J. C **76** (2016) no.7, 411, arXiv:1603.00385 [hep-ph].

[29] T. Plehn, M. Spira, and P. M. Zerwas, *Pair production of neutral Higgs particles in gluon-gluon collisions*. Nucl. Phys. **B479** (1996) 46–64, arXiv:hep-ph/9603205 [hep-ph]. [Erratum: Nucl. Phys. **B531** (1998) 655].

[30] D. de Florian and J. Mazzitelli, *Higgs Boson Pair Production at Next-to-Next-to-Leading Order in QCD*. Phys. Rev. Lett. **111** (2013) 201801, arXiv:1309.6594 [hep-ph].

[31] S. Borowka, N. Greiner, G. Heinrich, S. P. Jones, M. Kerner, J. Schlenk, U. Schubert and T. Zirke, *Higgs Boson Pair Production in Gluon Fusion at Next-to-Leading Order with Full Top-Quark Mass Dependence*. Phys. Rev. Lett. **117** (2016) no.1, 012001 arXiv:1604.06447 [hep-ph].

[32] S. Borowka, N. Greiner, G. Heinrich, S. P. Jones, M. Kerner, J. Schlenk and T. Zirke, *Full top quark mass dependence in Higgs boson pair production at NLO*. JHEP **1610** (2016) 107 arXiv:1608.04798 [hep-ph].

[33] D. de Florian and J. Mazzitelli, *Higgs pair production at next-to-next-to-leading logarithmic accuracy at the LHC*. JHEP **09** (2015) 053, arXiv:1505.07122 [hep-ph].

[34] S. Dawson, E. Furlan, and I. Lewis, *Unravelling an extended quark sector through multiple Higgs production?* Phys. Rev. **D87** (2013) no. 1, 014007, arXiv:1210.6663 [hep-ph].

[35] M. Gillioz, R. Grober, C. Grojean, M. Muhlleitner, and E. Salvioni, *Higgs Low-Energy Theorem (and its corrections) in Composite Models*. JHEP **10** (2012) 004, arXiv:1206.7120 [hep-ph].

[36] D. de Florian *et al.* [LHC Higgs Cross Section Working Group], *Handbook of LHC Higgs Cross Sections: 4. Deciphering the Nature of the Higgs Sector*. , arXiv:1610.07922 [hep-ph].

[37] J. Butterworth *et al.*, *PDF4LHC recommendations for LHC Run II*. J. Phys. G **43** (2016) 023001 arXiv:1510.03865 [hep-ph].

[38] S. Dulat, T.-J. Hou, J. Gao, M. Guzzi, J. Huston, P. Nadolsky, J. Pumplin, C. Schmidt, D. Stump, and C. P. Yuan, *New parton distribution functionsfrom a global analysis of quantum chromodynamics*, Phys. Rev. **D93** (2016) 033006, arXiv:1506.07443 [hep-ph].

[39] L. A. Harland-Lang, A. D. Martin, P. Motylinski, and R. S. Thorne, *Parton distributions in the LHC era: MMHT 2014 PDFs*, Eur. Phys. J. **C75** (2015) 204, arXiv:1412.3989 [hep-ph].

[40] NNPDF Collaboration, R. D. Ball et al., *Parton distributions for the LHC Run II*, JHEP **04** (2015) 040, arXiv:1410.8849 [hep-ph].

[41] **ATLAS, CMS** Collaboration, G. Aad *et al.*, *Combined Measurement of the Higgs Boson Mass in pp Collisions at $\sqrt{s} = 7$ and 8 TeV with the ATLAS and CMS Experiments*. Phys. Rev. Lett. **114** (2015) 191803, arXiv:1503.07589 [hep-ex].

[42] M. Spira, A. Djouadi, D. Graudenz, and P. M. Zerwas, *Higgs boson production at the LHC*. Nucl. Phys. **B453** (1995) 17–82, arXiv:hep-ph/9504378 [hep-ph].

[43] R. Harlander and P. Kant, *Higgs production and decay: Analytic results at next-to-leading order QCD*. JHEP **0512** (2005) 015, arXiv:hep-ph/0509189 [hep-ph].

[44] C. Anastasiou, S. Beerli, S. Bucherer, A. Daleo, and Z. Kunszt, *Two-loop amplitudes and master integrals for the production of a Higgs boson via a massive quark and a scalar-quark loop*. JHEP **01** (2007) 082, arXiv:hep-ph/0611236 [hep-ph].

[45] U. Aglietti, R. Bonciani, G. Degrassi, and A. Vicini, *Analytic Results for Virtual QCD Corrections to Higgs Production and Decay*. JHEP **01** (2007) 021, arXiv:hep-ph/0611266 [hep-ph].

[46] M. Muhlleitner and M. Spira, *Higgs Boson Production via Gluon Fusion: Squark Loops at NLO QCD*. Nucl. Phys. **B790** (2008) 1–27, arXiv:hep-ph/0612254 [hep-ph].

[47] R. Bonciani, G. Degrassi, and A. Vicini, *Scalar particle contribution to Higgs production via gluon fusion at NLO*. JHEP **11** (2007) 095, arXiv:0709.4227 [hep-ph].

[48] C. Anastasiou, S. Beerli, and A. Daleo, *The Two-loop QCD amplitude $gg \to h$,H in the Minimal Supersymmetric Standard Model*. Phys. Rev. Lett. **100** (2008) 241806, arXiv:0803.3065 [hep-ph].

[49] M. Muhlleitner, H. Rzehak, and M. Spira, *SUSY-QCD Corrections to MSSM Higgs Boson Production via Gluon fusion*. PoS **RADCOR2009** (2010) 043, arXiv:1001.3214 [hep-ph].

[50] R. V. Harlander and M. Steinhauser, *Hadronic Higgs production and decay in supersymmetry at next-to-leading order*. Phys. Lett. **B574** (2003) 258–268, arXiv:hep-ph/0307346 [hep-ph].

[51] R. V. Harlander and M. Steinhauser, *Supersymmetric Higgs production in gluon fusion at next-to-leading order*. JHEP **0409** (2004) 066, arXiv:hep-ph/0409010 [hep-ph].

[52] G. Degrassi and P. Slavich, *On the NLO QCD corrections to Higgs production and decay in the MSSM*. Nucl. Phys. **B805** (2008) 267–286, arXiv:0806.1495 [hep-ph].

[53] G. Degrassi and P. Slavich, *NLO QCD bottom corrections to Higgs boson production in the MSSM*. JHEP **1011** (2010) 044, arXiv:1007.3465 [hep-ph].

[54] R. V. Harlander, F. Hofmann, and H. Mantler, *Supersymmetric Higgs production in gluon fusion*. JHEP **02** (2011) 055, arXiv:1012.3361 [hep-ph].

[55] G. Degrassi, S. Di Vita, and P. Slavich, *On the NLO QCD Corrections to the Production of the Heaviest Neutral Higgs Scalar in the MSSM*. Eur. Phys. J. **C72** (2012) 2032, arXiv:1204.1016 [hep-ph].

[56] A. Belyaev, M. Drees, O. J. P. Eboli, J. K. Mizukoshi, and S. F. Novaes, *Supersymmetric Higgs pair production at hadron colliders*. Phys. Rev. **D60** (1999) 075008, arXiv:hep-ph/9905266 [hep-ph].

[57] A. A. Barrientos Bendezu and B. A. Kniehl, *Pair production of neutral Higgs bosons at the CERN large hadron collider*. Phys. Rev. **D64** (2001) 035006, arXiv:hep-ph/0103018 [hep-ph].

[58] B. Batell, M. McCullough, D. Stolarski, and C. B. Verhaaren, *Putting a Stop to di-Higgs Modifications*. JHEP **09** (2015) 216, arXiv:1508.01208 [hep-ph].

[59] A. Agostini, G. Degrassi, R. Gröber and P. Slavich, *NLO-QCD corrections to Higgs pair production in the MSSM* JHEP **1604** (2016) 106, arXiv:1601.03671 [hep-ph].

[60] G. Degrassi, P. Slavich, and F. Zwirner, *On the neutral Higgs boson masses in the MSSM for arbitrary stop mixing*. Nucl. Phys. **B611** (2001) 403–422, arXiv:hep-ph/0105096 [hep-ph].

[61] A. Dedes and P. Slavich, *Two loop corrections to radiative electroweak symmetry breaking in the MSSM*. Nucl. Phys. **B657** (2003) 333–354, arXiv:hep-ph/0212132 [hep-ph].

[62] M. Spira, HPAIR *home page*. http://tiger.web.psi.ch/hpair/.

[63] A. Brignole and F. Zwirner, *Radiative corrections to the decay $H \to h\ h$ in the minimal supersymmetric standard model*. Phys. Lett. **B299** (1993) 72–82, arXiv:hep-ph/9210266 [hep-ph].

[64] S. Heinemeyer and W. Hollik, *The Decay h0 → A0 A0: A Complete one loop calculation in the MSSM*. Nucl. Phys. **B474** (1996) 32–56, arXiv:hep-ph/9602318 [hep-ph].

[65] V. D. Barger, M. S. Berger, A. L. Stange, and R. J. N. Phillips, *Supersymmetric Higgs boson hadroproduction and decays including radiative corrections*. Phys. Rev. **D45** (1992) 4128–4147.

[66] A. Dobado, M. J. Herrero, W. Hollik, and S. Penaranda, *Selfinteractions of the lightest MSSM Higgs boson in the large pseudoscalar mass limit*. Phys. Rev. **D66** (2002) 095016, arXiv:hep-ph/0208014 [hep-ph].

[67] D. T. Nhung, M. Muhlleitner, J. Streicher, and K. Walz, *Higher Order Corrections to the Trilinear Higgs Self-Couplings in the Real NMSSM*. JHEP **11** (2013) 181, arXiv:1306.3926 [hep-ph].

[68] M. Brucherseifer, R. Gavin, and M. Spira, *Minimal supersymmetric Higgs boson self-couplings: Two-loop $O(\alpha_t\alpha_s)$ corrections*. Phys. Rev. **D90** (2014) no. 11, 117701, arXiv:1309.3140 [hep-ph].

[69] M. Mühlleitner, D. T. Nhung, and H. Ziesche, *The order $\mathcal{O}(\alpha_t\alpha_s)$ corrections to the trilinear Higgs self-couplings in the complex NMSSM*. JHEP **12** (2015) 034, arXiv:1506.03321 [hep-ph].

[70] S. Heinemeyer, W. Hollik, and G. Weiglein, *FeynHiggs: A Program for the calculation of the masses of the neutral CP even Higgs bosons in the MSSM*. Comput. Phys. Commun. **124** (2000) 76–89, arXiv:hep-ph/9812320 [hep-ph].

[71] S. Heinemeyer, W. Hollik, and G. Weiglein, *The Masses of the neutral CP - even Higgs bosons in the MSSM: Accurate analysis at the two loop level*. Eur. Phys. J. **C9** (1999) 343–366, arXiv:hep-ph/9812472 [hep-ph].

[72] G. Degrassi, S. Heinemeyer, W. Hollik, P. Slavich, and G. Weiglein, *Towards high precision predictions for the MSSM Higgs sector*. Eur. Phys. J. **C28** (2003) 133–143, arXiv:hep-ph/0212020 [hep-ph].

[73] M. Frank, T. Hahn, S. Heinemeyer, W. Hollik, H. Rzehak, and G. Weiglein, *The Higgs Boson Masses and Mixings of the Complex MSSM in the Feynman-Diagrammatic Approach*. JHEP **02** (2007) 047, arXiv:hep-ph/0611326 [hep-ph].

[74] T. Hahn, S. Heinemeyer, W. Hollik, H. Rzehak, and G. Weiglein, *High-Precision Predictions for the Light CP -Even Higgs Boson Mass of the Minimal Supersymmetric Standard Model*. Phys. Rev. Lett. **112** (2014) no. 14, 141801, arXiv:1312.4937 [hep-ph].

[75] A. Djouadi and J. Quevillon, *The MSSM Higgs sector at a high M_{SUSY}: reopening the low tanβ regime and heavy Higgs searches*. JHEP **10** (2013) 028, arXiv:1304.1787 [hep-ph].

[76] L. Maiani, A. D. Polosa, and V. Riquer, *Bounds to the Higgs Sector Masses in Minimal Supersymmetry from LHC Data*. Phys. Lett. **B724** (2013) 274–277, arXiv:1305.2172 [hep-ph].

[77] A. Djouadi, L. Maiani, G. Moreau, A. Polosa, J. Quevillon, and V. Riquer, *The post-Higgs MSSM scenario: Habemus MSSM?* Eur. Phys. J. **C73** (2013) 2650, arXiv:1307.5205 [hep-ph].

[78] A. Djouadi, L. Maiani, A. Polosa, J. Quevillon, and V. Riquer, *Fully covering the MSSM Higgs sector at the LHC*. JHEP **06** (2015) 168, arXiv:1502.05653 [hep-ph].

[79] E. Bagnaschi *et al.*, *Benchmark scenarios for low* $\tan\beta$ *in the MSSM* Tech. Rep. LHCHXSWG-2015-002, CERN, Geneva, Aug, 2015.

[80] G. Lee and C. E. M. Wagner, *Higgs bosons in heavy supersymmetry with an intermediate m_A*. Phys. Rev. **D92** (2015) no. 7, 075032, arXiv:1508.00576 [hep-ph].

[81] A. D. Martin, W. J. Stirling, R. S. Thorne, and G. Watt, *Parton distributions for the LHC*. Eur. Phys. J. **C63** (2009) 189–285, arXiv:0901.0002 [hep-ph].

[82] A. D. Martin, W. J. Stirling, R. S. Thorne, and G. Watt, *Uncertainties on alpha(S) in global PDF analyses and implications for predicted hadronic cross sections*. Eur. Phys. J. **C64** (2009) 653–680, arXiv:0905.3531 [hep-ph].

[83] A. D. Martin, W. J. Stirling, R. S. Thorne, and G. Watt, *Heavy-quark mass dependence in global PDF analyses and 3- and 4-flavour parton distributions*. Eur. Phys. J. **C70** (2010) 51–72, arXiv:1007.2624 [hep-ph].

[84] A. Bartl, H. Eberl, K. Hidaka, T. Kon, W. Majerotto, and Y. Yamada, *QCD corrections to Higgs boson decays into squarks in the minimal supersymmetric standard model*. Phys. Lett. **B402** (1997) 303–313, arXiv:hep-ph/9701398 [hep-ph].

[85] H. Eberl, K. Hidaka, S. Kraml, W. Majerotto, and Y. Yamada, *Improved SUSY QCD corrections to Higgs boson decays into quarks and squarks*. Phys. Rev. **D62** (2000) 055006, arXiv:hep-ph/9912463 [hep-ph].

[86] M. Carena, S. Heinemeyer, O. Stål, C. E. M. Wagner, and G. Weiglein, *MSSM Higgs Boson Searches at the LHC: Benchmark Scenarios after the Discovery of a Higgs-like Particle*. Eur. Phys. J. **C73** (2013) no. 9, 2552, arXiv:1302.7033 [hep-ph].

[87] E. Bagnaschi, R. V. Harlander, S. Liebler, H. Mantler, P. Slavich, and A. Vicini, *Towards precise predictions for Higgs-boson production in the MSSM*. JHEP **06** (2014) 167, arXiv:1404.0327 [hep-ph].

[88] J. Grigo, J. Hoff, K. Melnikov, and M. Steinhauser, *On the Higgs boson pair production at the LHC*. Nucl. Phys. **B875** (2013) 1–17, arXiv:1305.7340 [hep-ph].

[89] F. Maltoni, E. Vryonidou, and M. Zaro, *Top-quark mass effects in double and triple Higgs production in gluon-gluon fusion at NLO*. JHEP **11** (2014) 079, arXiv:1408.6542 [hep-ph].

[90] J. Grigo, J. Hoff, and M. Steinhauser, *Higgs boson pair production: top quark mass effects at NLO and NNLO*. Nucl. Phys. **B900** (2015) 412–430, arXiv:1508.00909 [hep-ph].

[91] R. K. Ellis, I. Hinchliffe, M. Soldate and J. J. van der Bij, *Higgs Decay to tau+ tau-: A Possible Signature of Intermediate Mass Higgs Bosons at the SSC* Nucl. Phys. B **297** (1988) 221,

[92] B. Mele, P. Nason, G. Ridolfi *QCD radiative corrections to Z boson pair production in hadronic collisions* Nucl. Phys. B **357**, (1991), 409

[93] T. Hahn, *Generating Feynman diagrams and amplitudes with FeynArts 3* Comput. Phys. Commun. **140** (2001) 418, arXiv:0012260 [hep-ph].

[94] Wolfram Research Inc., *Mathematica, Version 11.1* Champaign, IL, 2017

[95] M. Jamin and M. E. Lautenbacher, *TRACER: Version 1.1: A Mathematica package for gamma algebra in arbitrary dimensions* Comput. Phys. Commun. **74** (1993) 265.

[96] T. Hahn and M. Perez-Victoria, *Automatized one loop calculations in four-dimensions and D-dimensions* Comput. Phys. Commun. **118** (1999) 153 arXiv:9807565 [hep-ph].

[97] G. Degrassi and P. Slavich, *On the radiative corrections to the neutral Higgs boson masses in the NMSSM*. Nucl. Phys. **B825** (2010) 119–150, arXiv:0907.4682 [hep-ph].

[98] S. Liebler, *Neutral Higgs production at proton colliders in the CP-conserving NMSSM*. Eur. Phys. J. **C75** (2015) no. 5, 210, arXiv:1502.07972 [hep-ph].